1

Characterization of Water/Oil Interfaces

R. Miller J. Krägel
Max-Pianck-lnstitut, Berlin, Germany

V. B. Fainerman
Institute of Technical Ecology, Donetsk, Ukraine

A. V. Makievski
Max-Planck-lnstitut, Berlin, Germany, and
Institute of Technical Ecology, Donetsk, Ukraine

D. O. Grigoriev
Max-Planck-lnstitut, Berlin, Germany, and
St. Petersburg State University, St. Petersburg, Russia

F. Ravera L. Liggieri
Istituto di Chimica Fisica Applicata dei Materiali
CNR, Genoa, Italy

D. Y. Kwok
Massachusetts Institute of Technology, Cambridge,
Massachusetts

A. W. Neumann
University of Toronto, Toronto, Ontario, Canada

I. INTRODUCTION

The behavior of disperse systems, such as foams and emulsions, is very complex and there have been only few attempts to derive qualitative and quantitative relationships between their stability and physicochem-ical parameters of the stabilizing adsorption layers. The starting point of most of these approaches is the hydrodynamic theory of thinning of a liquid film between two bubbles or drops according to Reynolds (1) and Levich (2). A simplified picture of the general scenario in an emulsion is the following. When two droplets of equal size approach each other the contact area between the two drops is deformed such that a plane parallel film results (3). The liquid between the two film surfaces flows out until a critical film thickness is reached. In this situation, the two drops can repel each other, form a flock (coagulate), or coalesce to form one larger drop. Coalescence occurs when the film between the drops is not stable enough and ruptures (4). The film thining based on the Reynolds model assumes planar and completely rigid surfaces, which is not the case for films stabilized by adsorption layers of finite dilational elasticity (5).

Barnes (6) and Tadros and Vincent (7) demonstrated the importance of a number of factors on emulsion properties and stability, among them the relative volume of the dispersed phase, i.e., the volume fraction, and the average size of the droplet, the bulk viscosity of each phase, and also the nature and concentration of the emulsifier. The latter must be of vital importance as there are no stable emulsions or foams known without the presence of surface-active compounds. Sometimes this becomes not immediately visible in some systems as stabilizers may be inherent in many natural emulsions or foams.

Some approaches analyzed directly the influence of the stabilizing adsorption layers and concluded that there is a dependence of the stability of an emulsion on the interfacial concentration and the sum of inter-molecular interactions (8—10). Murdoch and Leng (11) pointed out the role of bulk and interfacial rheological parameters to describe these processes. This concept was further treated by several authors (12—14). A very comprehensive approach was given by Wasan and co-workers (15,16) who considered the surface shear and dilational rheology, and also some hydrody-namic parameters in their analysis of emulsion films.

In a number of experimental works evidence of the direct effect of adsorption-layer properties on the emulsion (foam) behavior has been discussed. A correlation between film rupture and dilational elasticity for a number of cationic surfactant systems has been shown by Bergeron (17) and also by Espert et al. (18). Dickinson (19) explains that the flocculation behavior of an emulsion requires a deep understanding of how different factors affect the structure and interactions of adsorbed layers, in particular of interfacial protein layers. Various differences in the flocculation are observed depending on the amount of adsorbed surface-active material during emulsification. In emulsion formation, rigid adsorption layers (due to surface-tension gradients, high elasticities) can yield smaller droplets as pointed out by Williams and Janssen (20). The effect of ionic strength and surface charge on emulsion stability has been studied recently (21—23). This might have various ways of action, such as salting out of surfactants and hence changing their surface activity, and changes in the disjoining pressure in the emulsions film. The special effects of ionic surfactants will not be further discussed in this chapter.

The most advanced summary of the importance of the adsorption layer properties on the behavior of an emulsion, i.e., its stability or breakdown, was given recently by Ivanov and Kralchevsky (24). In their review, Ivanov and Kralchevsky demonstrate the importance of the surfactant effect not only qualitatively but also give some general relationships. To evaluate the mass balance for a film under deformation they give the flux at the film surface $z = h/2$ (25):

$$\Gamma_o \frac{1}{r}\frac{\partial(rv_r)}{\partial r} - D_s \frac{\partial \Gamma_o}{\partial c_o}\frac{\partial^2 c}{\partial r^2} = \pm D\frac{\partial c}{\partial z} \qquad (1)$$

where v_r is the radial component of the mean mass flow, and r and z are cylindrical coordinates.

The three terms correspond to convection, surface, and bulk diffusion. At very small film thickness h the bulk diffusion term can be neglected in respect to the surface diffusion term. However, this does not take into consideration surfactant flux from the heterogeneous phase, i.e., from inside the emulsion drops.

With respect to the rheological parameters they come to the conclusion that surface elasticity effects are superior to surface viscosity effects. This, however, applies to pure surfactant layers and may be different for pure protein or mixed surfactant/protein adsorption layers. It has been stressed also by Langevin (26), in her review on foams and emulsions, that studies on the dynamics of adsorption and dilational rheology studies for mixed systems, in particular surfactant-polymer systems, are desirable in order to understand these most common stabilizing systems.

The analysis given for the surfactant effect on the thinning rate has shown that a flux from inside the emulsion drops is much less effective than the surfactant present in the homogeneous phase. It will be shown below, however, that almost all surfactants are usually soluble in both liquid phases of an emulsion so that obviously the distribution coefficient will be the parameter which controls the efficiency of a surfactant with respect to film thinning.

In this chapter an overview is given on the possibilities for a quantitative characterization of adsorption layers at liquid/liquid interfaces. After a general introduction to the fundamental thermodynamic relationships and particular ideas on surfactant and protein adsorption, the process of adsorption-layer formation is discussed on the basis of the most frequently used methodology, the measurement of dynamic interfacial tensions. This will also include measurements of extremely low interfacial tensions and the effect of inter-facial transfer between the two liquid phases.

Additional information on interfacial layers can be gained from rheological and ellipsometry experiments. There is quite a number of different experimental setups used to determine surface rheological parameters (27). New possibilities to determine surface dilational parameters arise from oscillating-drop experiments. Using axisymmetric drop shape analysis (ADSA) the change in interfacial ten-

sion becomes accessible as a function of the drop surface area when the drop deformations are considerably slow. For faster changes, i.e., higher oscillation frequencies, the oscillating-drop technique, as an analog of the pulsating-bubble method (28) has been recently developed (29). Studies of the interfacial shear rheology are described on the basis of a number of experimental methods; however, only a few of the existing techniques are suitable for investigations of liquid/liquid interfacial layers. Special emphasis is placed on torsion pendulum experiments (30).

III. ADSORPTION ISOTHERMS

A. Adsorption Isotherms

Interfacial layers at the interface between two immiscible liquid phases are characterized by large gradients in local properties, such as density, tensor of pressure, dielectric permittivity, and concentration of the dissolved components. The profile of the local concentration depends on properties of the dissolved substances. For substances which do not adsorb at the water/oil interface but are soluble in both phases, the concentration in the interfacial layer is between the equilibrium concentrations in the two phases (Fig. la).

The presence of a sharp maximum inside the inter-facial layer (Fig. 1B) is characteristic of surface-active components. Surface-inactive components can even show a minimum in the local concentration (Fig. 1C). Especially important for the stabilization of emulsions is the adsorption behavior of surfactants at the water/oil interface. To describe such systems makes it necessary to know the adsorption isotherm, to establish relationships between the concentration of a component in the interfacial layer and the bulk phases, and to derive equations of state giving the interfacial tension as a function of the interfacial layer composition. The derivation of these equations is based on the assumption that in equilibrium the temperature and the chemical potentials of any component have identical values in all parts of the system.

B. Chemical Potentials of Interfacial Layers

The chemical potentials of nonionic components within the interfacial layer μ^s_i depend on the composition of the layer and its surface tension γ. The dependence of μ^s_i on the composition of a surface layer is given by the known relation (31):

$$\mu_i^s = \mu_i^{0s}(T, P, \gamma) + RT \ln f_i^s \qquad (2)$$

where $\mu^{0s}_i(T, P, \gamma)$ is the standard chemical potential of component ; and depends on temperature T, pressure P, and surface tension γ,f_i are the activity coefficients. The standard chemical potential can be presented as a function of pressure and temperature only, if one introduces an explicit dependence of $\mu^{0s}_i(T, P, \gamma)$ on surface tension into Eq. (2) (31). This equation for the chemical potentials is the well-known Butler equation (32):

$$\mu_i^s = \mu_i^0 s + RT \ln f_i^s - \gamma\omega_i \qquad (3)$$

where ω_i is the partial molar area of the ith component. In this equation, in contrast to Eq. (2), the standard chemical potential $\mu^{0s}_i(T, P) = \mu^{0s}_i$ is already independent of the surface tension.

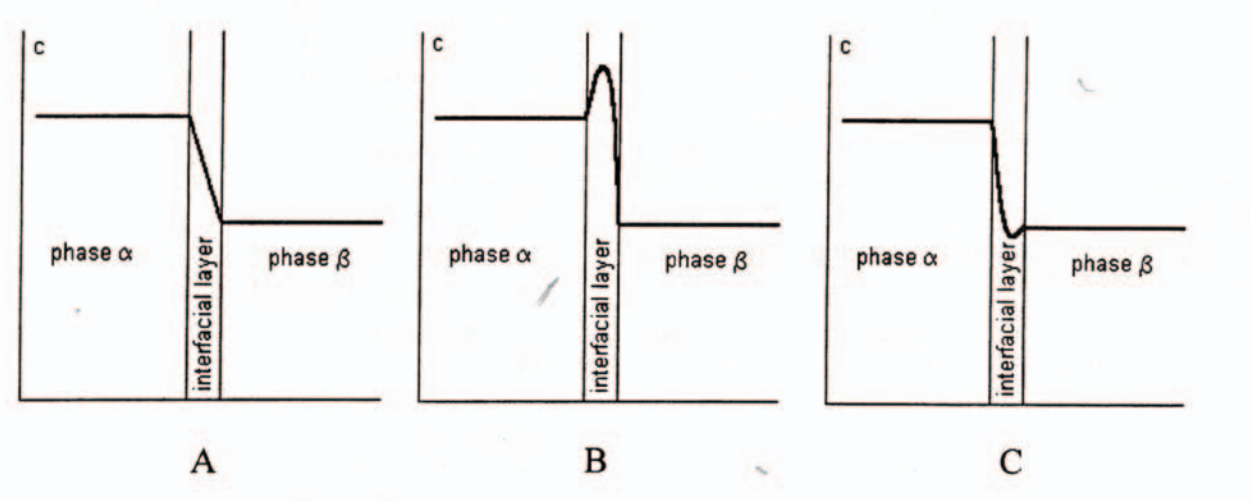

Figure 1 Change of local concentration in the interfacial layer.

Equations of state for surface layers and adsorption isotherms can be derived by equating the expressions for the chemical potentials at the surface, Eq. (3), to those in the bulk solution:

$$\mu_i^{\alpha} = \mu_i^{0\alpha} + RT \ln f_i^{\alpha} x_i^{\alpha} \quad (4)$$

The standard chemical potentials in Eq. (4), $\mu_i^{0\alpha}$, depend on pressure and temperature. At equilibrium this yields:

$$\mu_i^{0s} + RT \ln f_i^{s} x_i^{s} - \gamma\omega_i = \mu_i^{0\alpha} + RT \ln f_i^{\alpha} x_i^{\alpha} \quad (5)$$

Note that in equilibrium Eq (4) and (5) are suitable for both bulk phases, water and oil. Now the standard state has to be formulated. For the solvent (i = 0) usually a pure component is assumed, and

$$\mu_0^{0s} - \gamma_0\omega_0 = \mu_0^{0\alpha} \quad (6)$$

For the i surface-active components, infinite dilution (x^{α}_i 0) as the standard state is experimentally easier to access than the pure state (31, 33). It should be mentioned that setting the activity coefficients equal to unity for infinite dilution is not necessarily consistent with the same unit value of the activity coefficient for pure components. Therefore, an additional normalization of the potentials of the components should be performed. Indicating parameters at infinite dilution by the subscript 0, and those in the pure state by the superscript 0, the two standard potentials are interrelated by

$$\mu_{(0)i} = \mu_i^0 + RT \ln f_{(0)i} \quad (7)$$

for both phases α and the surface phase s. In combination with Eq. (5) this leads to

$$\mu_{0i}^{s} + RT \ln x_i^{s}\big|_{x_i^{\alpha}\to 0} - \gamma_0\omega_i = \mu_{0i}^{\alpha} + RT \ln x_i^{\alpha}\big|_{x_i^{\alpha}\to 0} \quad (8)$$

$$\mu_{0i}^{\alpha} - \mu_{0i}^{s} = -\gamma_0\omega_i + RT \ln K_i \quad (9)$$

where $K_i = (x_i^s/x_i^{\alpha})_{x_i^{\alpha}\to 0}$ are the distribution coefficients at infinite dilution. In a similar way it is possible to obtain from Eq. (4) an expression for the distribution coefficient of a component between two volume phases:

$$\mu_{0i}^{\alpha} - \mu_{0i}^{\beta} - RT \ln K_i^0 \quad (10)$$

where $K_i^0 = (x_i^{\beta}/x_i^{\alpha})_{x^{\alpha}\to 0}$. For a certain concentration the equilibrium distribution of a component between the oil and water phases (phases α and β) depends on the activity coefficients:

$$\frac{x_i^{\alpha}}{x_i^{\beta}} = K_i^0 \frac{f_i^{\beta}}{f_i^{\alpha}} \quad (11)$$

From Eqs (5) and (6) the following relationship results:

$$\ln \frac{f_0^s x_0^s}{f_0^{\alpha} x_0^{\alpha}} = -\frac{(\gamma_0 - \gamma)\omega_0}{RT} \quad (12)$$

and from Eqs (5) and (9) one obtains:

$$\ln \frac{f_i^s x_i^s / f_{(0)i}^s}{K_i f_i^{\alpha} x_i^{\alpha} / f_{(0)i}^{\alpha}} = -\frac{(\gamma)_o - \gamma)\omega_i}{RT} \quad (13)$$

The additional (normalizing) activity coefficients introduced in Eq. (7) can be incorporated into the constant K_i which enters Eq. (13). For further derivation it is necessary to express the surface molar fractions, x_j^s, in terms of their Gibbs adsorption values Γ_j. For this we introduce the degree of surface coverage, i.e., $\Gamma_j\omega_j$ or $\theta_j = \Gamma_j\omega_{\Sigma}$. Here, ω_{Σ} is the average partial molar area of all components. It is necessary to choose a proper ω_0 and the average partial molar surface area ω_{Σ} for all components or states. However, the use of a realistic surface demand for ω_0 (approximately 0.1 nm_2 for one H_2O molecule) will contradict experimental data. Let us consider first that there is only one dissolved species, and assume that the surface layer and bulk behave ideally. For $\omega_0 = \omega_1$, Eqs (12) and (13) transform into the well-known equations of von Szyszkowski (34) and Langmuir (35)

$$\Pi = \gamma_0 - \gamma = \frac{RT}{\omega_1}\ln(1 + K_1 x_1^{\alpha}) = \frac{RT}{\omega_1}\ln(1 + b_1 c_1) \quad (14)$$

$$\Gamma_1 = \frac{1}{\omega_1}\frac{b_1 c_1}{1 + b_1 c_1} \quad (15)$$

respectively, where the constant b_1 is the surtace-to-bulk distribution coefficient related to the concentration c rather than to the mole fraction x. In order to derive Eq. (14) we have to use a surface-layer model in which the molar surface area of the solvent in Eqs (12) and (13) is chosen equal to the molar surface area of the surfactant. This requirement can be satisfied (36-39) if one chooses the position of the dividing surface in such a way that the total adsorption of the solvent and surfactant are equal to $1/\omega_1$, i.e.

$$\Gamma_0 + \Gamma_1 = 1/\omega_1 = \Gamma_1^{\infty} \quad (16)$$

For a saturated monolayer ($\Gamma_1 = 1/\omega_1$), the dividing surface defined by Eq. (16) coincides with the dividing surface of the Gibbs convention, for which Γ_0=0. For Γ_1 = 0, however, the convention of Eq. (16) shifts the dividing surface towards the bulk solution by the distance $\triangle = (\omega_1 c_0^{\alpha})^{-1}$ as compared to the Gibbs convention (40). For large molecules, such as proteins ($\omega \gg \omega_0$), the value of $\triangle$ becomes negligibly small, and therefore for any adsorption the Lu-

cassen-Reynders' dividing surface practically coincides with the Gibbs' dividing surface. Reasons for this choice of the dividing surface have been discussed in (31, 41—45).

For surfactant mixtures or single molecules having several adsorption states within the surface the corresponding values of ω_i differ and the definition of the dividing surface transforms into a more general relationship:

$$\sum_{i=0}^{n} \Gamma_i = 1/\omega_\Sigma \tag{17}$$

Equations defining an average molecular area demand for all surfactant components of a mixture, taking into account different ω_i have been proposed by Lucassen-Reynders (38, 39) and Joos and coworkers (33, 41). An example in which the contribution of each component to ω_Σ is determined by its adsorption relative to the other adsorptions (31, 38) is

$$\omega_\Sigma = \left(\sum_{i\geq 1} \Gamma_i \omega_i\right) \Big/ \left(\sum_{i\geq 1} \Gamma_i\right) \tag{18}$$

If dissolved components are ionized, and a separation of charges takes place, resulting in the formation of an electric double layer (EDL), then the electrochemical potential (46—18) has to be used instead of the chemical potential [cf. Eq. (21)]:

$$\mu_i^S = \mu_i^{0S}(T, P, \gamma) + RT \ln f_i^S x_i^S + z_i F \psi \tag{19}$$

where F is the Faraday constant, z_1 is the charge of the ion, and ψ is the electric potential.

Unfortunately, in this case the dependence of the standard potential on the surface tension cannot be excluded, in contrast to the derivation presented for nonionized components. In the solution bulk outside the DEL no charge separation takes place, therefore the chemical potential μ^α_1 for both ionized and non-ionized components obeys the same equation [Eq. (4)].

C. Mixtures of Nonionic Surfactants

Assuming ideality of the bulk solution, and using the surface coverage θ_1 instead of the mole fractions in the form $x_i^s = \theta_i = \Gamma_i \omega_i$ or $\theta_i = \Gamma_i \omega_\Sigma$, the equation of state for a nonideal surface layer can be obtained from Eq. (12):

$$\Pi = -\frac{RT}{\omega_0}\left[\ln\left(1 - \sum_{i\geq 1} \theta_i\right) + \ln f_0^s\right] \tag{20}$$

and the adsorption isotherm from Eq. (13):

$$K_i c_i = \frac{\theta_i f_i^s}{\left(1 - \sum_{i\geq 1} \theta_i\right)^{n_i} (f_0^s)^{n_i}} \tag{21}$$

where c_1 are the bulk concentrations, and $n_i = \omega_i/\omega_0$. Activity coefficients determined by intermolecular interactions (enthalpic nonideality, $f^{sh}{}_i$) can be calculated using the regular solution theory (49—51). Lucassen-Reynders (45) has derived the following expression for the activity coefficient of any surface-layer component for the nonideal entropy of mixing:

$$\ln f_k^{sE} = 1 - n_k \sum_i (\theta_i/n_i) \tag{22}$$

As the enthalpy and the entropy are active in the Gibbs free energy, this additivity results in

$$f_i^s = f_i^{sH} \cdot f_i^{sE} \quad \text{or} \quad \ln f_i^s = \ln f_i^{sH} + \ln f_i^{sE} \tag{23}$$

For solutions of two surfactants the substitution of Eqs (22) and (23) into Eqs (20) and (21) leads to (31)

$$\Pi = -\frac{RT}{\omega_0}\left[\ln(1-\theta_1-\theta_2) + \theta_1\left(1-\frac{1}{n_1}\right) + \theta_2\left(1-\frac{1}{n_2}\right) + a_1\theta_i^2 + a_2\theta_2^2 + a_{12}\theta_1\theta_2\right] \tag{24}$$

$$b_i c_i = \frac{\theta_i}{(1-\theta_1-\theta_2)^{n_i}} \exp(-2a_i\theta_i - 2a_{12}\theta_j) \cdot \exp\left[(1-n_i)(a_1\theta_i^2 + a_2\theta_2^2 + a_{12}\theta_1\theta_2)\right] \tag{25}$$

where a_1, a_2 and a_{12} are constants; $b_1 = K_1 \exp(n_i - a_i - 1)$; $i = 1, 2$; and $j = 1, 2 (j \omega i)$. One can easily verify that all known equations describing the interfacial state of solutions of one or two surfactants involving both intermolecular interaction and nonideality of entropy [cf. (33, 36, 37, 52—72)] are limiting cases of Eqs (24) and (25). If the enthalpy of mixing is ideal, i.e., $a_1 = a_2 - a_{12} = 0$, then the following relations result (46, 57, 58):

$$\Pi = -\frac{RT}{\omega_0}\left[\ln(1-\theta_1-\theta_2) + \theta_1\left(1-\frac{1}{n_1}\right) + \theta_2\left(1-\frac{1}{n_2}\right)\right] \tag{26}$$

$$b_i c_1 = \frac{\theta_i}{(1-\theta_1-\theta_2)^{n_i}} \tag{27}$$

If the entropy of mixing for surface-layer components is ideal, that is, $n_1 - n_2 = 1$, then the generalized Frumkin equation of state and adsorption isotherm (36, 37, 52—55) are obtained:

$$\Pi = -\frac{RT}{\omega_0}[\ln(1-\theta_1-\theta_2) + a_1\theta_1^2 + a_2\theta_2^2 + a_{12}\theta_1\theta_2] \tag{28}$$

$$b_i c_i = \frac{\theta_i}{(1-\theta_1-\theta_2)}\exp(-2a_i\theta_i - 2a_{12}\theta_j) \tag{29}$$

For the solution of a single surfactant, i.e., for $0_2 = 0$ and $c_2 = 0$, these last expressions transform into the usual Frumkin equations (52):

$$\Pi = -\frac{RT}{\omega_0}[\ln(1-\theta) + a\theta^2] \tag{30}$$

$$bc = \frac{\theta}{(1-\theta)}\exp(-2a\theta) \tag{31}$$

Finally, for an ideal surface layer of an *n*-component ideal bulk solution, Eqs (20) and (21) transform into a generalized Szyszkowski-Langmuir equation of state:

$$\Pi = -\frac{RT}{\omega_0}\ln\left(1 - \sum_{i\geq 1}\Theta_i\right) \tag{32}$$

and a generalized Langmuir adsorption isotherm given by Eq. (27) with all $n_i = 1$. A direct consequence of the equality of all ω_i is that the adsorption ratio of two surfactants remains constant when their concentrations are varied in the same proportion, i.e., at constant c_1/c_2. However, for surfactant molecules with different ω_i Eq. (13) predicts increasingly preferential adsorption of the smaller molecule with increasing surface pressure. This has been shown experimentally (46) and is conveniently illustrated theoretically for ideal surface behavior by the following equation:

$$\frac{\Gamma_1}{\Gamma_2} = \frac{b_1 c_1}{b_2 c_2}\exp\left(\frac{\Pi(\omega_2 - \omega_1)}{RT}\right) \tag{33}$$

implying that a smaller molecule will expel a larger one from the surface when their total concentration is increased at constant c_1/c_2.

D. Surface Layers of Surfactants Able to Change Orientation

Equations which describe reorientation of surfactant molecules within the surface layer can be derived from Eqs (20) and (21) (31, 42, 43). Reorientation results in a variation of the partial molar area ω_i. If we assume that the solvent-surfactant and surfactant-surfactant intermolecular interactions do not depend on the state of surfactant molecules at the surface (ω_i), it follows from the regular solution theory [cf. (49—51)] for the convention of Eq. (17) that

$$\ln f_0^{sH} = a\Gamma_\Sigma^2\omega_\Sigma^2 \tag{34}$$

$$\ln f^{sH_i} = a(1-\Gamma_\Sigma\omega_\Sigma)^2,\ i \geq 1 \tag{35}$$

where a is a constant, and $\Gamma_\Sigma = \Sigma_{i\geqslant 1}\Gamma_i$ is the total adsorption of surfactant in all states. For our choice of the dividing surface, Eq. (22) can be transformed into

$$\ln f_i^{sE} = 1 - \omega_i\sum_{j\geq 0}\Gamma_j = 1 - n_i, \qquad i \geq 1 \tag{36}$$

$$\ln f_0^{sE} = 1 - \omega_0\sum_{j\geq 0}\Gamma_j = 0 \tag{37}$$

It is seen that the convention $\upsilon_0 = \upsilon_\Sigma$ means that the entropie contribution to it vanishes. Using Eqs (23) and (34)-(37), from Eqs (30) and (31), and with $K_i = K = a$ constant, one obtains:

$$\Pi = -\frac{RT}{\omega_\Sigma}[\ln(1-\Gamma_\Sigma\omega_\Sigma) + a(\Gamma_\Sigma\omega_\Sigma)^2] \tag{38}$$

$$bc = \frac{\Gamma_i\omega_\Sigma}{(1-\Gamma_\Sigma\omega_\Sigma)^{n_i}}\exp(-n_i)\exp[-2a\Gamma_\Sigma\omega_\Sigma + a(1-n_i)(\Gamma_\Sigma\omega_\Sigma)^2] \tag{39}$$

where $b = k\exp(-a-1)$

If $K_1 \neq K_2$ [in this case $b_1 = b_2(\omega_1/\omega_2)\alpha$, where α is a constant (42)], and for surfactant molecules which can adsorb in two states (1 and 2) with different partial molar areas ω_1 and $\omega_2(\omega_1 > \omega_2)$ the adsorption isotherm [Eq. (21)] can be expressed as

$$b_2 c = \frac{\Gamma_2\omega_\Sigma}{(1-\Gamma_\Sigma\omega_\Sigma)^{\omega_2/\omega_\Sigma}} = \left(\frac{\omega_2}{\omega_1}\right)^\alpha\frac{\Gamma_1\omega_\Sigma}{(1-\Gamma_\Sigma\omega_\Sigma)^{\omega_1/\omega_\Sigma}} \tag{40}$$

where $\Gamma_\Sigma = \Gamma_1 + \Gamma_2$ is the total adsorption, and ω_Σ is the mean partial molar area:

$$\omega_\Sigma = \frac{\omega_2 + \omega_1\cdot\beta\cdot\exp[\Pi(\omega_2-\omega_1)/RT]}{1+\beta\cdot\exp[\Pi(\omega_1-\omega_1)/RT]} \tag{41}$$

The parameter β in Eq. (41) considers that the adsorption activity of surfactant molecules is larger in state 1 than in state 2 (42, 43):

$$\beta = \left(\frac{\omega_1}{\omega_2}\right)^\alpha\exp\left(\frac{\omega_1-\omega_2}{\omega_\Sigma}\right) \tag{42}$$

An important relationship follows from Eq. (40) for two states 1 and 2 (31, 33, 43):

$$\frac{\Gamma_1}{\Gamma_2} = \beta\exp\left[\frac{\Pi(\omega_2-\omega_1)}{RT}\right] \tag{43}$$

The dynamic surface pressure in the framework of the two-states model is defined by

$$\Pi = -(RT/\omega_\Sigma)\ln(1 - \Gamma_\Sigma\omega_\Sigma) \quad (44)$$

Let us consider the results obtained for $C_{10}EO_8$ for the water/hexane interface using the pendent-drop method (73). Figure 2 shows the experimental and theoretical interface-tension isotherms.

The theoretical calculations were performed with different models: the reorientation, Langmuir, and Frumkin models. The experimental results are in perfect agreement with the reorientation model and the Frumkin equations, while the Langmuir model is completely invalid. However, for the Frumkin equations a value of a = -10.8 for the interaction parameter is obtained which is quite unrealistic. Thus, one can conclude that the model of interacting molecules is inapplicable for $C_{10}EO_8$ at the water/oil interface. The values of geometric parameters (ω_1 and ω_2) for the $C_{10}EO_8$ molecule at the water/air and water/oil interfaces are rather similar to each other, while the α values are quite different: 3.0 at the water/air interface, and 6.5 at the water/oil interface (73). Thus, the adsorption activity of oxyethylene groups at the hex-ane/water interface is significantly higher than that at the air/water interface. The dependencies of the adsorptions in states 1 and 2 on the interfacial pressure for the two interfaces are shown in Fig. 3.

E. Models of Interfacial Layer of Ionized Molecules

The Lucassen-Reynders approach considers the surface as a two-dimensional solution described by Eq.

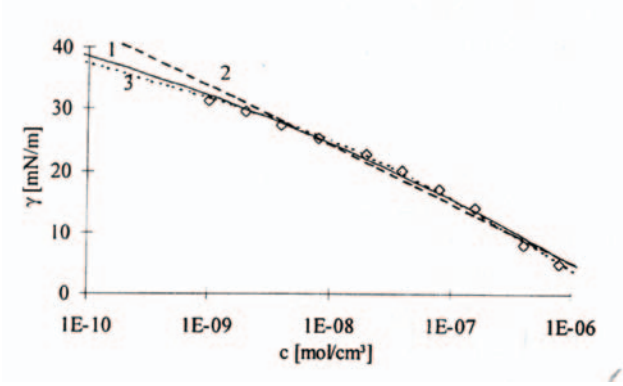

Figure 2 Surface tension isotherm for $C_{10}EO_8$ at water/hexane interface (Γ); theoretical isotherms:

1 - reorientational model ($\omega_{min} = 4.82 \times 10^5$ m^2/mol, $\omega_{max} = 1.09 \times 10^6$ m^2/mol, $\alpha = 6.5$);

2 - Langmuir model ($\omega = 5.8 \times 10^5$ m^2/mol);

3 - Frumkin model ($\omega = 3.8 \times 10^5$ m^2/mol, a = -10.8), according to Ref. 73.

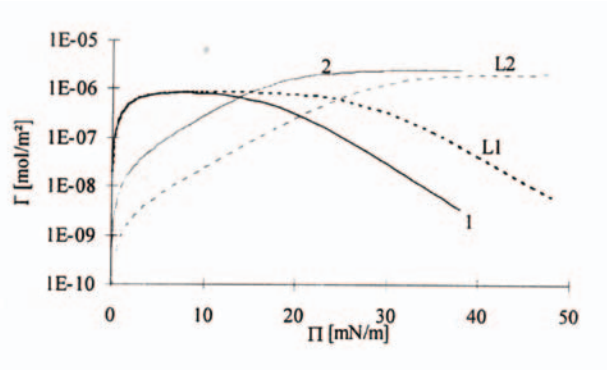

Figure 3 Dependencies of the adsorption in the state 1 (curves 1 and L1) and 2 (curves 2 and L2) on the interfacial pressure for the two-state model at the water/air (curves 1 and 2) and water/hexane (curves L1, L2) interfaces; according to Ref. 73.

(3) and applied to an electroneutral dividing surface which contains only electroneutral combinations of ions (36, 37, 55). Any additional effects of ionization in this approach should be accounted for in the activity coefficients f_i. The surface equation of state is still given by Eq. (12), but the distribution of surfactant between surface and solution bulk is now obtained for electroneutral combinations of ions, say R and X for an anionic surfactant RX (where R^- is the surface-active ion and X^+ is the counterion). This means that for both surface and bulk the average ionic product $(c_R c_X)^{-1/2}$ replaces the molar concentration c_i (36—38, 64). This does not make any difference to the adsorption isotherm if there is only one salt RX, but it does when the solution contains in addition an inorganic electrolyte with the same counterion X^+ as the surfactant, for example, a salt XY. In such a case it is necessary to take into account the average activity of surface-active ions and all counter-ions in the solution.

Using the conditions which require the ionic equilibrium to exist in the bulk $(\mu^\alpha_{RX} = \mu^\alpha_R + \mu^\alpha_X)$ and surface layer $(\mu^s_{RX} = \mu^s_R + \mu^s_X)$ one obtains from Eqs (3) and (4) the relation:

$$\ln \frac{f^s_R f^s_X S^s_R x^s_X}{K f^\alpha_R f^\alpha_X X^\alpha_R X^\alpha_X} = -\frac{(\gamma_o - \gamma)\omega_{RX}}{RT} \quad (45)$$

As the surface layer is electroneutral, and therefore $X^s_R = X^s_S$, then from Eqs (12) and (40) for nonideal (Frumkin) surface layers and nonideal bulk solutions of one ionic surfactant, with or without additional nonsurface active electrolyte, the adsorption isotherm follows

$$b(c_R - c_{X^+})^{1/2} f_\pm = \frac{\Theta}{1-\Theta}\exp(-2a\Theta) \quad (46)$$

where $f_\pm$ is the average activity coefficient in the solution bulk, $\Theta=\Gamma_{RX}/\Gamma_{RX}^{\infty}$, $c_{X+}= c_{RX}$ and C_{XY} and $C_{R+} = C_{RX}$, and due to the surface-layer electroneutral-ity $\Gamma_R=\Gamma_X=\Gamma_{RX}/2$. For ideal surface layers ($a = 0$), Eq. (41) is reduced to (6, 7, 25):

$$\theta = \frac{bf_\pm(c_R c_X)^{1/2}}{1 + bf_\pm(c_R c_X)^{1/2}} \quad (47)$$

corresponding to the following Π(c) relationship:

$$\Pi = RT\Gamma_{RX\infty}\ln\left[bf_\pm(c_{RX}c_{X^-})^{1/2}+1\right] \quad (48)$$

A surface-tension isotherm assuming surface-layer nonideality was presented in Refs (36, 37 and 55). For a nonideal surface layer, the unit value which enters the right-hand side of Eq. (48) should be replaced by the activity coefficient of the solvent in the surface layer. It was shown in Refs 36, 37, 55 and 65 that Eq. (48) describes the surface- and interfacial-tension of anionic and cationic surfactant solutions quite well in a wide range of added inorganic electrolyte.

Let us consider now the case when a solution contains a mixture of two anionic (or cationic) surfactants (e.g., homologues R_1X and R_2X with a common coun-teron X^+) with addition of inorganic electrolyte XY. In such systems the counterion concentration X^+ is given by the sum of concentrations of R_1X, R_2X, and XY. After consideration of the surface-to-bulk distribution of both electroneural combinations of ions, the surface-pressure isotherm for ideal surface layers can be written in the form:

$$\Pi = RT\Gamma_{RX\infty}\ln\left[(b_1 f_{1\pm})^2 c_{R_1X}c_{X^-} + (b_2 f_{2\pm})^2 c_{R_2X}c_{X^-})^{1/2} + 1\right] \quad (49)$$

One can easily see that Eq. 49 is the straightforward consequence of Eqs (3) and (4) for the compositions of ions within the surface layer $x_i^s=(x^s_{Ri}x^s_X)^{1/2}$ and within the solution bulk $x_i^\alpha=(x^\alpha_{Ri}x^\alpha_X)^{1/2}$, provided that the following conditions are satisfied: $x^s_{R1}+X^s_{R2}=x^s_X$ (surface-layer electroneutrality), $x^s_0 + X^s_{R1} + X^S_{R1} + x^s_x = 1$ (the balance between molar portions of all components within the surface layer), and $\Gamma_0 + \Gamma_{R1} + \Gamma_{R2} + \Gamma_X = \Gamma_{RX\infty}$ (dividing surface chosen after Lucassen-Reynders). For nonideal surface layers, the activity coefficient should enter the right-hand side of Eq. (49), instead of unity.

Finally, very large effects on adsorption and surface pressure have been described for mixtures of anionic RX (R^-X^+) and cationic RY (R^+Y^-) surfactants in the solution. In such systems, the adsorption is represented almost completely by the equimolar composition R^-R^+ which has a very high surface activity without any noticeable contribution of R^-X^+ and R^+Y^- over a large range of mixing ratios (74). Thus, one can describe the surface tension of this mixture for ideal surface layers by

$$\Pi = RT\Gamma_{R^-R^+\infty}\ln\left[b_{R^-R^+}f_\pm(c_{RX}c_{RY})^{1/2}+1\right] \quad (50)$$

The adsorption equilibrium constant for the composition R^-R^+ can be approximated by the constants of adsorption equilibrium of R^-X^+ and R^+Y^- in the individual solutions (65):

$$b_{R^-R^+} = (b_{RX}b_{RY})/V \quad (51)$$

where V is the average molar volume of the surfactant.

The advantages of the electroneutral surface-layer model presented above can be regarded also as deficiencies, because this model cannot be used to describe the structure of the surface layer, electric potential of the surface, etc. In addition, no satisfactory treatment of the adsorption of proteins and other polyelectrolytes can be given, if the contribution from DEL into the surface pressure of the adsorption layer is neglected. As no equivalent to the Butler equation exists for the case of ionized layers, the procedure used to derive the equation of state for surface layers should be based on the Gibbs adsorption equation and a model adsorption isotherm equation. The isotherm can also be derived from the theoretical analysis of the expressions for the electrochemical potentials of ions. For the solution of a single ionic surfactant RX, with the addition of inorganic electrolyte XY, starting from Eqs. (19) and (2) one obtains the adsorption isotherm:

$$Kf_R c_R = \frac{\theta}{1-\Theta)}\exp(-2a\Theta)\exp\left(\frac{z_R F\psi}{RT}\right) \quad (52)$$

when f_R is the activity coefficient of the ion R in the solution bulk, Θ. Equation (52) is similar to that derived by Davies (46, 47), and reproduced by other authors (48, 75—80).

For our system, the Gibbs adsorption equation has the form:

$$-d\gamma = \Gamma_R d\mu_R^\alpha + \Gamma_X d\mu_X^\alpha + \Gamma_Y d\mu_Y^\alpha \quad (53)$$

Clearly, the Gibbs dividing surface is used in Eq. (53), where $\Gamma_0 = 0$. The adsorption isotherm [Eq. (52)] involves another definition of the dividing surface (Lucassen-Reynders' surface with $\Gamma_0 \neq 0$), which inevitably introduces some deficiency when a solution of Eqs (52) and (53) is simultaneous used. For a fixed concentration of inorganic

electrolyte in ideal bulk solutions Eq. (53) becomes [see (48)]

$$\frac{\partial\gamma}{\partial c_R} = \Gamma_R \frac{\partial\mu_R^\alpha}{\partial c_R} + \Gamma_X \frac{\partial\mu_X^\alpha}{\partial c_R} \tag{54}$$

The values of adsorption for the ions R^- and X^+ can be calculated from the integration over the total solution volume, i.e.,

$$\Gamma_i = \int_0^\infty [c_i(y) - c_{i0}]\mathrm{d}y \tag{55}$$

where c_{i0} is the concentration of the ions outside the DEL and y is the spatial coordinate. The concentration of ions within the DEL in Eq. (55) can be calculated from the Gouy-Chapman theory. Finally, the relation:

$$\frac{\partial\gamma}{\partial c_R} = RT\frac{\Gamma_R}{c_R} + \frac{2RT}{F}\left(\frac{2\varepsilon RT}{c_R + c_Y}\right)^{1/2} \times \left[\cosh\left(\frac{z_R F\psi^0}{2RT}\right) - 1\right] \tag{56}$$

follows from Eqs (54) and (55) [see (48, 75, 79)], where ψ^0 is the electric potential of the surface, and ε is the dielectric permittivity. Introducing now the value Γ_R [cf. adsorption isotherm, Eq. (52)] into Eq. (56) and performing the integration, one obtains the equation of state for surface layers of ionic surfactant solution (46, 48, 75):

$$\Pi = -RT\Gamma_{RX\infty}[\ln(1-\Theta) + a\Theta^2] + \frac{4RT}{F}(2\varepsilon RTc_\Sigma)^{1/2}[\cosh\varphi - 1] \tag{57}$$

where C_Σ is the total concentration of ions within the solution, and $\varphi = z_i F\psi^0/2RT$. It can be thus seen that the inter-ion interaction results in an additional surface-pressure jump. The electric potential is determined by the surface-charge density:

$$\sinh\varphi = z_R\Gamma_R F/(8\varepsilon RTc_\Sigma)^{1/2} \tag{58}$$

It was taken into account in the models developed in Refs 75, 78 and 80 that some portion of the counter-ions is bound to surface-active ions within the Stern-Helmholtz (S-H) layer, while another (unbound) portion is located within the diffuse region of the DEL. The equivalent relations of Eqs (56)-(58) in this case contain the difference Γ_R —- $\gamma^s X$ instead of Γ_R, where $\Gamma^s x$ is the adsorption of counterions localized within the monolayer. It follows from the model described by Eqs (56)-(58) that if all counterions are localized within the monolayer (within the S-H layer), then $\triangle\Pi = 0$. However, in this case an additional contribution to the surface pressure $\triangle\Pi$ also exists (81). This contribution is negative, and its value is significantly lower than that given by Eq. (57) for the case of a DEL formation. Examples of a successful application of Eqs (52) and (57) to experimental $\Pi(c_{RX})$ curves are given in Refs 48 and 75.

It was shown in Refs 75 and 80 that the portion of adsorbed surface active 1:1 charged ions which becomes bound to the counterions within the S-H layer is approximately 70—90%, that is, the surface layer is almost electroneutral. These results explain why Lucassen-Reynders' theory can be successfully applied to those systems. It can be shown additionally that for compositions of ion the effect produced by the DEL vanishes. For compositions of ions Eq. (55) can be presented in the form:

$$(\Gamma_R\Gamma_X)^{1/2} = \int_0^\infty [(c_R(y)c_X(y))^{1/2} - (c_{R0}c_{X0})^{1/2}]\mathrm{d}y \tag{59}$$

The integration domain on the right-hand side of Eq. (59) can be split into two intervals: 0 to H and H to ∞, respectively, where H is the thickness of the S-H layer. For symmetric 1:1 charged electrolytes the contribution to adsorption caused by the diffuse part of the DEL vanishes, and only the contribution of the S-H layer should be considered. Certainly, for a nonsym-metric electrolyte, say a protein, one cannot exclude the contribution by the DEL in the framework of the composition approach, and in these cases the model of a charged monolayer should be preferred.

F. Adsorption of Proteins

The adsorption isotherm [Eq. 21], and also the equation of stage [Eq. 20] with proper account for Coulomb contributions can be used as a basis to describe adsorption layers of proteins. Here, one has to keep in mind that the subscript i refers to various states of the pro ten molecule at the surface. The problems arising from a nonideality of the surface layer, the dependence of the K_i values on the state of large molecules at the interface, and the inter-ion interactions within the adsorption layer have been properly considered in Refs 44, 82 and 83.

Assuming an enthalpic contribution of the Frumkin type and taking into account the contribution of the DEL one can transform the equation of state for the surface layer [Eq. 57] into

$$\Pi = -\frac{RT}{\omega_\Sigma}\left[\ln(1-\Gamma_\Sigma\omega\Sigma) + a(\Gamma_\Sigma\omega_\Sigma)^2\right] + \frac{4RT}{F}(2\varepsilon RTc_\Sigma)^{1/2}[ch\varphi - 1] \quad (60)$$

where $\Gamma_\Sigma = \Sigma_{l\geq 1}\Gamma_i$ is the total adsorption of the protein in all states. For protein solutions at high ion concentrations the Debye length $\lambda = (\varepsilon RT/F^2c_\Sigma)^{1/2}$ is small. This means that for protein solutions the DEL thickness can be smaller than the adsorption layer thickness. Therefore, the concentration of ions in Eqs (59) and (60) is just their concentration within the adsorption layer. It follows from Eqs (59) and (60) that for large C_Σ the approximation $\varphi \ll 1$ can be used. After simplification one obtains the following equation of state and adsorption isotherm for nonideally charged surface layers of a protein (83):

$$\Pi = -\frac{RT}{\omega_\Sigma}\left[\ln(1-\Gamma_\Sigma\omega_\Sigma) - a_{el}\Gamma_\Sigma^2\omega_\Sigma^2\right] \quad (61)$$

$$b_1 c = \frac{\Gamma_1\omega_\Sigma}{(1-\Gamma_\Sigma\omega_\Sigma)^{\omega_1/\omega_\Sigma}}. \quad (62)$$

where $a_{el} = z^2F/\omega_\Sigma(8\varepsilon RTc_\Sigma)^{1/2}$ and z is the number of unbound unit charges in the protein molecule. The total adsorption amount in these equations can be expressed via the adsorption in state 1:

$$\Gamma_\Sigma = \Gamma_1\sum_{i=1}^{n} i^\alpha \exp\left[-\frac{(i-1)\Pi\omega_1}{RT}\right] \quad (63)$$

Here, a is a constant which determines the variation in surface activity of the protein molecule in the rth state with respect to state 1 characterized by a minimum partial molar area $\omega i = \omega_{min}$; $b_i = b_1 l^\alpha$ can be either an integer or fractional, and the increment is defined by $\triangle i = \triangle\omega/\omega_1$. For $\alpha = 0$ one obtains $b_i = b_1 = a$ constant, while for $\alpha > 0$ the b_i increase with increasing ω_i. The value of the mean partial molar area for all states, and the adsorption in any *i*th state can be expressed by

$$\omega_\Sigma = \omega_1\left(\sum_{i=1}^{n} i^{(\alpha+1)}\exp\left(-\frac{i\Pi\omega_1}{RT}\right)\right)\Big/\left(\sum_{i=1}^{n} i^\alpha\exp\left(-\frac{i\Pi\omega_1}{RT}\right)\right) \quad (64)$$

$$\Gamma_i = \Gamma_\Sigma\left(i^\alpha\exp\left[-\frac{(i-1)\Pi\omega_1}{RT}\right]\right)\Big/\left(\sum_{i=1}^{n} i^\alpha\exp\left[-\frac{(i-1)\Pi\omega_1}{RT}\right]\right) \quad (65)$$

respectively. The main feature of the theoretical model [Eqs (61—65)] is the self-regulation of both the state of the adsorbed molecules and the adsorption-layer thickness by the surface pressure (82—84). The mechanism of self-regulation is inherent in the Butler equation [Eq. (3)], from which all the main equations are derived.

From Eq. (65) one can calculate the portion of adsorbed molecules which exist in the state ω_i. The dependencies of the distribution function Γ_i/Γ_{max} on &#omega969$_i$ and the area per protein molecule in the maximum of the distribution function are shown in Fig. 4. It is seen that the adsorption layer of proteins is characterized by an almost complete denaturation at low surface pressure while at large surface pressures the adsorption layer is composed of molecules in a state with a minimum molecular surface area demand.

A theoretical model for concentrated protein solution was developed in Refs 83 and 85. The calculations performed according to this theory shows good agreement with the experimental data: the adsorption increases significantly while Π remains constant. Theoretical studies of the adsorption behavior for mixtures of the globular protein HSA and nonionic surfactants were performed in (86). An anomalous surface tension increase of the mixtures at low surfactant concentrations was found experimentally and explained theoretically.

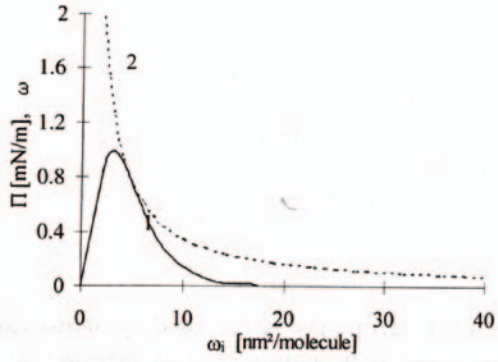

Figure 4 Distribution of protein adsorption in various states Γ_i with respect to the surface area ψ_i covered by the protein molecule in the adsorption layer at Π = 1.2 mN/m (1), and an area per protein molecule in the maximum of the distribution function as a function of surface pressure (2); parameters used; M = 24,000 g/mol, ω_{max} = 40 nm²/molecule, ω_{min} = 2 nm²/molecule, Hω= 1 nm²/molecule, a_{el} = 1 00, and α = *1*, according to Ref. 31.

III. DYNAMIC INTERFACIAL TENSIONS

Numerous methodologies have been developed for the measurement of surface and interfacial tensions as outlined in Refs (87—90). Methods such as the Wilhelmy plate, Du Noüy ring, and capillary-rise techniques are less suitable for liquid/gas interfaces, while a method like the bubble-pressure method is particularly applicable only to a liquid/gas system. Alternative approaches to obtaining liquid-liquid interfacial tension are generally based on drop methods. Overviews of the most frequently used drop methods are given in a monograph, where the pendant-drop (91), drop-volume (92), spinning-drop (93), and drop-pressure methods (94) have been described in detail. This section describes interfacial tension techniques, and gives reference to more details in the literature and experimental examples for a selection of liquid/liquid interfaces.

A. Axisymmetric Drop Shape Analysis (ADSA)

In essence, the shape of a drop is determined by a combination of interfacial tension and gravity effects. Surface forces tend to make drops spherical whereas gravity tends to elongate a pendant drop or flatten a sessile drop. When gravitational and interfacial tension effects are comparable then, in principle, one can determine the interfacial tension from an analysis of the shape of the drop.

The advantages of pendant and sessile drop methods are numerous. In comparison with a method such as the Wilhelmy plate technique, only small amounts of the liquid are required. Drop-shape methods easily facilitate the study of both liquid-vapor and liquid-liquid interfacial tensions (95, 96). Also, the methods have been applied to materials ranging from organic liquids to molten metals (97) and from pure solvents to concentrated solutions. There is no limitation to the magnitude of surface or interfacial tension that can be measured. The methodology works as well at 10^3 mJ/m^2 as at 10^{-3} mJ/m^2 as at 10^{-3} mJ/m^2. Since the profile of the drop may be recorded by photographs or digital image representation, it is possible to study interfacial tensions in dynamic systems, where the properties are time dependent.

In many emulsion or microemulsion systems, the interfacial tension between the oil-rich phase and the aqueous solution is very low (or ultralow), which presents considerable difficulties for many experimental methodologies. The most commonly employed approach for measuring ultralow interfacial tension is the spinning-drop technique (98). However, ADSA has also been used to study these systems and possesses a number of advantages over the spinning-drop technique: higher accuracy, more versatile environmental control (high pressure and temperature), and ability to study time-dependent effects. The problem of extremely low interfacial tensions is discussed in more detail in Sec. IV.

A typical set-up for ADSA is shown in Fig. 5.

In brief, via the CCD camera (1) with objective (2) and the frame grabber (3), an image of the shape of a drop (9) is transferred to a computer, where by using the ADSA software the coordinates of this drop are determined and compared to profiles calculated from the Gauss-Laplace equation of capillarity. The only free parameter in this equation, the interfacial tension Y, is obtained at optimum fitting of the drop-shape coordinates. The dosing system (7) allows one to change the drop volume and hence the drop surface area. This possibility is used in dilational relaxation experiments as outlined in Sec. VI.

B. Drop Volume Tensiometry

In recent years the drop-volume method has gained a reputation as a standard technique (99, 100). Its major advantage is that it can be applied to both liquid/gas and liquid/liquid interfaces. Although its experimental conditions and theoretical description are well established for a

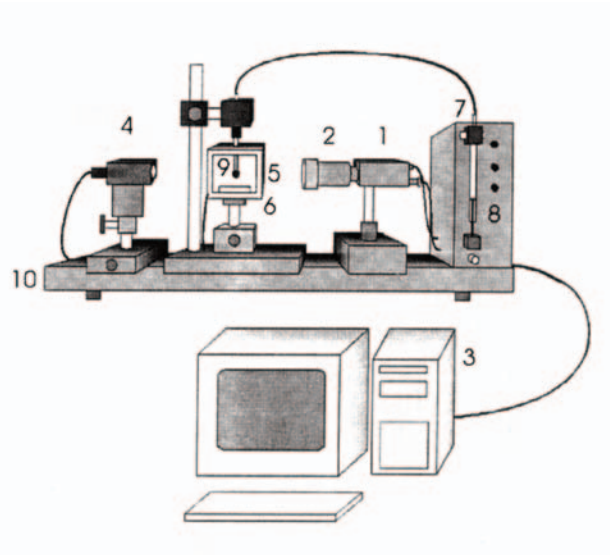

Figure 5 Schematic of a pendant-drop apparatus, 1 - CCD, 2 - objective, 3 - PC with frame grabber, 4 - light, 5 -measuring cell, 6 - holder, 7 - dosing system, 8 - syringe, 9 - capillary with drop, 10 - optical bench.

standard range of drop formation times it has only been very recently that a number of peculiarities have been observed and discussed. Commercial instruments based on this principle are widely used in practice now, such as the automatic drop-volume tensiometer TVT1 from Lauda, Germany.

In Fig. 6 the principle of a drop volume apparatus is shown as an example. The motor controller—-encoder system (3, 4) linked with a syringe (2) provides a constant and accurate dosing rate while the light barrier (7) is used to detect each detaching drop. Thus, the time in between two drop signals multiplied by the dosing rate gives the drop volume. The dosing system is linked via an interface (8) to the serial port of a PC (9).

The PC software controls complete measurement programs, i.e., drop-volume measurements for a liquid can be performed at different dosing rates. After each measurement the surface tension as a function of time is calculated and plotted as a graph. Other types of automated drop-volume instruments are designed in a similar way.

There are three different measurement modes available with the drop-volume method, which can yield different data. However, taking all peculiarities into consideration, the results obtained by the different procedures are the same. The dynamic version of the drop-volume method is the classical procedure for the measurement of interfacial tensions. This mode consists of creating a continuous formation of drops at the tip of a capillary by means of an accurate dosing system. The interfacial tension is calculated from the average volume measured for several subsequent drops.

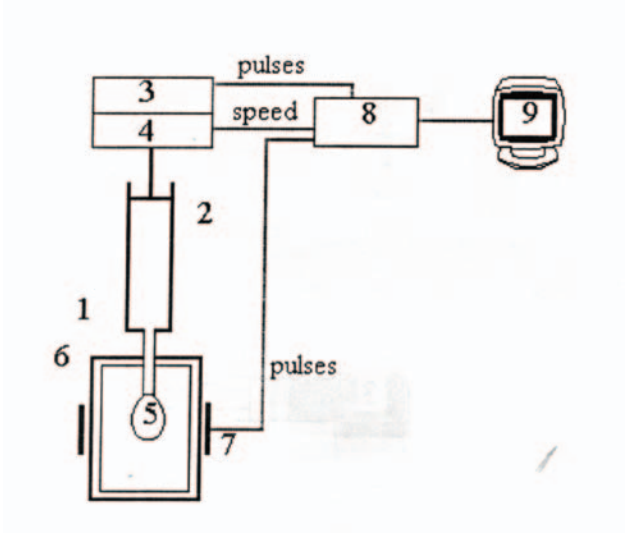

Figure 6 Principle of an automated drop volume instrument, according to the TVT1 of Lauda, Germany; 1 - capillary, 2 - syringe, 3 and 4-motor controller-encoder system, 5 - drop, 6 - temperature control jacket, 7 - light barrier, 8 -electronic interface, 9 - **IBM PC**.

The diffusion-controlled adsorption kinetics for the adsorption process is given by the classical Ward and Tordai equation (101) derived more than half a century ago:

$$\Gamma = 2c_0\left(\frac{Dt}{\pi}\right)^{1/2} - 2\left(\frac{D}{\pi}\right)^{1/2}\int_0^t c(0, t-\xi)\mathrm{d}(\xi^{1/2}) \quad (66)$$

where Γ is the dynamic adsorption, D is the diffusion coefficient, c_0 and c(0, t) are the bulk and subsurface concentrations, respectively, and ξ is a dummy integration variable. The theoretical model to describe the adsorption kinetics of a surfactant at the surface of a continuously growing drop until detachment was first derived by Pierson and Whittaker (102). In analogy with the equation of Ward and Tordai, Eq. (66), the following integral equation was derived (103):

$$\Gamma(t) = 2c_o\sqrt{\frac{3Dt}{7\pi}} - \sqrt{\frac{D}{\pi}}t^{-2/3}\int_0^{3/7t^{7/3}} \frac{c\left(0, \frac{7}{3}\xi^{3/7}\right)}{\left(\frac{3}{7}t^{7/3} - \xi\right)^{1/2}}\mathrm{d}\xi \quad (67)$$

A numerical analysis of this rather complex integral equation showed that the rate of adsorption at the surface of a growing drop with a linear volume increase, as is the case in drop-volume experiments, is about one-third of that at a surface with constant area (92). From experience of adsorption kinetics studies, this approximation for the effective age of one-third of the drop formation time is sufficiently accurate to interpret dynamic interfacial tensions (104—106).

The use of an equation as complex as Eq. (67) requires a lot of numerical calculations so that approximate solutions are very favorable. The first model to describe the adsorption at the surface of a growing drop was derived by Ilkovic in 1938 (107). The boundary conditions were chosen such that the model corresponded to a mercury drop in a polarography experiment. These conditions, however, are not suitable for describing the adsorption of surfactants at a liquid-drop surface. Delahay and coworkers (108, 109) used the theory of Ilkovic and derived an approximation suitable for the description of adsorption kinetics at a growing drop. The relationship was derived only for the initial period of the adsorption process:

$$\Gamma(t) = 2c_o\sqrt{\frac{3Dt}{7\pi}} \quad (68)$$

The relationship already indicates a correlation between the rate of adsorption at a growing drop surface and a stationary interface: the adsorption at a growing drop surface is 3/7 times slower, which is close to 1/3, as discussed before.

The interfacial tension change with time at a growing drop as given by Joos and Van Uffelen (110) has the form:

$$\Delta\gamma(t) = \gamma(t) = \gamma_{eq} = \xi B\sqrt{(2n+1\alpha}\frac{(1+\alpha t)^n - (1-\zeta)}{\sqrt{(1+\alpha t)^{2n+1} - 1}} \quad (69)$$

where γ_{eq} is the equilibrium surface tension, $\xi = (\Gamma(t)/\Gamma_e)^2$, $\zeta = (\Gamma_e - \Gamma(t))/\Gamma(t)$,

$$B = \frac{RT\Gamma_{eq}^2}{c_0}\sqrt{\frac{\pi}{4D}} \equiv \left(\frac{d\gamma(t)}{d(t_{ef}^{-1/2})}\right)_{t\to\infty} \quad (70)$$

R is the gas constant, T is the temperature, and $t_{ef} = t/(2\pi+1)$ is the effective adsorption time. Equation (70) follows immediately from Eq. (69) for $\alpha t \gg 1$. The initial drop has a size less than a hemisphere with the radius equal to the capillary radius r_{cap} (68) so that the drop area can be given by $A_o = 1.5\pi r^2_{cap}$. The area of a drop after the break off of the liquid bridge can be described by

$$A(t) = (4\pi)^{1/3}(3V)^{2/3} + A_0 \approx 4.83V^{2/3} + A_0 \quad (71)$$

where V is the drop volume. The value of *at in* Eq. (69) can be obtained from Eq. (63):

$$\alpha t = \left(\frac{A(t)}{A_0}\right)^{1/n} - 1 \quad (72)$$

Thus, for any time t the value of a can be calculated from Eqs (71) and (72). If we assume a Langmuir-Szyszkowski adsorption isotherm and interfacial tension equations, the parameters ξ and ζ can be expressed via the values of the dynamic and equilibrium interfacial pressures, $\Pi(t)$ and Π_{eq} as

$$\xi = \left[\frac{1 - \exp(-\Pi(t)RT\Gamma_\infty)}{1 - \exp(-\Pi_{eq}/RT\Gamma_\infty)}\right]^2 \quad (73)$$

$$\xi = \frac{\exp(-\Pi(t)/RT\Gamma_\infty) - \exp(-\Pi_{eq}/RT\Gamma_\infty)}{1 - \exp(-\Pi_{eq}/RT\Gamma_\infty} \quad (74)$$

where $\Pi_{eq} = \gamma_o - \gamma_{eq}$, $\Pi(t) = \gamma_0 - \gamma(t)$, γ_o is the interfacial tension of pure liquids, and F^ the limiting adsorption value. The respective approximations are useful in order to interpret quantitatively experimental drop-volume results.

C. Capillary Pressure Tensiometry

The capillary pressure tensiometry (CPT) method has been developed for measuring the interfacial tension of pure liquids and is based on the simple relationship for the capillary pressure:

$$\Delta P = \frac{2\gamma}{R} \quad (75)$$

which is a linear relationship between the capillary pressure $\triangle P$ and the drop curvature (l/R). Thus, from ($\triangle P$, l/R) data during the growth of a drop, γ can be calculated by fitting a Imear relationship. A possible CPT set-up used by Passerone *et al.* (Ill) is shown in Fig. 7.

The cell is made up of two principal bodies connected by the capillary and containing the two liquids. The cell has been fully constructed in PTFE, PCTFE, and glass to improve the cleaning and filling procedures. The capillary is hand made from a Pyrex glass pipe down on a flame, cut perpendicularly to its axis and then carefully fine grounded. The drop is formed on the inner radius a which is typically in the range 0.25-0.35 mm.

The pressure signal is measured with a pressure transducer placed in contact with the liquid forming the drop. The variation in the pressure difference between the two phases is due to variations in the capillary pressure since all other hydrostatic contributions remain constant. The signal is sampled with a typical frequency of 25 Hz by a PC board.

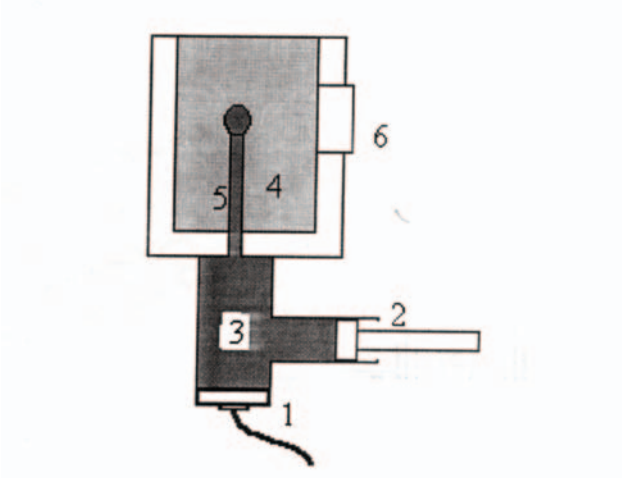

Figure 7 Sketch of capillary pressure tensiometer for pressure derivative and expanded-drop experiments; 1 - pressure transducer, 2 - injection system, 3 - liquid, 1,4 - liquid 2; 5 -capillary with drop, 6 - optical window.

D. Dynamic Interfacial Tensions of Various Systems

When liquid/liquid systems are studied a number of peculiarities have to be considered, the most important of them being the solubility of surfactants in both adjacent liquid phases. There is a striking difference in studies at a liquid surface where only very few surfactants show a comparable phenomenon, the evaporation from the adsorption layer. If the surfactant is soluble in both phases but adsorbs only from one (typically from the aqueous phase) the surfactant is transferred across the interface and desorbs into the oil phase (for details see Sec. V).

In general there are three cases for the adsorption process at a liquid/liquid interface:

1. The surfactant is present in the water phase only.
2. The surfactant is present in the oil phase only.
3. The surfactant is present in both phases with an equilibrium surfactant concentration distribution.

The theoretical solution of models 1 and 2 is a generalized Ward and Tordai equation [Eq. (66)] and was first proposed by Hansen (112):

$$\Gamma(t) = \frac{2}{\sqrt{\pi}}\left[c_{1o}\sqrt{D_1 t} - \left(\sqrt{D_1} + K\sqrt{D_2}\right)\int_0^{\sqrt{t}} c_1(0, t-\xi)\mathrm{d}\sqrt{\xi}\right] \tag{76}$$

Case 3 is described by the same Ward and Tordai equation; however, D has to be replaced by the effective diffusion coefficient defined as $D_{ef} = \sqrt{D_1} + K\sqrt{D_2}$.

As an example to demonstrate the solubility of a surfactant in water and also in the adjacent oil phase, here nonane was used, and measurements with Triton X-45 solutions were performed as follows. At the beginning the container in which the drops of the Triton solution were formed contained only pure nonane. The volume of aqueous solution was 300 ml while that of nonane was 10 ml. The experimental results are shown in Fig. 8.

The drops (500 in each run) are formed such that for each flow rate 10 drops are formed and are averaged, starting with the largest flow rate. During the first four runs the obtained $\gamma(t)$ curves change. From the fifth run on no significant changes are observed so that this state refers to the case of adsorption from both adjacent phases, i.e., the equilibrium distribution of the Triton between nonane and water has been reached. Only experiments for this case allow a quantitative interpretation as the experimental conditions can be given in the theoretical model.

Experimental results for solutions of other Tritons have been reported in Ref 113. From these studies it was concluded that the distribution coefficient for Triton X-45 is significantly higher than for Triton X-405. To visualize the significant differences in dynamic surface tensions measured for the three cases discussed above, the results of experiments with Triton X-45 are reported in Fig. 9. It is obvious that for case 3 the adsorption process is the fastest as adsorption takes place from both adjacent liquid phases.

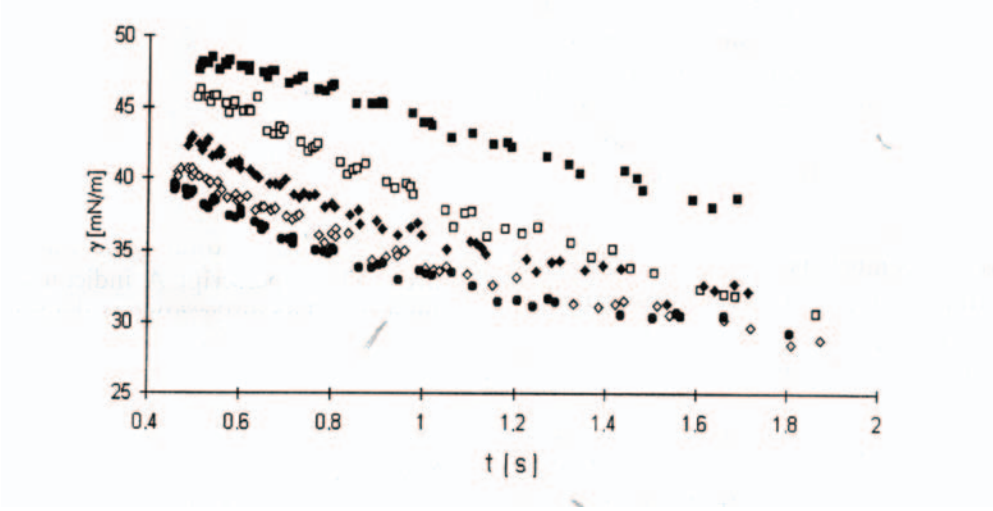

Figure 8 Dynamic interfacial tension of Triton X-45 solutions as a function of $\sqrt{t}$; $c_o = 1.2 \times 10^{-8}$ mol/cm^3, 5 subsequent runs; according to Ref. 113.

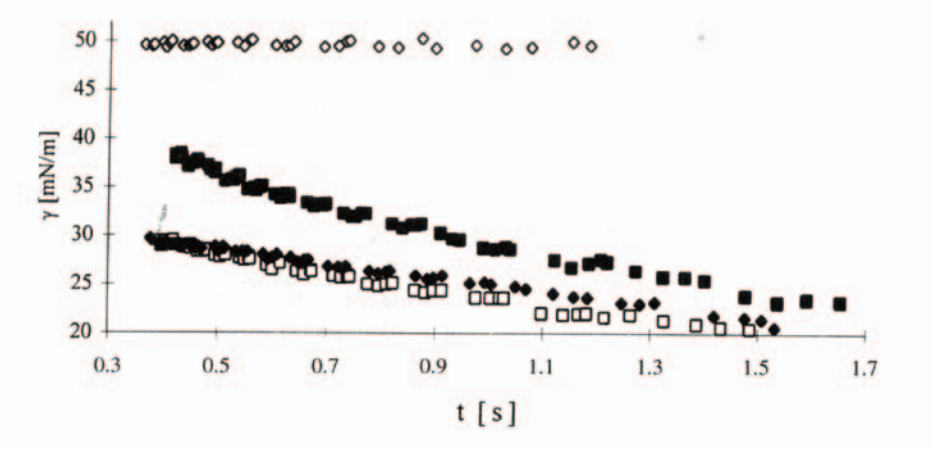

Figure 9 Dynamic interfacial tension of a Triton X-45 solution as a function of $\sqrt{t}$; $c_o = 2.4 \times 10^{-8}$ mol/cm^3 for the three different cases (a) (■) (B), (b) (◆), and (c) (□); and in absence of Triton X-45 (◇), according to Ref. 113.

In the two other cases (1 and 2) the adsorption is much slower due to adsorption from one phase only and moreover due to the loss of adsorbed molecules via desorption into the second liquid phase. It was emphasized in Refs 113-115 that when dealing with liquid/liquid interfaces one always faces the problem that surfactant molecules are soluble in both adjacent liquids and hence adsorption from one phase generally leads to a transfer across the interface. Experiments particularly dedicated to this transfer are discussed in Sec. V.

IV. EXTREMELY LOW INTERFACIAL TENSIONS

The measurement of ultralow interfacial tension has been of continued interest (98, 116-128) both in fundamental research and in industrial applications, particularly in surfactant-based (enhanced) oil recovery - an attempt to recover remaining oil reserves by reducing the oil/water interfacial tension through microemul- sions (117, 120, 125, 129, 130). Typically, oil is recovered in a primary process by the natural energy of a reservoir. However, as much as 40-60% of the original oil can remain trapped in porous rocks due to capillary retention force. A secondary process of water injection with surfactant is therefore used to facilitate further oil displacement.

Microemulsions are homogeneous mixtures of water and oil with thermodynamically stable oil droplets of diameters ranging from 100 to 1000 A. The interfacial tension is typically less than 0.001 mJ/m and, as a comparison, that for an oil/water system without surfactant is about 50 mJ/m. The reduction in the interfacial tension decreases the capillary retention force significantly and enables oil droplets to deform and maneuver easily through pores in the rock medium (117).

In the remainder of this section we discuss the thermodynamic consequences and the experimental possibilities for the measurement of ultralow interfacial tensions.

A. Thermodynamic Consequences

Surface/interfacial tension is a well-defined thermodynamic property (131). It is the energy required to display a unit new interfacial area. From classical Gibbsian thermodynamics, the various modes of energy transfer between the system and the surroundings can be formulated by a relation called a fundamental equation: the fundamental equation (131, 132) of an interface between two bulk phases is given by

$$U^A = U^A(S^A, A, N^A) \tag{77}$$

where U, S, N, and A are, respectively, the internal energy, entropy, total mole number, and interfacial area. The superscript A indicates the property of an interface. The differential of the fundamental equation is given by

$$dU^A = \left[\frac{\partial U^A}{\partial U^A}\right]_{A,N^A} dS^A + \left[\frac{\partial U^A}{\partial A}\right]_{S^A,N^A} dA + \left[\frac{\partial U^A}{\partial N^A}\right]_{S^A,A} dN^A \tag{78}$$

The intensive parameters, i.e., temperature T, interfacial tension γ, and interfacial chemical potential μ^A, are now defined from the fundamental equation as

$$T = \left[\frac{\partial U^A}{\partial S^A}\right]_{A,N^A} \tag{79}$$

$$\gamma = \left[\frac{\partial U^A}{\partial A}\right]_{S^A,N^A} \tag{80}$$

and

$$\mu^A = \left[\frac{\partial U^A}{\partial N^A}\right]_{S^A,A} \tag{81}$$

Equation (78) can be written in the differential form of a property relation as

$$dU^A = TdS^A + \gamma dA + \mu^A dN^A \tag{82}$$

where the terms TdS^A, γdA, and $\mu^A dN^A$ correspond respectively to the heat transfer, mechanical work, and chemical work in the system. Here, we look at the mechanical work done (dW^A) due to interfacial tension:

$$dW^A = \gamma dA = \left[\frac{\partial U^A}{\partial A}\right]_{S^A,N^A} dA \tag{83}$$

Obviously lowering the value of γ can decrease significantly the mechanical work required for a given dA. It would be of interest to reduce γ as much as possible if the aim is to minimize the surface work. The question then arises as to how low the interfacial tension can get.

Since U^A is the internal energy of an interface, an interface must exist between two bulk phases, for a finite value of interfacial tension. The consequence of Eq. (82) is that a stable interface requires a positive value of interfacial tension, implying that energy must be increased if the interfacial area is to be increased. If this were not the case then, even in the absence of an external agent to apply energy, the interfacial area would keep increasing as this would lead to a decrease in energy - a decrease in energy is always thermodynamically favorable. This would continue until complete molecular dissolution was reached. However, we know that this cannot be true for a stable interface. The implication is that, for a thermodynamically stable system, an experimental value of (ultralow) interfacial tension is always finite and larger than zero.

B. Experimental Possibilities

Numerous techniques have been developed to measure the interfacial tensions of a liquid/fluid interface (87, 89). Among the commonly used ones, drop-shape methods are very promising for ultralow interfacial tensions: they are based on the idea that the shape of a sessile or pendant drop is determined by the balance betwen surface/interfacial tension and an external force, such as gravity. Two such techniques are axi- symmetric drop shape analysis (ADSA) and the spinning-drop technique (SDT). ADSA (133-135) determines the liquid/fluid interfacial tensions from the shape of axisymmetric menisci due to gravitational force. SDT (136-139) employs a similar strategy: instead of gravity, a known centrifugal force is applied for drop deformation. Figure 10 displays a schematic of these effects on drop shape.

Consider a liquid drop immersed in a surrounding liquid medium that is enclosed in a cylindrical glass tube rotating about its horizontal axis (Fig. 10). At zero angular velocity ϖ, the droplet behaves as an inverted sessile drop inside the tube. As ϖ increases, the drop starts to rotate about the axis of rotation. The higher the ϖ, the more deformed the droplet is. At sufficiently high ϖ the shape of the droplet can be approximated by a cylinder with rounded ends. Vonnegut

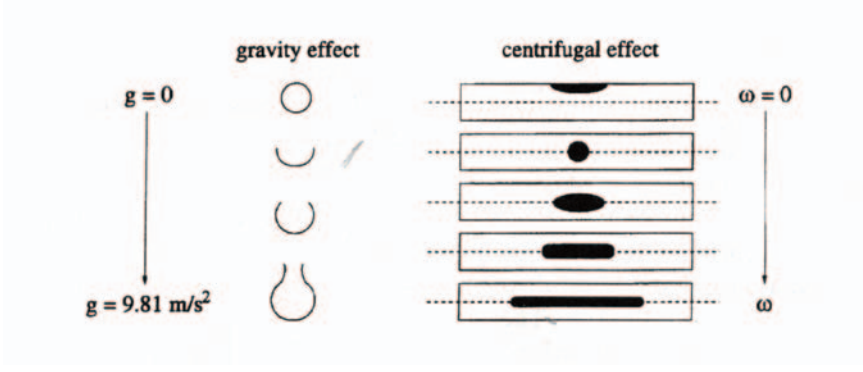

Figure 10 A schematic of the effects of gravity and centrifugal forces on drop shape.

(136) has shown that, in the case of a cylindrical droplet, the interfacial tension can be calculated from

$$\gamma = \frac{\Delta\rho\varpi^2 r^3}{4} \qquad (84)$$

where $\triangle$p and r are, respectively, the density difference between the liquid/fluid interface and the radius of the deformed cylindrical droplet at high ϖ. Thus, knowing $\triangle$p, r, and ϖ allows the determination of interfacial tension and this is the basic principle of the spinning-drop technique. Equation (84) is often referred to as the Vonnegut equation. A detailed description of ADSA for determining the liquid/fluid interfacial tensions has been described in Sec. III.

C. Axisymmetric Drop Shape Analysis and Spinning Drop Technique

Both ADSA and SDT have advantages and disadvantages. Here, we summarize them in the following two categories: range of applicability and experimental difficulty.

1. Range of Applicability

The range of applicability of ADSA is broad. It has been applied to a variety of studies on the time dependence of liquid/fluid interfacial tensions in the presence of surfactants (140-142, 196), film balance experiments with insoluble (143-145) and soluble films (146, 147), polymer melt experiments (148, 149), pressure (150) and temperature dependence (151) of interfacial tensions, drop size dependence of contact angles and line tension (152, 153), and static (154) and dynamic (155, 156) contact-angle measurements. SDT, on the other hand, is solely restricted to surface/interfacial tension measurements (136,137). It has been applied to polymer melt experiments (157-161) and to situations where the interfacial tension is as low as 10^{-1} mJ/ m^2 (116, 118-120, 125-127). In contrast to the pendant/sessile drop used by ADSA, the "external" centrifugal force can be varied continuously by changing the angular velocity ω in order to minimize experimental error and to ensure that the system is sufficiently close to gyrostatic equilibrium. A disadvantage of SDT is the fact that only the equilibrium interfacial tension can be obtained.

2. Experimental Difficulty

As compared to the pendant-drop arrangement in ADSA, the set-up of SDT is more complex. For example, it can be a very frustrating task to fill the liquid (or bubble) in the matrix inside the cylindrical tube so that it is free of air bubbles and so that escape of volatile components during operation is prevented. This can be a serious problem when dealing with highly viscous polymers (159-162). As the cylindrical drop radius r in Eq. (79) is raised to the third power, reliable experimental results require careful radius calibration. One experimental difficulty of ADSA is that the pendant-drop arrangement may not be appropriate for measurements of ultralow interfacial tension, as the interfacial tension might not withstand the weight of the droplet, i.e., the gravitational effect overpowers that of the interfacial tension. This can be overcome by an inverted sessile-drop arrangement used by Kwok *et al.* (98). Experimental examples are given in the next section.

D. Experimental Examples

In several instance (98, 127), ADSA ultralow inter-facial-tension measurements are available for the same systems for which SDT has been performed. Ultralow interfacial tension measurements by ADSA were by means of an inverted sessile-drop set-up of Aerosol OT (AOT) in NaCl/water solution in an n-heptane matrix solution.

1. Aerosol OT (AOT) in Aqueous Solution of NaCl Water and n-Heptane

Figure 11 displays the interfacial-tension results from ADSA, for 0.415 mM AOT in aqueous solution of 0.0513 M NaCl/water and n-heptane. The interfacial tension decreases from about 0.05 mJ/m^2 to an equilibrium value of 0.01 mJ/m^2 in 12 min. A different result is given in Fig. 12 for 0.420 mM AOT.

It can be seen that the interfacial tension reaches an equilibrium value in a much shorter time, decreasing from about 0.026 to 0.006 mJ/m to 0.006 mJ/m^2 in 2 min. Increasing the AOT concentration decreases both the interfacial tension value and the time required to reach equilibrium. The results given in Figs 11 and 12 agree well with those published by Aveyard *et al.* (127) using SDT. The interfacial-tension values reported by Aveyard *et al.,* estimated from their graph, are $\approx$ 0.01 and $\approx$ 0.003 ml/m^2, respectively, from 0.415 and 0.420 mM AOT. The choice of the method depends on the specific application and is largely a matter of convenience, equipment available, and the issues discussed in Sec. IV.B.

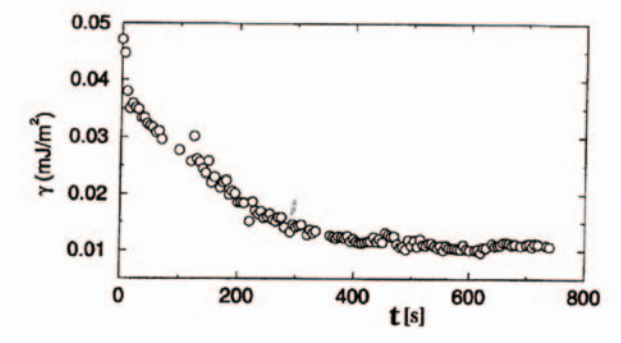

Figure 11 Interfacial tension vs. time for 0.415 mM AOT in solution of 0.0513 M NaCl/water and n-heptane.

V. SURFACTANT TRANSFER ACROSS THE INTERFACE

The study and description of adsorption processes in liquid-liquid systems deserves some specific consideration because, in most cases, the behavior of these systems is more complex in comparison with that of liquid-air systems.

The principal characteristic of such systems is the solubility of the surfactant in both phases, which is practically never negligible. This implies that the theoretical modeling of the adsorption dynamics needs to consider the transfer of surfactant across the interface during the process and that any experimental study needs careful definition of the initial partition state. Moreover, in most cases the relative volumes of the bulk phases may become an important parameter influencing the adsorption dynamics (114, 115).

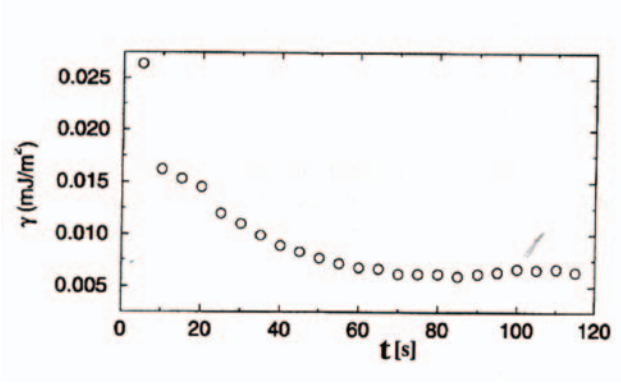

Figure 12 Interfacial tension vs. time for 0.420 mM AOT in solution of 0.0513 M NaCl/water and n-heptane.

For these reasons knowledge of the partition properties of the systems is a mandatory requirement for characterization of the dynamic behavior of such a system and for an adequate evaluation of the equilibrium adsorption properties.

These properties can be characterized by the distribution coefficient K_i of each adsorbing component *i.* This parameter can be denned as the ratio between the equilibrium concentrations of the surfactant in the two phases, and can be expressed in terms of basic thermodynamic parameters [cf. Eq. (10)]. In fact, considering a solute in two liquids α and β, under the hypothesis of dilute and ideal solutions, the ratio between the equilibrium concentrations c_α and β can be written as (163):

$$K = \frac{c_\alpha}{c_\beta} = \frac{v_\alpha}{v_\beta} \exp\left(-\frac{\mu_\alpha^0 - \mu_\beta^0}{RT}\right) \tag{85}$$

where K is the distribution coefficient for a one-surfactant system, υ_α and υ_β are the molar volumes, $\mu_\alpha{}^0$ and $\mu_\beta{}^0$ are the standard chemical potentials, R is the gas constant, and T is the absolute temperature.

Surfactant solutions are typically very diluted, meaning that the hypothesis of the ideal solution is usually satisfied so that, at least at submicellar concentration, K is independent of the concentration, and depends only on the temperature.

Although describing properties of the bulk liquids, in surfactant solutions the value of K strongly influences the adsorption dynamics at the liquid-liquid interface. For example, in adsorption and diffusion processes in water-oil systems, knowledge of the K value is fundamental in interpreting the experimental data (114, 115, 164, 169).

Moreover, the transfer of surfactant between the liquid phases can also have an impact on the interface stability. In fact it has been shown (170, 171) that, depending on the ratio between the diffusion coefficients in the two phases, the transfer of matter across the interface can give rise to interfacial instabilities.

A. Measurement of the Partition Coefficient

The straightforward way for evaluating K is the measurement of the bulk concentration after equilibration of the immiscible phases.

However, when the partition coefficients of mono-meric surfactants have to be evaluated, the utilization of common

analytical techniques is very limited—-and often impossible—-due to the very low values of the concentrations.

The specific surface-active property of the surfactant can be exploited to set up an indirect method for the evaluation of the concentration of a surfactant solution, based on the measurement of the surface tension. In fact, by using the γ—-*c* isotherm as a calibration curve, *c* can be evaluated by the equilibrium.

Thus, for a surfactant in an immiscible couple—-for example water and oil—-*K* can be measured according to the following methodology (172):

1. First, a *c*—-γ isotherm is obtained by measuring the equilibrium surface tension of solutions, prepared with oil-saturated water, as a function of the surfactant concentration.
2. A volume V_w of aqueous solution with initial concentration c_{0w} is brought into contact with a volume V_0 of pure oil for a time long enough (days) to warrant achievement of the partition equilibrium.
3. The equilibrium surface tension γ_{eq} of the aqueous phase is then measured and its concentration c_w is evaluated by using the γ—c isotherm as a calibration curve.
4. Finally, from the surfactant mass balance, *K* can be calculated as

$$K = \frac{V_w}{V_o}\left(\frac{c_{w0}}{c_w} - 1\right) \tag{86}$$

The error in this measurement is

$$\Delta K = \frac{V_w}{V_o}\left[\frac{(c_{w0} - c_w)}{c_w}\left(\frac{\Delta V_w}{V_w} + \frac{\Delta V_o}{V_o}\right) + \frac{c_{w0}}{c_w}\left(\frac{\Delta c_{w0}}{c_{w0}} + \frac{\Delta c_w}{c_w}\right)\right] \tag{87}$$

where $\triangle V_W$, $\triangle V_o$, and $\triangle c_{w0}$ are the errors in V_w, V_0, and c_{w0}, respectively, and the error in c_w is given by

$$\Delta c_w = \left|\frac{\partial c_w}{\partial \gamma_{eq}}\right| \Delta \gamma_{eq} \tag{88}$$

which can be calculated by the best fit $\gamma_{eq\text{-}cw}$ isotherm.

The meaning and the values of the various terms in Eqs (87) and (88) have been widely discussed in Ref. 172. One of the points resulting from this discussion is that, in order to minimize this error, some experimental parameters, such as the liquid volumes and the concentration range, must be suitably chosen.

The values of *K* for some surfactants in a water-hexane system are reported in Table 1. As shown, it is easy to evaluate *K* with an error of the order of 10%. The surfactants listed in Table 1 belong to different classes of nonionic surfactants, and the values of *K* show that the patitioning is never negligible.

To verify achievement of the partition equilibrium, the ratio between the surfactant concentration in the two phases can be monitored as a function of the time in which the liquids are brought into contact. As shown in Fig. 13, after some time this value reaches a plateau, indicating achievement of the partition equilibrium.

Table 1 Measured Partition Coefficient *K* in Water/Hexane System; All Data at 20°C

Surfactant	K	Range of c_w (mol/cm^3)
C_8DMPO	0.14 ± 0.02	2e − 7 ÷ 4e − 6
C_{10}DMPO	1.30 ± 0.05	6 − e8 ÷ 2e − 6
C_{12}DMPO	7.7 ± 0.3	4e − 8 ÷ 2e − 7
C_{13}DMPO	34.7 ± 0.6	1e − 8 ÷ 5e − 8
Triton X-405	0.098 ± 0.004	2e − 8 ÷ 2e − 7
Triton X-100	0.82 ± 0.03	2e − 8
$C_{10}E_5$	1.65 ± 0.04	5e − 9 ÷ 4e − 8
$C_{10}E_8$	0.49 ± 0.05(15°C)	–
	0.85 ± 0.08	4e − 8 ÷ 1e − 7
	1.5 ± 0.1 (25°C)	–
	1.7 ± 0.2 (30°C)	–
	2.3 ± 0.3 (35°C)	–
$C_{16}E_{20}$	0.14 ± 0.02	1e − 9 ÷ 2e − 9

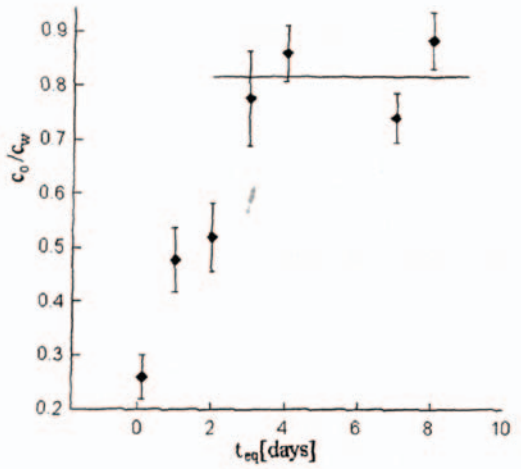

Figure 13 Dependence of the ratio between the concentration in hexane and in water on the time of contact of the two phases.

According to Eq. (85) the measurement of K as a function of the temperature allows the difference of chemical potential of the surfactant in the two phases and of the transfer enthalpy to be evaluated.

In fact (163), by the reasonable assumption that the exponential term is much more sensitive to the temperature change than to the molar volumes, Eq. (85) leads to

$$\frac{\partial \ln K}{\partial T} = -\frac{1}{R}\frac{\partial}{\partial T}\left(\frac{\mu_{i\alpha}^0 - \mu_{i\beta}^0}{T}\right) \tag{89}$$

By basic thermodynamics arguments the chemical potential and the molar enthalpy are linked by

$$\frac{\partial}{\partial T}\frac{\mu_i}{T} = -\frac{\overline{H}_1}{T^2} \tag{90}$$

Thus, Eq. (88) can be written:

$$\frac{\partial \ln K}{\partial (1/T)} = -\frac{\Delta \overline{H}_i^0}{R} \tag{91}$$

where $\overline{H}_i^0 = \overline{H}_{i\alpha}^0 - \overline{H}_{i\beta}^0$ is the molar standard enthalpy of transfer.

Equation (91) allows the evaluation of the molar standard enthalpy of transfer. For example (173), for $C_{10}E_8$ in water-hexane (Fig. 14), a linear relationship exists between In(K) data and $1/T$; thus, it is possible to calculate $\Delta \overline{H}_i^0$ from the slope of the best-fit straight line, which in this case gives $\Delta \overline{H}_i^0 = 5.7\ 10^4$ J/mol.

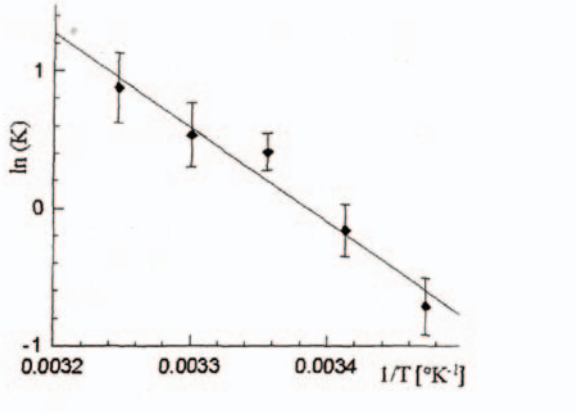

Figure 14 Logarithm of the partition coefficients of $C_{10}E_8$ in water/hexane vs. the inverse of temperature. The slope of the straight line represents the standard enthalpy of transfer.

B. Effect of Partitioning on Dynamic Adsorption Process

As far as the adsorption dynamics at liquid—liquid interfaces is considered, the partitioning of the surfactants between the two phases has an important role.

In spite of the extensive knowledge of adsorption dynamics at liquid-vapour surfaces, only a few works have been devoted to the study of dynamic and equilibrium propeties of adsorption at liquid-liquid interfaces so that, today, there is an evident lack of data for these systems, and the theoretical approaches developed for liquid-vapour surfaces need to be specified for liquid-liquid interfaces.

For most surfactants it is possible to assume a local equilibrium between the interface and the layer just in contact with it, often called the sublayer. In this case, adsorption is controlled by diffusion since the adsorption Γ varies according to the net diffusion flux. Thus, by considering a plane interface betwen two semi-infinites liquid phases 1 and 2, characterized respectively by the diffusion coefficients D_1 and D_2, it is

$$\frac{d\Gamma}{dt} = -D_1 \left.\frac{\partial c}{\partial x}\right|_{x=0} + D_2 \left.\frac{\partial c}{\partial x}\right|_{x=0^-} \tag{92}$$

where the x unit vector is taken as perpendicular to the interface and directed towards the liquid 1, and the interface is located in $x = 0$. Owing to the local equilibrium condition, for $t > 0$, the sublayer concentrations $c_{10}(t) = c(0^+, t)$ and $c_{20}(t) = c(0\ t)$ are always at partition equilibrium:

$$c_{20}(t) = K c_{10}(t) \tag{93}$$

The classical problem of adsorption dynamics is the prediction of the evolution of $\Gamma(t)$ for a "freshly" formed interface—i.e., with $\Gamma(0) = 0$—between two liquids with initial surfactant concentrations:

$$c(x, 0) = c_1^\infty \text{ for } x > 0$$
$$c(x, 0) = c_2^\infty \text{ for } x < 0 \qquad (94)$$

By solving Eq. (92) with the boundary condition (Eq. (93)] and initial conditions [Eq. (94)], one obtains:

$$\Gamma(t) = 2\left[c_1^\infty\sqrt{\frac{D_1 t}{\pi}} + c_2^\infty\sqrt{\frac{D_2 t}{\pi}}\right] - \frac{1}{\sqrt{\pi}}\int_0^t\left[\sqrt{D_1} + K\sqrt{D_2}\right]\frac{c_{01}(\chi)}{\sqrt{t-\chi}}d\chi \qquad (95)$$

which is a generalization of the Ward-Tordai equation (174, 175) derived for a monophasic system.

Owing to the local equilibrium condition, the equilibrium isotherm can be used at any t to describe the relationship beween Γ and c_{01}, in order to solve Eq. (95).

This straightforward generalization of the mono-phasic approach to the study of liquid-liquid adsorption dynamics is only possible by assuming local equilibrium conditions. In fact, only in that case are we allowed to use the relationship [Eq. (92)] between the two sublayer concentrations. At present, no theories exist for the description of liquid-liquid adsorption dynamics when the local equilibrium condition is not satisfied. For liquid-vapor systems, some models, often called mixed adsorption dynamics, are available to describe this situation. However, the specification of these models for liquid-liquid systems poses severe problems. Luckily, the local equilibrium condition —and then the diffusion-controlled approach - is suitable for describing adsorption dynamics for most non-ionic surfactants. A description of the adsorption dynamics for liquid—liquid systems, considering the presence of energetic adsorption barriers at the two sides of the interface, has been given in Ref. 165.

The models of adsorption from semi-infinite bulk phases predict in any case a monotonic relaxation of the interfacial tension even in the presence of transfer of matter into the second phase. In particular, if the initial bulk concentrations are at partition equilibrium the adsorption asymptotically reaches its equilibrium value, otherwise the system achieves a stationary state.

For some applications, however, the assumption of semi-infinite bulks is not realistic. This can be, for example, the case of the bubbling of drops of surfactant solution in a liquid, which requires one to study the adsorption dynamics in finite volumes.

The effect on adsorption dynamics of the transfer across the interface is particularly remarkable when systems of limited volume are considered which are initially far from the partitioning equilibrium. A first theoretical approach to this problem has been given in Ref. 169, where stirred bulks are considered.

More recently (114, 115, 176), the adsorption dynamics of C_{13} dimethyl phosphine oxide (C_{13}DMPO), C_{12}DMPO, and C_{10}DMPO at freshly formed water-hexane interfaces has been investigated as a function of the initial partition conditions and of the relative volumes between the two liquids. As shown in Table 1 some of these surfactants have large values for the partition coefficients, which enhances the influence of the transfer.

At first, a drop of surfactant aqueous solution was formed in a cell filled with pure hexane, such that a ratio $Q + 10^{-3}$ existed between the volume of the drop (supplying phase) and that of the hexane (recipient phase). The dynamic interfacial tension $\gamma(t)$ was monitored by a computer-enhanced pendant-drop technique. The evolution of γ for some initial concentrations of aqueous solution is shown in Fig. 15A—C for C_{13}DMPO, C_{12}DMPO, and C_{10}DMPO, respectively.

Owing to the limited amount of surfactant in the drop, the interfacial tension passes through a minimum when the net number of molecules adsorbing at the interface from the inner phase equates with the net number of molecules desorbing in the external phase. It is important to notice that, in these dynamic conditions, the interfacial tension can reach values which are well below the equilibrium values, which can be relevant for some technological processes such as the control of droplet size or emulsification.

Similar experiments have been run by forming a drop of hexane inside the cell filled with the surfactant aqueous solution, in order to obtain a volume ratio $Q = 1000$ between the supplying and recipient phases. The measured dynamic interfacial tensions for this kind of experiment are shown in Fig 16A—C for C_{13}DMPO, C_{12}DMPO, and C_{10}DMPO, respectively. In this configuration the interfacial tension minima disappear since the internal phase is rapidly saturated and a monotonic relaxation behavior is observed.

A diffusion-controlled model can be applied to describe these experiments, in which a spherical drop of radius R_1 is considered embedded in a spherical shell of radius R_2 representing the external phase. The volume ratio Q can be adjusted by varying the R_1/R_2 ratio.

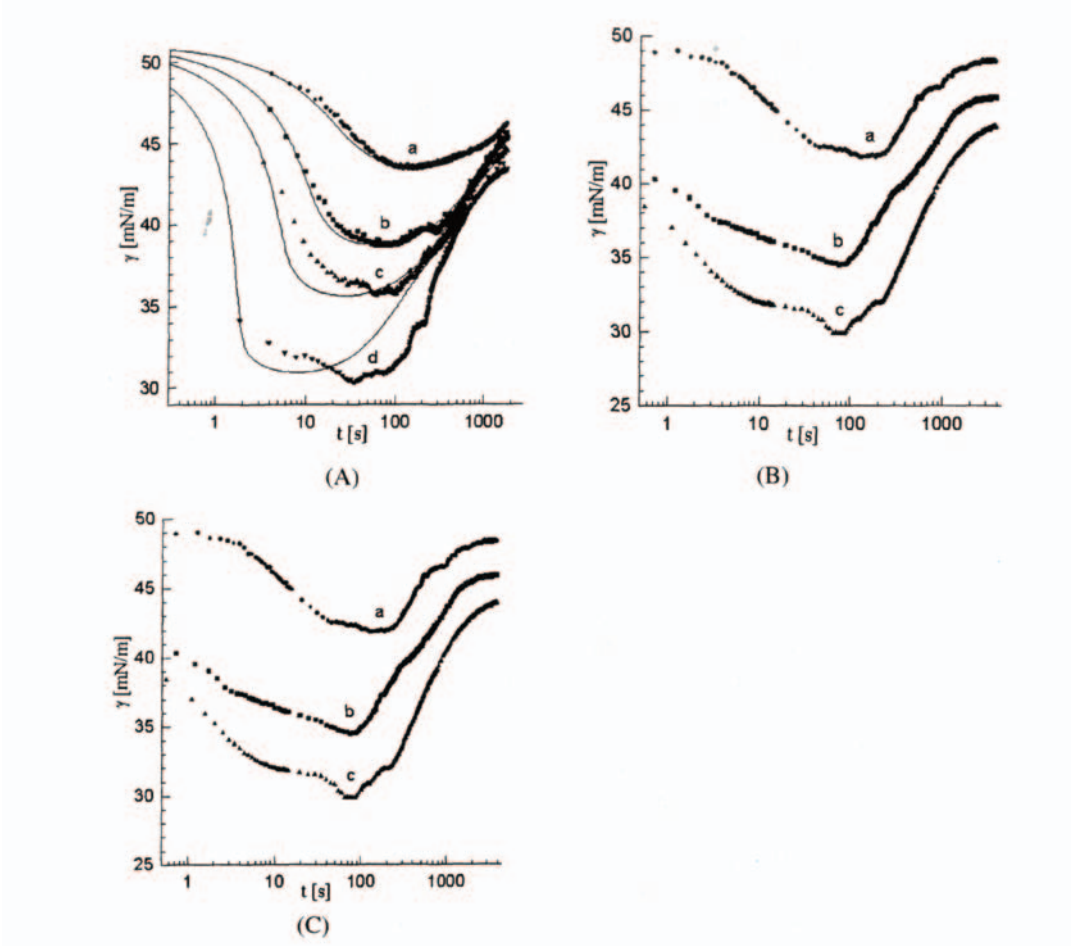

Figure 15 Dynamic interfacial tension for the adsorption with transfer of surfactant of C_nDMPO at a water/hexane interface. The phase supplying the surfactant is a drop of aqueous solution formed in hexane initially free from surfactant. The water/oil volume ratio is Q = 10^{-3}. The solid curves are calculated from the model. The given concentrations are the initial values in water; (A) C_{13}DMPO: $C_0 = 1 \times 10^{-8}$ (a), 2×10^{-8} (b), 3×10^{-8} (c), 5×10^{-8} mol/cm^3 (d); (B) C_{12}DMPO: $C_0 = 2 \times 10^{-8}$ (a), 5×10^{-8} (b), 8×10^{-8} mol/cm^3 (c); (C) C_{10}DMPO: $C_0 = 2 \times 10^{-7}$ (a), 3×10^{-7} (b), 1×10^{-6} mol/cm^3 (c).

The model is characterized by the following set of equations:

$$\frac{d\Gamma}{dt} = -D_1 \left.\frac{\partial c}{\partial r}\right|_{r=R_1^-} + D_2 \left.\frac{\partial c}{\partial r}\right|_{r=R_1^+} \tag{91}$$

where $c = c(r, t)$ is the surfactant concentration at time t and at distance r from the origin of the coordinates. This equation is equivalent to Eq. (92) and has to be used as a boundary condition at the interface $r = R_1$ for the diffusion problem in the bulk phases described by the Fick equations:

$$\begin{aligned} \frac{\partial c}{\partial t} &= D_1\left(\frac{\partial^2 c}{\partial r^2} + \frac{2}{r}\frac{\partial c}{\partial r}\right) \text{ for } 0 < r < R_1 \\ \frac{\partial c}{\partial t} &= D_2\left(\frac{\partial^2 c}{\partial r^2} + \frac{2}{r}\frac{\partial c}{\partial r}\right) \text{ for } R_1 < r < R_2 \end{aligned} \tag{96}$$

The initial conditions are:

$$\begin{aligned} c(r, 0) &= c_0 \text{ for } 0 < r < R_1 \\ c(r, 0) &= 0 \text{ for } R_1 < r < R_2 \end{aligned} \tag{97}$$

or exactly the opposite, when the surfactant is initially contained in the external phase. Another boundary condition is

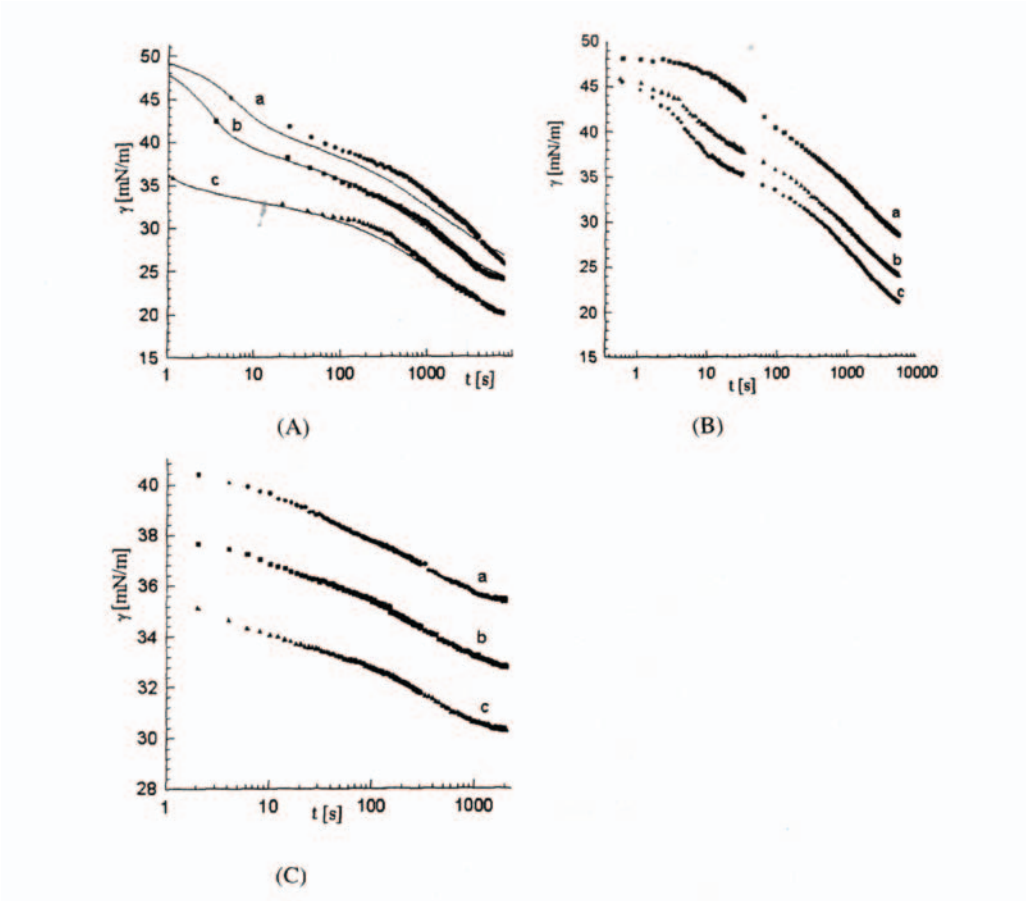

Figure 16 Dynamic surface tension during the adsorption with transfer of surfactant of C_nDMPO at a water/hexane interface. A drop of hexane initially free from surfactant is formed in the aqueous solution containing the surfactant. The water/oil volume ratio is $Q = 1000$. The solid curves are calculated from the model. The given concentrations are the initial values in water; (A) C_{13}DMPO: $C_0 = 1.5 \times 10^{-8}$ (a), 2.3×10^{-8} (b), 5.3×10^{-8} mol/cm^3 (c); (B) C_{12}DMPO: $C_0 = 1\ 10^{-8}$ (a) 2×10^{-8} (b), 3×10^{-8} mol/cm3 (c), (C) C_{10}DMPO: $C_0 = 3 \times 10^{-8}$ (a), 5×10^{-8} (b), 8×10^{-8} mol/cm^3 (c).

needed to express the closure of the system:

$$\left.\frac{\partial c}{\partial r}\right|_{r=R_2^-} = 0 \qquad (98)$$

Finally, since the interface is considered at local equilibrium with both the adjacent phases, the two boundary concentrations are assumed to be at partition equilibrium:

$$c(R_1^-, t) = k_p c(R_1^+, t)) \qquad (99)$$

and the equilibrium relation holds between the boundary concentration $c(R_1^-, t)$ and the adsorption Γ:

$$\Gamma = \Gamma(c(R_1^-, t)) \qquad (100)$$

This set of equations can be solved according to the finite difference scheme given in Ref. 177, by using the values of the isotherm parameters obtained by equilibrium measurements and the values of K reported in Table 1. The model describes the general features observed for the systems and predicts the appearance of the minima in $y(t)$ when $Q < 1$.

Moreover, as shown in Figs 15a and 16a, the calculated $y(t)$ agrees well with the measured dynamic inter-facial tension, in paticular at the lower concentrations. For larger concentrations, the deviation increases. It is possible that, at these concentrations, the adoption of a spherical symmetry for the model is no longer adequate, as the drop deforma-

tion is no longer negligible owing to the low values reached by y.

VI. INTERRACIAL DILATIONAL RHEOLOGY

Dilational rheological experiments are based on area changes by keeping the shape of the interface constant. Models for the exchange of matter, which sets in after a compression or expansion of the interface, are generally applicable to both harmonic and transient types of relaxations (178). Stress-relaxation experiments may yield results different from those obtained from measurements on small disturbances as the composition of the surface layer can vary (179). Overviews on experimental and theoretical aspects of dilational rheology were given recently in Refs 180—182.

The damping of capillary waves at interfaces is the classic version of all dilational relaxation methods at interfaces. The response of the system is measured in terms of a relative damping of the propagated wave (183, 184). Recent work was focused on modifications of the theoretical background for this technique as well as on experimental improvements (185—187). One of the more recently developed methods to investigate surface relaxations of adsorption layers due to harmonic disturbances is the oscillating-bubble method. The technique involves the generation of radial oscillations of a gas. The theory of pulsating bubbles in surfactant solutions has been further developed (188, 189). Another group of measurements suitable for studying the dilational rheology of interfacial layers are stress-relaxation experiments performed by Joos and cowor-kers (190—192). All these methods are applicable for studies at liquid/gas interfaces but less suitable for liquid/liquid interfaces. For example, the capillary wave technique can be in principle applied to a water/oil interface; however, the experiment is connected with a number of problems, mainly the huge demand in highly purified oil (193, 194). Also, the overflowing cylinder, one of the effective stress-relaxation experiments for the water/air surface (195), has been successfully used for measurements at the water/oil interface, but again the large amount of solvent needed for an experiment restricts the application of this method.

A. Pendant-drop Experiments

This technique has been used for relation experiments in the transient as well as harmonic perturbation mode (196-199) and is suitable also for liquid/liquid interfaces (200, 201). The principle set-up of this method has been already described in detail above as a method to investigate the dynamics of adsorption. The computer-controlled motor-driven dosing system can, however, be used to change the volume, and hence its interfacial area in different ways. The most easy area disturbances are step-wise increases or decreases, but also trapezoidal or zig-zag area change can be easily performed. Moreover, the technique allows even harmonic changes of the interfacial area; however, owing to the finite time needed for obtaining the video images only low frequencies can be handled (199, 202).

Due to the changes in the interfacial area a compression or expansion of the adsorption layers is generated which induces a relaxation process in order to re-establish its equilibrium state. By monitoring the evolution of interfacial tension with time the dilational elasticity and the relaxation mechanism can be obtained.

In Fig. 17 some typical interfacial tension changes are shown which have been obtained for a trapezoidal area change of an aqueous protein solution drop in tetradecane. The elasticity can be calculated from the initial jump of the $\gamma(t)$ dependence immediately following an expansion or compression.

The change in interfacial tension during a sinusoidal surface area change for a sunflower oil drop in a protein solution at a comparatively low oscillation frequency is shown in Fig. 18. Due to the time required for image acquisition in the ADSA experiments faster oscillations are not possible without the use of VCR (with a frame frequency of 25 Hz one can perform oscillation experiments at a maximum frequency of 1 Hz).

B. Drop-oscillation Experiments

The principle set-up of a drop pressure method has been already described in detail above as a method to investigate

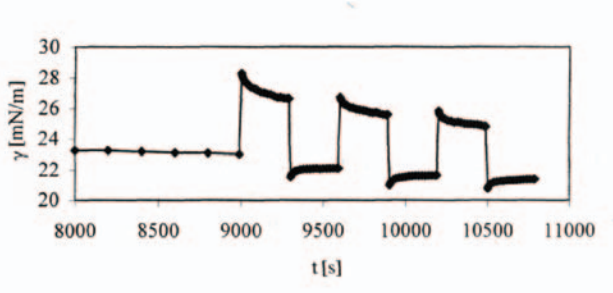

Figure 17 Dependence of dynamic surface pressure on time for periodic trapezoidal deformations of a solution drop surface (5×10^{-7} M HSA) in tetradecane.

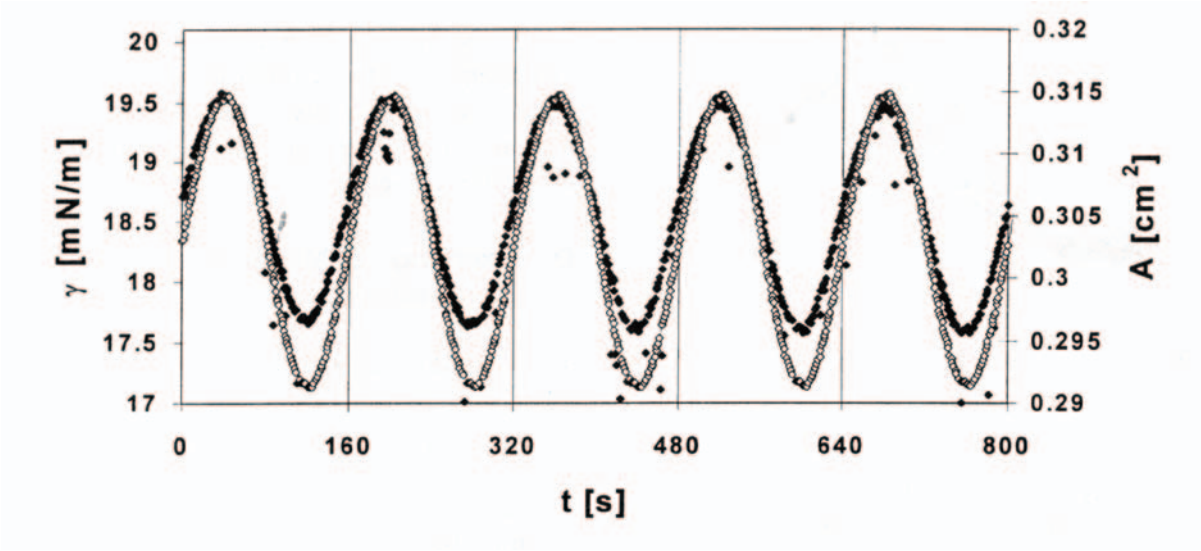

Figure 18 Harmonic oscillation of the interfacial tension y and drop surface area *A* of a sunflower oil drop immersed into an aqueous β-lactoglobulin solution (10^{-6} M/l), frequency $f = 0.00625$ Hz, according to Ref. 201.

the dynamics of adsorption (203, 204). This set-up can essentially be used for transient relaxation experiments (205).

The drop-shape oscillation technique as developed by Tian *et al*. (206, 207) is another technique suitable for closing the gap in the experimental methods for liquid/liquid interfaces. This method is based on the analysis of drop-shape oscillation modes and yields again the matter-exchange mechanism and the dila-tional interfacial elasticity. The method is similar to the transient relaxation methods applicable only for comparatively low oscillation frequencies.

A recently developed method allows harmonic changes of the drop surface area in a wide range of frequencies. Figure 19 shows the principle set-up for the oscillating-drop method (29).

The most important components of this set-up are, in analogy to the oscillating-bubble instrument, the pressure sensor, the piezo driver (189), and the capillary. The wetting behavior of the capillary is the key problem as it can control the size of the drop significantly. For the present situation, the capillary inner surface is hydrophobized to be wetted by the oil while the head and outer surface are hydrophilic to be wetted by the aqueous solution under study. The piezo driver and pressure sensor are directly controlled via an interface by the computer. The software allows one to generate a drop oscillation of definite frequency and amplitude while the pressure change is continuously read by the pressure sensor and registered on the computer. From the frequency dependence of the pressure amplitude and phase shift between pressure and drop area change the dilational elasticity and exchange of matter of the interfacial layer are calculated. In Fig. 20 the pressure amplitude measured for a tetradecane drop in water is shown as a function of the oscillation frequency. Up to a frequency of about 100 Hz the expected constant pressure difference due to changes in the radius of curvature of the drop is obtained. At higher frequencies additional contributions from the hydrodynamics of the two liquids arise and have to be considered in the data analysis.

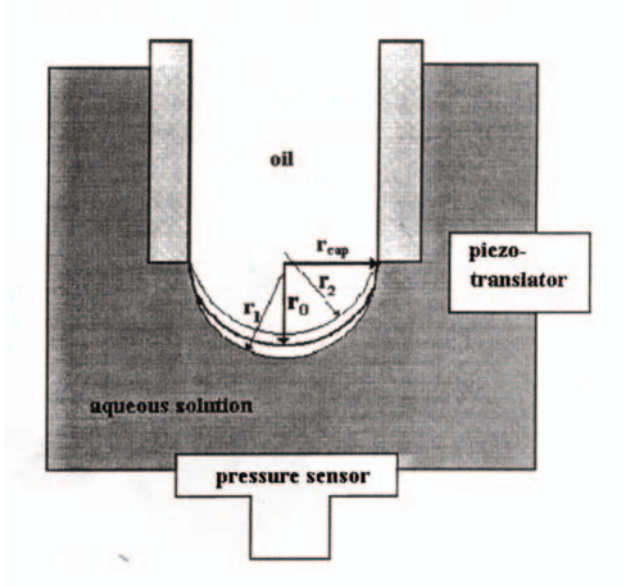

Figure 19 Schematic of an oscillating drop set-up.

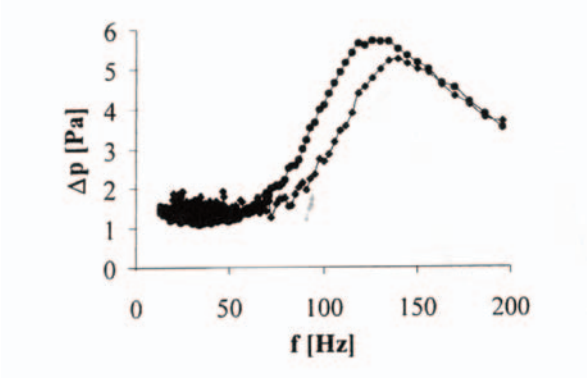

Figure 20 Frequency dependence of the capillary pressure amplitude for an oil drop in water, two runs.

C. Emulsion Film Relaxations

In addition to the study of interfacial rheology, studies on thin-film rheology are of particular practical interest. The first ideas were proposed by Kim *et al*. (208). The formation of a foam film can be arranged at the tip of two coaxial capillaries via two independent pumps as described in Ref. 209 (see Fig. 21). Such an assembly was used by Wege *et al*. (210) to exchange the bulk phase of a drop in order to perform penetration experiments at the drop surface. The three stages comprise the formation of an oil drop (dark gray) in water (light gray) as stage 1, and the subsequent formation and increase of a water drop inside this oil drop (stages 2 and 3). The size of the emulsion film and its thickness can be adjusted by actions of the respective pumps.

An oscillation of the foam film can be performed such that the film thickness changes with the area, or can be even kept constant by well-adjusted simultaneous oscillations of both fluid volumes. The coaxial arrangement of two capillaries seems to be an ensemble which allows an easily automated repeat formation of a foam film after an unwanted film rupture. This experimental set-up is under development now.

D. Exchange of Matter Theory for an Oscillating Drop

The exchange of matter theory for a harmonic inter facial area perturbation:

$$A = A_0(1 + \delta \sin \varpi t) \tag{101}$$

and a diffusional transport of surfactant molecules in the bulk phases given by Pick's equation for a drop of radius R_0 in a second infinite liquid:

$$\frac{\partial c}{\partial t} = D_1 \frac{\partial^2 c}{\partial x^2} \text{ at } \infty < x < R_0 \text{ (outside the drop)} \tag{102}$$

$$\frac{\partial c}{\partial t} = D_2 \frac{\partial^2 c}{\partial x^2} \text{ at } 0 < x < R_0 \text{ (inside the drop)} \tag{103}$$

require appropriate initial and boundary conditions. As a useful initial condition one can assume for both cases an equilibrium state of the adsorption layer. The boundary conditions for a bubble and a foam film, however, differ from each other significantly. The boundary condition at the interface reads:

$$\frac{d\Gamma}{dt} + \Theta\Gamma = \frac{\partial c}{\partial x} \text{ at } x = R_0 \tag{104}$$

where Θ = d In A/dt is given by Eq. (101). If one assumes only small oscillation ($\delta < 0.1$) we obtain:

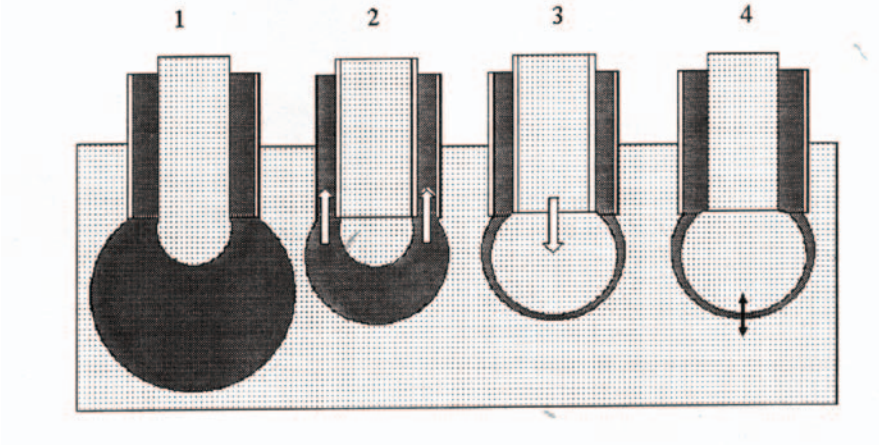

Figure 21 Steps for the formation of an emulsion film at the tip of a capillary.

$$\Theta = \frac{\mathrm{d}}{\mathrm{d}t}\frac{\delta \sin \varpi}{1 + \delta \sin \varpi t} \cong \delta \varpi \cos \varpi t \qquad (105)$$

The second boundary condition required for the solution of the transport problem is

$$\frac{\partial c}{\partial x} = 0 \ at \ x = 0 \qquad (106)$$

To complete the mathematical problem a relationship Γ(c), a so-called adsorption isotherm, is needed. For the simple case of bubble or drop oscillations (with the surfactant only outside the drop) a solution was derived in Ref. 189 in analogy to the capillary wave theory (183, 184).

For the emulsion film case, independent of the type of the function Γ(c) no analytical solution is available and numerical methods have to be applied. To obtain a link to the experiment, an additional relationship, equivalent to the adsorption isotherm, is required, relating the surface concentration Γ with the measured capillary pressure $P = 2\gamma/r$ in the bubble or film pressure of the curved foam film, which in turn is proportional to the surface pressure n.

Transient as well as harmonic relaxation experiments give access to the dilational rheology of the studied interface or film (211). The definition of the dilational elasticity E is given by the relation:

$$E = -\mathrm{d}\gamma/\mathrm{d} \ln \Gamma = \mathrm{d}\Pi/\mathrm{d} \ln \Gamma \qquad (107)$$

From changes of the surface pressure Π with time the elasticity can be obtained, while the phase shift between the generation of area oscillations and the pressure oscillation response is a measure of the exchange of matter [introduced by Lucassen as dilational viscosity, cf. (180)].

A systematic analysis of the stability of bubble and drop oscillations in open and closed cells has been performed recently and hydrodynamic limits have been given as a function of the geometry of the bubble and capillary as well as of the bulk properties of the two adjacent liquids (212, 213).

E. Summary

An experimental technique dedicated to studies of the dynamic and mechanical properties of adsorption layers at the liquid/liquid interface is described with respect to its impact on the characterization of emulsions. A recently developed oscillating-drop technique gives access to the surface rheology of adsorption layers composed of surfactants and/or proteins. The same methodology seems to be suitable for direct investigations of single emulsion-film properties for which a relevant modification of the experimental set-up is proposed.

On the basis of theories for oscillating bubbles, new models for the exchange of matter for surfactant adsorption layers will have to be developed, taking into consideration the effect of surfactant transfer across the interface and the peculiarities of transport in thin emulsion films.

VII. INTERFACIAL SHEAR RHEOLOGY

The interfacial shear Theological parameters are the analogs of the three-dimensional equivalents of shear elasticity and viscosity, though there are complications for interfaces where material can be exchanged between the interface and the bulk phase during the measurement.

The rate of film thinning in emulsions depends on the interfacial rheology because the flow of fluid is coupled with the flow of interfacial elements. A high interfacial shear viscosity can promote emulsion stabi lity by retarding film thinning and hence the rate of droplet coalescence. The understanding of interfacial rheology in real emulsions is very complicated due to the fact that there are usually a large number of differ ent surface-active components present. This makes it difficult to interpret the rheology of such systems in terms of the respective physicochemical properties of the interface.

The general framework of interfacial rheology has been dealt with systematically by several previous authors: Joly (214), Goodrich (215), Lucassen (216), Edwards *et al.* (217), and Noskov and Loglio (218). Reviews on interfacial rheology in general have been published by Warburton (219) and Miller and cowor-kers (27, 220). Several researchers have attempted to correlate emulsion stability with interfacial tension and interfacial rheology. The literature up to 1988 has been reviewed by Malhotra and Wasan (221). An introduction to the subject of food emulsions was published by Lucassen-Reynders (222) and more recently by Murray and Dickinson (223) and Murray (224).

A. Methods

Different techniques for the study of shear rheology of interfacial layers have been developed over the years; however, they are mostly suited for liquid/gas inter faces. The early instruments were constructed to measure the interfacial shear viscosity under constant shear conditions. In more complex systems, nonlinear effects, shear-rate dependencies of the viscosity, and viscoelastic properties are

also evident. For measure ments at liquid/liquid interfaces two types of rhe-ometers are commonly used-the deep channel and the biconical bob rheometers (both techniques will be discussed later). Warburton (225) proposed an oscillat ing ring surface rheometer which exploits the phenom enon of mechanical resonance. Benjamins and van Voorst Vader (226) introduced a sensitive method using a concentric ring system which is placed in the interface. The outer ring is driven at a particular fre quency and small amplitude, while a torque is applied to the inner ring to keep it stationary.

The oscillatory deep-channel rheometer described by Nagarajan and Wasan (227) can be used to examine the rheological behavior of liquid/liquid interfaces. The method is based on monitoring the motion of tracer particles at an interface contained in a channel formed by two concentric rings, which is subjected to a well-defined flow field. The middle liquid/liquid interface and upper gas/liquid interface are both plane horizon tal layers sandwiched between the adjacent bulk phase. The walls are stationary while the base moves. In the instrument described for dynamic studies of viscoelastic interfaces the base oscillates sinusoidally. This move ment induces shear stresses in the bottom liquid that are transmitted to the interface. The interfaces are viewed from above through a microscope attached to a rotary micrometer stage which is coaxial to the cylinders.

The interfacial motion is determined from the movement of a small (100 μm) inert particle placed at the interface. This measurement is sometimes not easy since the particle must be positioned precisely. The measurement is most accurate if the reference is chosen to be the midpoint of the oscillation, where the velocity is maximum. The rheological parameters are calculated from a hydrodynamic analysis for two moving adjacent immiscible liquids incorporating interfacial rheological models. Mechanical considerations restrict the maximum possible frequency of this instrument to about 1 Hz.

Many proposed techniques rely on measuring the rotational motion of a knife-edged disk when placed in the plane of the interface. This arrangement is the two-dimensional equivalent of a Couette viscometer. The biconical disc is often suspended from a torsion wire and different constructions have been devised for monitoring and/or controlling the deflection of the disk in response to the rotation of the disk (228, 229). There is one great advantage of the Couette-type device: the technique can be easily applied to liquid/gas and liquid/liquid interfaces. The sensitivity of this technique is poorer than that of a deep-channel rheometer owing to additional drag on the disk by the bulk phases. However, the biconical disk technique is more widely used, probably because of easier experimental handling. For the biconical disk technique there are some limitations for the interpretation of the results. The shear deformation of the interface can be transferred by a constant low strain-rate experiment or as a very short and small deflection of the biconical disk. In the former experiment the deformation is transferred continuously and sometimes causes the destruction of the interfacial layer. If such a breakdown of the interfacial structure takes place a completely different interfacial layer state will be measured. The latter experimental set-up enables one to prevent the destruction of the interfacial layer. The damped oscillation behavior of the torsion pendulum provides the information on the surface shear rheology; however, for highly nonlinear systems it is difficult to interpret the experimental results.

The biconical bob oscillatory interfacial rheometer of Nagarajan et al. (230) is designed to measure the dynamic viscoelastic response of a liquid-liquid interface subjected to a small-amplitude oscillatory shear stress. This instrument is used to examine the rheological behavior of interfaces in the presence of surfactants, in particular of macromolecules. The rheological parameters are calculated from a hydro dynamic analysis incorporating a linear viscoelastic interfacial rheological model. The general response of this instrument has been compared with that of the oscillatory deep-channel interfacial rheometer, which is capable of similar measurements. Measurements of interfacial viscoelasticity for the same liquid-liquid system with the two rheometers are shown to be comparable. This study demonstrates the intrinsic nature and, therefore, the instrument independence of these rheological properties. Accurate measurements of interfacial shear viscoelasticity can be carried out over a wide range of systems by combining the rheometers. A similar experimental set-up was proposed by Miller et al. (231) and a schematic is given in Fig. 22.

This torsion pendulum rheometer developed for studies of adsorption layers at the water/air interface been modified in order to allow measurements at the water/oil interface. Instead of a ring with a sharp edge a biconical disk has been used. A detailed description of this device has been given elswhere (232). Basically, a small shear deformation of the interface of the system under study is produced by a freely oscillating, hanging titanium disk. The interfacial meniscus is positioned at the edge of the disk, with the interface contained in a concentric glass vessel. The interfacial shear field is generated in the gap between the edge of the disk and the wall of the measuring vessel. Using this device, interfacial shear elasticities and viscosities as a function of adsorption time can be determined by measuring the amplitude ratio and the shift of the eigenfrequency of the pendulum with respect to a surfactant-free interface. A linear

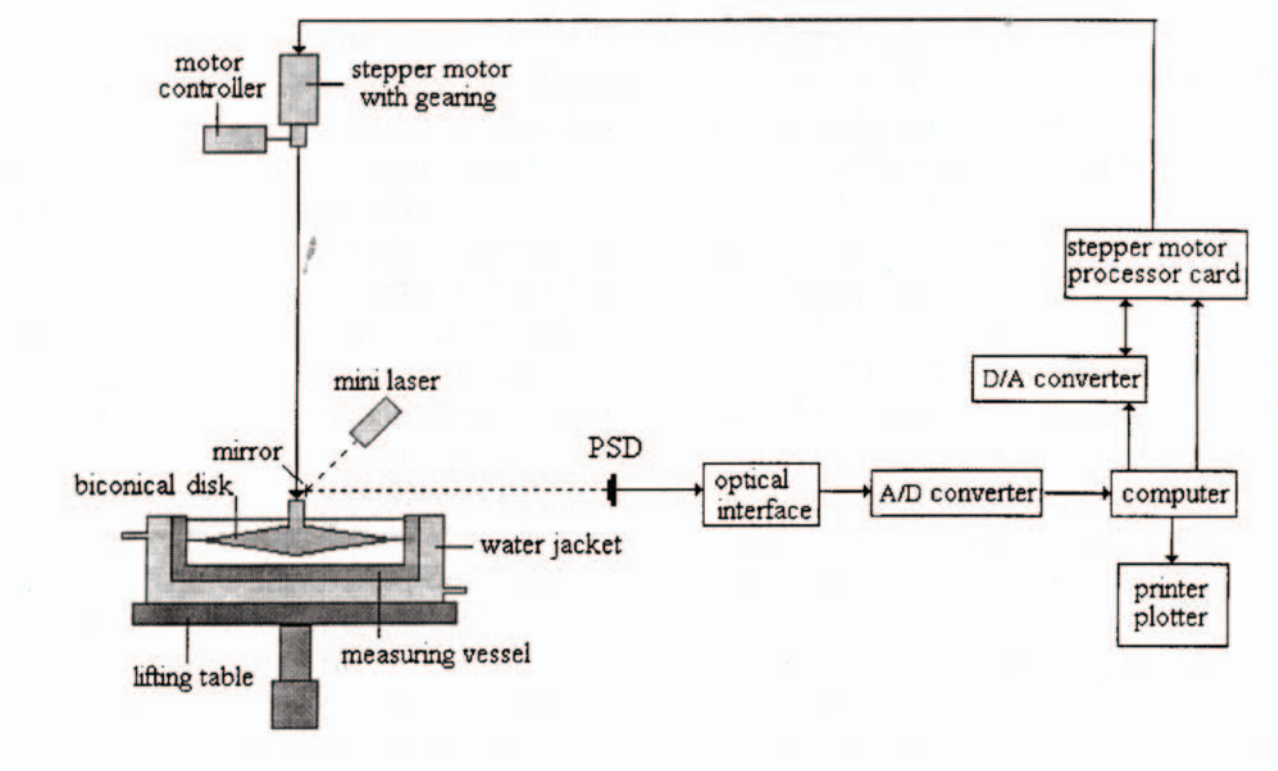

Figure 22 Schematic view of an interfacial shear rheometer at liquid/liquid interfaces.

viscoelastic model is used to describe the viscoelastic properties of the interfacial layer. For a tungsten wire of 100 μm diameter and 30 cm length the eigenfrequency is of the order of 0.1 Hz. All rheological experments have to be performed with very small deflection angles (≤2°) so as to minimize disruption of the interfacial layers. The pendulum experiment, which lasts approximately 30 s, can be repeated every 10 min over a long perod. Unfortunately, this method does not allow large changes in the deformation frequency, as needed for a complete characterization of the viscoelasticity of an interfacial layer. The lower limitation of this instrument is determined by the fact that the bulk phases also exert a drag on the disk. Therefore, the measured effect induced by the interfacial layer must be high enough to be detected. The upper limitation is given by highly nonlinear systems, such as concentrated layers of macromolecules. For such systems it is often difficult to interpret the data obtained from the damped oscillation.

B. Experimental Results

Interfacial rheological measurements are made on macroscopic interfaces. For the most part, the range of applied stresses, strains, and shear rates do not mirror the vigorous, nonequilibrium conditions of the practical process of emulsification. Nevertheless, interfacial rheology is an efficient and powerful detection technique, which may enhance our knowledge on formation, structure, properties, and behavior of interfacial layers formed in oil/water systems. Lakatos and Lakatos-Szabo (233) determined the interfacial shear rheology of different crude oil/water systems in a wide temperature and shear-rate range in the presence of nonionic emulsifiers (oxyethylated nonylphenols with EO numbers between 10 and 40). They observed that the interfacial viscosity, the nonNewtonian flow behavior, and the activation energy of the viscous flow drastically decrease in the presence of these surfactants. The modification of the rheolog-

ical properties increase with decreasing EO number, and increasing surfactant concentration and temperature. Opawale and Burgess (234) studied the interfacial shear rheology of different liophilic nonionic surfactants of the sorbitan fatty acid ester type with the aim of selecting appropriate emulsifiers for water-in-oil emulsions under different conditions. For these investigations they used an oscillatory ring surface rheometer. The effects of bulk concentration, temperature, and the presence of salt in the aqueous phase on the interfacial properties of surfactant films were determined. The surfactants exhibited mainly viscoelastic properties. The authors conclude that interfacial association of inverse micelles and/or surfactant multilayer formation are probably responsible for the observed viscoelasticity. The addition of sodium chloride to the aqueous phase and increase in temperature influenced the viscoelastic properties. Mohammed *et al*. (235) studied the effect of demulsifiers on the interfacial rheology and emulsion stability of water-in-crude oil emulsions. The results indicated that the demulsifier used is poor at displacing the naturally occurring asphaltene surfactants from the crude oil/water interface, but if they adsorb at the interface first they prevent the formation of the stable, rigid asphaltene films.

The interaction between polymers and surfactants is one of the most important problems in enhanced oil recoverry. Interfacial shear viscosity is sensitive to surface-active species adsorbed at the oil/water interface. Therefore, interfacial shear viscosity measurements are very useful for investigating the interfacial layer formation by adsorption from mixed polymer-surfactant solutions. Cardenas-Valera and Bailey (236) examined the interfacial rheological properties of spread films of poly(ethylene oxide)/poly(methylmethacrylate) (PEO/ PMMA) graft copolymers at toluene/water and toluene-n-heptane/water interfaces. The interfacial shear viscosity was determined from the damped oscillation of a torsion pendulum. The largest viscosity was exhibited by a monolayer spread at the toluene-n-heptane/water interface. Emulsions prepared with this sytem showed the lowest coalescence rate, indicating that at this interface the graft copolymer forms a coherent film which retards interdroplet film drainage. The results show that films with larger values of the interfacial rheological parameters produce a more stable emulsion owing to an increase in the mechanical strength of the interfacial film and its ability to respond to local thickness variations.

Zhang and coworkers (237, 238) studied aqueous solutions of polyacrylamide (PAAM) mixed with three different surfactants at the hexadecane/water interface, using a rotational torsion viscometer. The structure of the interfacial films were shown to be dependent on the shear rate. Based on the experimental results, a mechanism for PAAM-surfactant interactions was proposed. The interfacial viscosity decreased with ionic surfactant concentration. They supposed that the polymer-surfactant interaction model changes with surfactant concentration. For nonionic surfactants the interfacial viscosity was relatively higher and independent of the concentration.
The authors did not find an indication that the interaction model changes by increased nonionic surfactant concentration.

In pharmaceutical and food technology, emulsion proteins are often used as stabilizers. The importance of interfacial shear rheological properties on protein stabilized emulsions was reviewed by Murray and Dickinson (223) and Murray (224). The influence of covalent cross-linking with transglutaminase on the time-dependent surface shear viscosity of adsorbed milk protein films at the n-tetradecane/water interface has been investigated by Faergemand *et al*. (239). They studied the influence of sodium caseinate, $\alpha_{(S1)}$-casein, β-casein, and β-lactoglobulin. Proteins were adsorbed from 10^{-3}wt % aqueous solutions at pH 7, and apparent surface viscosities were recorded at 40°C in the presence of various enzyme concentrations. Results for casein systems showed a rapid enhancement in surface viscoelasticity due to enzymic cross-linking with a substantially slower development of surface shear viscosity for $\alpha_{(S1)}$-casein than for β-casein. While adsorbed β-lactoglobulin showed less relative increase in surface viscosity than the caseins, the results for β-lactoglobulin showed the presence of a substantial rate of crosslinking of the globular protein in the adsorbed state, whereas in bulk solution β-lactoglobulin was cross linked only after partial unfolding in the presence of dithiothreitol. A maximum in shear viscosity at relatively short times following addition of a moderate dose of enzyme was attributed to formation of a highly cross-linked protein film followed by its brittle fracture. Enzymic cross-linking or protein before exposure to the oil-water interface was found to produce a slower increase in surface viscosity than enzyme addition either immediately after interface formation or to the aged protein film.

Williams and Janssen (20) studied the behavior of droplets in a simple shear flow in the presence of a protein emulsifier. The effect of two structurally diverse protein emulsifiers, β-lactoglobulin and β-casein, upon the break-up behavior of a single aqueous droplet in a Couette flow field has been studied over a wide range of protein concentrations. It was found that β-casein and low concentrations of β-lactoglobulin cause the droplets to be at least as stable as expected from conventional theories based on the equilibrium interfacial tension. In such cases the presence of the emulsifier at the deforming interface is thought to enhance the interfacial elasticity. This effect can be characterized by

an effective interfacial tension, which is higher than the equilibrium value. High concentrations of β-lactoglobulin, on the other hand, have been shown to cause droplets to be less stable than would have been predicted from an equilibrium inter-facial tension model. It is thought that an interfacial protein network is formed, which limits the droplet deformation and makes the droplet interface rigid with respect to tangential stresses. As a result, the critical deformation and capillary number are found to be essentially independent of the viscosity ratio. It is proposed that the interfacial structure may be probed using a combination of interfacial shear and dilational rheological measurements. From this type of analysis it may be possible to predict the break-up stability of droplets.

Ogden and Rosenthal (240) studied the influence of solid particles (tristearin crystals) on the stability of protein-stabilized emulsions. A Couette-type torsion-wire surface-shear viscometer was used to measure the apparent interfacial shear viscosity of pH 7 ($I = 0.05$ M) buffered solutions of lysozyme, sodium caseinate, and Tween-40 in contact with either n-tetra-decane or purified sunflower oil. When proteins were present in the aqueous phase and tristearin crystals in the oil phase, a synergistic increase in the interfacial shear viscosity was observed. The magnitude of the increase appeared to be independent of the type of protein, but depended on the nature of the oil phase. This increase in the interfacial shear viscosity was not simply due to the presence of protein reducing the interfacial tension and thus affecting the adsorption behavior of the fat crystals. When the aqueous phase contained a small-molecule surfactant (Tween-40) instead of protein, keeping the same interfacial tension, a significantly smaller increase in the interfacial shear viscosity was observed. It therefore seems likely that when proteins are present, hydrophobic peptide residues interact with the tristearin crystals at the interface. More recently, Ogden and Rosenthal (241) studied the interaction of tristearin crystals with β-casein at the sunflower oil/water interface with the same measuring technique.

An example of shear viscosity measurements on a protein adsorption layer at a water/hexadecane interface, using the biconical disc technique (231), is shown in Fig. 23.

At first, step-by-step increases in the protein concentration results in only rather small increases in the shear viscosity. Above a certain concentration the viscosity increases very strongly. At the water/air interface, in most cases, a maximum in the concentration dependence of the shear viscosity is found, which can be discussed on the basis of conformational changes in the interfacial layer. At the interface between two liquids the situation seems to be more complicated and qualitatively different results are obtained. The differences may be connected with the additional freedom

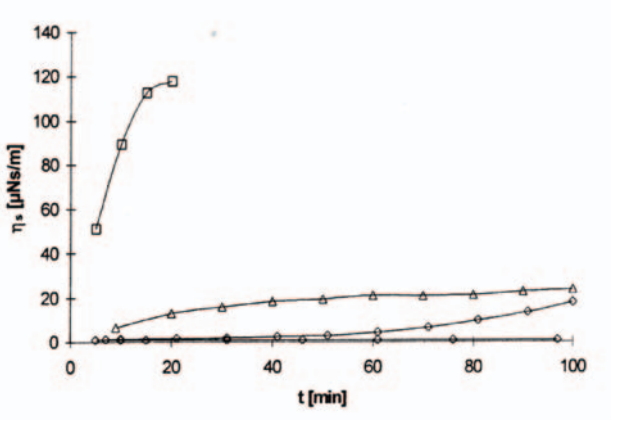

Figure 23 Interfacial shear viscosity of ABPI (bean protein) at the water/hexadecane interface; protein concentrations: 10^{-4}% (□), 2×10^{-4}% (△), 3×10^{-4}% (μ), 4×10^{-4}% (Γ).

of adsorbed protein molecules to entangle into the oil phase. In this way also, at higher concentration, an unfolding of adsorbed molecules at the water/oil interface can happen while at the water/air interface, owing to the restricted space, adsorbed molecules will have to remain in their native state as discussed by Wiistneck *et al*. (242).

VIII. ELLIPSOMETRIC STUDIES

The properties of adsorbed layers at liquid interfaces can be determined either indirectly by thermodynamic methods or directly by means of some particular experimental techniques, such as radiotracer and ellipsometry. For adsorbed layers of synthetic polymers or biopolymers the advantages of the ellipsometry technique become evident as it yields information not only on the adsorbed amount but also on the thickness and refractive index of the layer. The theoretical background of ellipsometry with regard to layers between two bulk phases has been described in literature quite frequently (243). In brief, the principle of the method assumes that the state of polarization of a light beam is characterized by the amplitude ratio $|E_p|/|E_s|$ and the phase difference ($\delta_p - \delta_s$) of the two components of the electric-field vector E. These two components E_p and E_s are parallel (p) and normal (s) to the plane of incidence of the beam and given by

$$E_p = |E_p|e^{i\delta_p}$$
$$E_s = |E_s|e^{i\delta_s} \quad (108)$$

Changes in the state of polarization upon reflection at an interface are given by

$$\tan\Psi = \frac{|E_p^r|/|E_s^r|}{|F_p^i|/|E_s^i|} \quad (109)$$

$$\Delta = (\delta_p^r - \delta_s^r) - (\delta_p^i - \delta_s^i) \quad (110)$$

where tan Ψ is the change in the amplitude ratio and △ is the relative phase change. The superscripts r and i denote the reflected and incident beams. These two parameters are the data usually determined in ellipsometric experiments; however, under special conditions it is possible to estimate only one (244, 245). In terms of the overall reflection coefficients of the parallel R_p and normal R_s components of the beam the total effect caused by the reflection can be written as

$$\rho = \frac{R_p}{R_s} = \frac{E_p^r/E_s^r}{E_p^i/E_s^i} = \tan\Psi e^{i\Delta} \quad (111)$$

This equation is the so-called basic ellipsometric equation. It contains R_p and R_s which depend on the optical properties of the reflecting system, the wavelength of the light λ the angle of incidence φ and the experimentally measurable parameters Ψand △. For the reflection at a clean interface, the R_p and R_s are the Fresnel coefficients (246) of the single uncovered interface. They depend only on the refractive indices of the two adjacent phases and the angle of incidence. For systems that do not absorb light the optical constants of the two bulk phases (ambient and substrate media) are usually obtained from the experimental values of Ψ and △ for the clean interface (denoted by subscript "0" via Eq. (111). For a layer-covered interface, multiple reflections and refractions take place within the layer (Fig. 24).

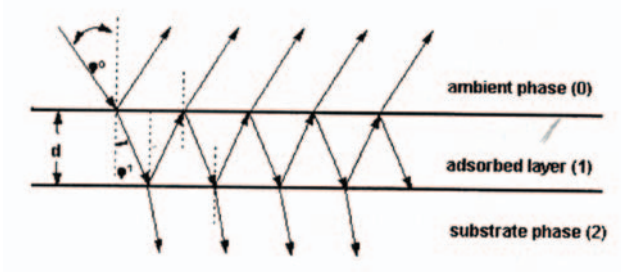

Figure 24 Multiple reflections and refractions in an inter-facial layer.

These effects are enclosed in the overall reflection coefficients as

$$R_j = \frac{r_{01j} + r_{12_j}e^{-2i\beta}}{1 + r_{01j}r_{12j}e^{-2i\beta}}, j = p, s \quad (112)$$

Equation (111), in terms of the ellipsometric angles △ and Ψ, then reads:

$$\rho = \tan\Psi e^{i\Delta}\frac{r_{01p} + r_{12p}e^{-2i\beta}}{1 + r_{01p}r_{12p}e^{-2i\beta}}\frac{1 + r_{01s}r_{12s}e^{-2i\beta}}{r_{01s} + r_{12s}e^{-2i\beta}} \quad (113)$$

In Eqs (112) and (113),r_{01j} and r_{12j} *(j - p, s)* denote the Fresnel reflections coefficients at the 0-1, 1-2 interfaces of the ambient medium (0), layer (1), and substrate medium (2) in the reflecting system; β is the phase change of the electromagnetic wave caused by the presence of the inter-facial layer.

$$\beta = \frac{2\pi d n_1 \cos\varphi_1}{\lambda} \quad (114)$$

Here, d is the thickness of the layer, $_1$ is its refractive index, and φ is the angle of refraction in the layer. When a thin nonadsorbing, plane-parallel, homogeneous, and isotropic layer, with d ≺λ is present at an interface between two phases (characterized by △ and Ψ Eq (113) yields (246):

$$\beta = \frac{2\pi d n_1 \cos\varphi_1}{\lambda} \quad (114)$$

where n_0 and n_2 are the refractive indices of ambient and substrate phases, respectively, φ is the angle of incidence, and . For systems with a nonabsorbing ultrathin layer the conditions of homogeneity and isotropy of the layer can be invalid (for instance, for insoluble monolayers in the state of a two-dimensional phase transition) (247, 248). In such cases, Eq. (115) can be rearranged to obtain the following relationship (which is exact up to the first-order terms in d/λ:

$$\delta\Delta = \Delta - \Delta_0 = -\left(\frac{4\pi d}{\lambda}\right)\left(\frac{\sin\varphi_0\tan\varphi_0 n_0}{1 - (n_0/n_2)^2\tan^2\varphi_0}\right) \times \left[\frac{n_\perp^2 - n_2^2}{n_0^2 - n_2^2} - \frac{n_0^2}{n_\parallel^2}\left(\frac{n_\parallel^2 - n_2^2}{n_0^2 - n_2^2}\right)\right] \quad (116)$$

In this equation the optical axis of the layer is assumed to be perpendicular to the interface; $n_\perp$ is the real part of the refractive index of the layer perpendicular to its optical

axis; $n_{||}$ is the real part of the refractive index of the layer parallel to the optical axis.

The solution of Eq. (113) [or its simplified modification, Eq. (114)] for the calculation of the reflection coefficients is a standard task and is described in the literature, for example, in Ref. 249. The inverse problem, calculation of the refractive index and thickness of the adsorbed layer from the measured ellipsometric angles $\triangle$, $\triangle_0$, Ψ, and Ψ is unfortunately not so trivial. An analytical solution of these equations is not possible, because the theory does not give explicit expressions for the optical parameters n_1 and $d$of the layer. Therefore, a numerical evaluation, including iteration procedures, is usually applied. Reasonable starting values for the optical properties of the layer are inserted in Eqs (113) or (115) and the iteration process is continued until a satisfactory agreement between the calculated and measured values of A and $\triangle$ has been reached. Modern computers and suitable software make such numeric calculations simple. For anisotropic, ultrathin adsorbed layers even a numerical solution of the basic ellipsometric equation in the respective form Eq. (115) is impossible. These layers have a negligible absorption and therefore the corresponding change in one of the two ellipsometric angles is not measurable ($\delta\Psi \approx 0$). In this connection the basic ellipsometric equation contains only one experimental parameters and three further parameters are to be evaluated. Therefore, it is clear that an infinite number of evaluated parameters can agree with the measured value of $\delta\triangle$.

To proceed and obtain some physical information, additional assumptions about some of the optical properties of the layer are needed (247, 248). These can be derived from sound theoretical considerations, taking into account the structure of the layer and peculiarities of the molecules forming the layer (247, 248).

Although the optical properties of the adsorbed layer by evaluation of the ellipsometric data obtained are quite interesting for its characterization, for inter-facial science the information about the amount adsorbed at an interface is especially important. In the calculation of this quantity, however, the problem appears to be of a proper proportionality between the layer properties provided by ellipsometry and the adsorbed amount. Recently, it was shown that for ultrathin adsorbed layers of conventional soluble surfactants ellipsometry is insufficient and additional experimental methods are required (245, 250). Relatively thick layers are also often not homogeneous in the bulk (substrate) normal to the interface. In this case the refractive index and the thickness of the layer calculated from the experimental values of $\delta\triangle$ and $\delta\triangle$ represent mean optical quantities. If, additionally, the refractive index n_1 is a linear function of the solute concentration in the layer:

$$n_1 = n_2 + \frac{dn}{dc}(c(z) - c(\infty)) \tag{117}$$

where $c(z)$ is the solute concentration in the layer as a function of the distance from the interface (z = 0) to the bulk, and c(∞) is the solute concentration in the solution. The adsorption Γ can be unambiguously calculated from the average layer thickness d_{av} and the average refractive index n_{lav}:

$$\Gamma = \frac{d_{av}(n_{1av} - n_2)}{dn/dc} \tag{118}$$

these simplifying assumptions are commonly used in the ellipsometric studies of different layers of synthetic polymers of biopolymers. At the same time it has been accentuated for such applications that the adsorbed amount can be determined more accurately than the layer thickness and refractive index, especially at low interfacial coverages (251).

Ellipsometry is a well-established experimental method for thin-film investigations and nowadays numerous modifications of experimental set-ups exist (252). When ultrafast measurements for monitoring very rapid processes is not necessary, a conventional PCSA null-ellipsometer set-up is often used. The scheme of such an apparatus is shown in Fig. 25. A low-capacity laser serves as light source (beam diameter of about 0.5-1 mm), and the beam passes through the first quarter-wave plate to produce circularly polarized light. The light is then linearly polarized by a Glan-Thompson prism mounted in a rotatable divided circle which can be read with a very high precision. The second quarter-wave plate and the analyzer (a second Glan-Thompson prism) are mounted in a similar manner as a polarizer. A photodiode detector is normally used. Both incidence and reflection arms are motorized and computer controlled; the highly precise motors rotating the polarizer and analyzer are also controlled by the computer.

For ellipsometric investigations of liquid/liquid interfaces numerous measuring cells have been developed. One example is presented schematically in Fig. 26.

For such ellipsometric experiments the cell must be very carefully positioned to place the interface between the two liquids exactly in the ellipsometer axis. The angle of incidence and the angle formed by the two side-walls of the cell must be equal with high accuracy to avoid changes in the state of light polarized upon passing through the cell.

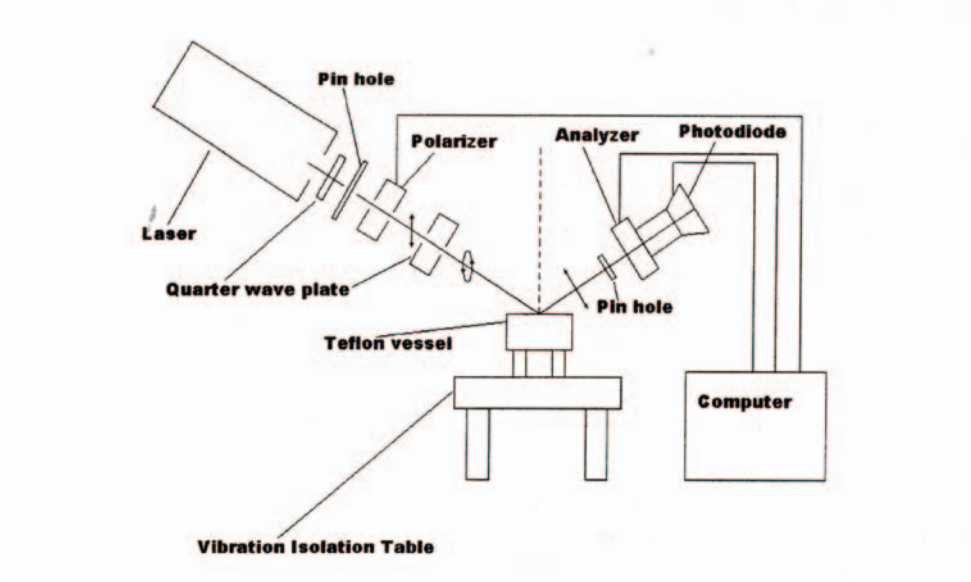

Figure 25 Principle of an ellipsometer set-up.

The measuring procedure by means of the PCSA null-ellipsometer is an experimental routine and typically computerized (253).

Although ellipsometry is well established as an experimental technique for the investigation of adsorbed layers, the number of studies at fluid/liquid interfaces is relatively small. Ellipsometry was used for investigation of the layer thickness between two immiscible liquids near the critical point (254, 255). This technique was also quite often used for in situ studies of the adsorption kinetics at an air/protein solution surface or polymer monolayers at an air/water interface (251, 256). It was also shown that ellipsometric results obtained at the same interface for conventional soluble surfactants or insoluble monolayers cannot be unambiguously interpreted by the standard formalism (244, 245, 247). The application of ellipsometry to the study of coalescence phenomena in emulsion systems was recently reported (257). The newly developed technique of dual-wavelength ellipsometry was used for investigation of the thinning of liquid films between two droplets in an emulsion. A comparison with independent methods shows satisfactory agreement and, hence, ellipsometry can also be applied to such systems.

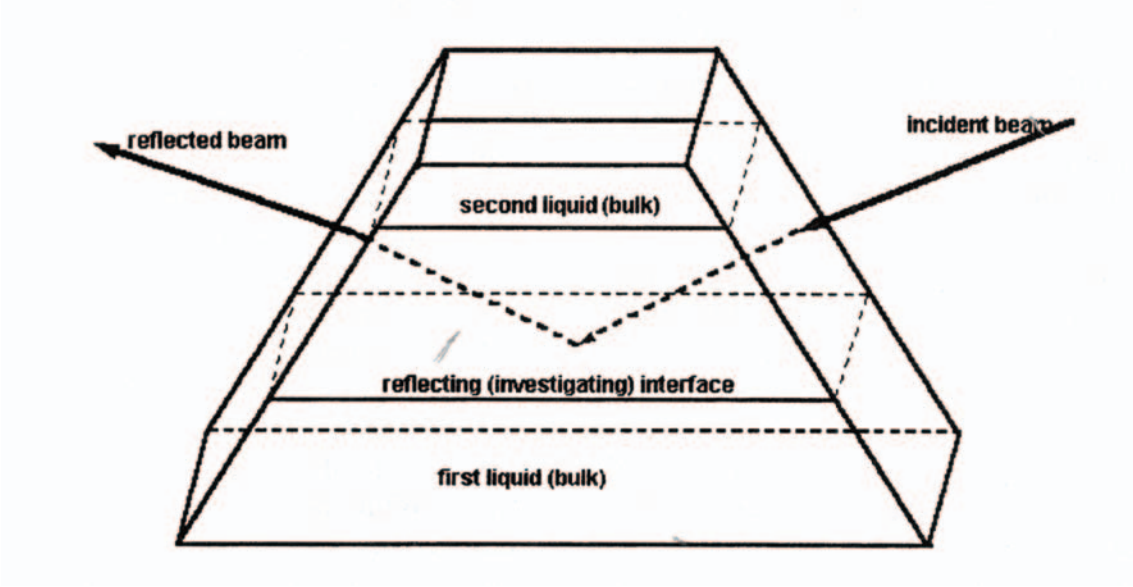

Figure 26 Measuring cell for ellipsometric studies at liquid/liquid interfaces.

IX. HLB CONCEPT

Surfactants are the compounds at an interface that reduce the interfacial tension. It follows from thermodynamics, that this property is due to the ability of these compounds to undergo the transfer from within an adjacent fluid (liquid or gas) phase to the interface. In fact, this ability is just the adsorption phenomenon. Clearly, an accumulation at the interface is possible for substances consisting of two parts, each of them separately exhibiting the affinity to one of the contacting phases. Such a property is characteristic of amphiphilic molecules possessing polar (hydrophilic) and nonpolar (lipophilic) parts.

With respect to the properties of polar groups, surfactants can be subdivided into ionic (cation- and anion-active, ampholytic, and zwitterionic) and nonionic surfactants. If the effect produced by the polar group of the surfactant molecule is more significant than that of the lipophilic group, this substance is soluble in water. It is less surface active as compared to any substance characterized by an optimum balance between the activities of hydrophilic and lipophilic groups. Similar conclusions can be drawn also with respect to the solubility in oil: here, the role of the lipophilic group is determining. Clearly, the efficiency of a surfactant is not determined solely by the amphiphilicity, but depends on the hydrophilic/lipophilic balance (HLB) characteristic for this compound. Therefore, this balance is an important characteristic of both the surfactant and the interface.

The first attempt to estimate this hydrophilic/lipophilic balance quantitatively was made by Griffin, who introduced a scale of HLB numbers (258). The initial aim for this classification of surfactants with respect to HLB numbers was to permit the optimum choice of emulsifiers. Subsequently the same method was applied to wetting agents, detergents, etc. The approach proposed by Griffin was further developed and generalized in a number of review papers (259, 260), presenting methods used to determine and calculate HLB numbers for various surfactants. Recently, the HLB concept was analyzed by Rusanov (261) and Kruglyakov (262). In this last book one can also find an extensive bibliography related to Griffin's HLB numbers. The Griffin HLB scale extends from 1 (for extremely lipophilic oleic acid) to 40 (extremely hydrophilic sodium dodecyl sulfate), with a mean HLB value taken to be 10. It is assumed that for the mixture of two or more surfactants, the HLB number additively depends on the HLB numbers of the individual surfactants. Therefore, to determine the HLB number for a surfactant, first the emulsifying ability of this substance is measured, and then that mixture of two surfactants with known HLB numbers is determined which possesses the same emulsifying ability. For the stabilization of oil-in-water emulsions, surfactants with HLB numbers in the range 9-12 are optimal, while to stabilize water-in-oil emulsions, more lipophilic surfactants, possessing HLB numbers in the range from 4 to 6 should be used. As an example, the HLB numbers data are listed below (Table 2) for Tritons X, the substances with the general chemical formula:

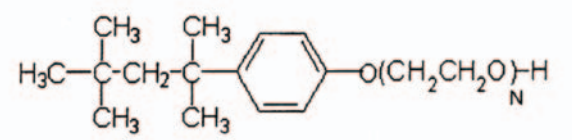

here N is the mean number of oxyethylene groups, and MW is the mean molecular weight.

The stability of an emulsion depends not only on the surfactant type, but also on the nature of the organic phase. To characterize the oil phase, the concept of a necessary (required) HLB number is used. This number is taken to be equal to the HLB number of the surfactant which ensures the best possible emulsification of the oil. Tables of necessary HLB numbers for various oils were published in Ref. 258. For example, with respect to oil-in-water emulsions, the necessary HLB number is 17 for oleic acid, 15 for toluene, 14 for xylene and cetyl alcohol, 10.5 to 12 for mineral oils, 7.5 to 8 for vegetable oils, 5 to 7 for vaseline, and 4 for paraffin. In Refs 263 and 264 the necessary HLB numbers for various oils are compared with the relative dielectric permittivity of the oil ε. In the series of saturated hydrocarbons, a weak inverse dependence between the necessary HLB number and e was observed (264); e.g., ε =

Table 2 HLB Numbers of Tritons X, According to *Sigma Chemical*

Triton	N	MW	HLB	Triton	N	MW	HLB
X-15	1	250	3.6	X-102	12–13	756	14.6
X-35	3	338	7.8	X-165	16	910	15.8
X–45	5	426	10.4	X-305	30	1526	17.3
X-114	7–8	536	12.4	X-405	40	1966	17.9
X-100	9–10	625	13.5	X-705	70	3286	18.7

2.036 and HLB = 8 for tetradecane, while ε = 1.8 9 and HLB = 10.5—11.0 for hexane. On the other hand, for various oils a slight increase of the necessary HLB number takes place with increasing dielectric permittivity. All empirical dependence between the necessary HLB number and surface tension or molar volume of oil were proposed, in Ref. 262. It should be noted that the necessary HLB values estimated for the same oil using various methods can differ from each other: for example, the data present in Refs 263 and 264 exceed those listed in Ref. 258.

The attempts to rationalize Griffin's HLB scale from a physicochemical point of view were made in a number of studies. Various correlations were shown to exist between the HLB numbers and the chemical structure or molecular composition of the surfactants. Correlations were also found between the HLB number and physicochemical properties of surfactants and their solutions, for example, surface and interfacial tension, solubility, and heat of solution, spreading and distribution coefficient, dielectric permittivity of the surfactant, cloud point and phase inversion point, critical micelle concentration, foaminess, etc. These studies are reviewed in Ref. 262. However, the correlations found are not generally applicable; moreover, the concept of the additivity of HLB numbers as such for mixtures of surfactants or oils cannot be proven expermentally when the surfactant characteristics are varied over a wider range (265).

An important contribution to the HLB concept was made by Davies (266, 267), where the so-called group numbers were introduced, that is, HLB numbers which correspond not to the molecule as a whole entity, but to the constituting groups (molecular structural units). Once the group numbers g_i are known, one can calculate the HLB number from the chemical formula of a surfactant using the equation:

$$\mathrm{HLB} = 7 + \sum_i g_i \qquad (119)$$

For hydrophilic groups g; > 0, while for lipophilic groups $g_i < 0$. The group numbers for some groups calculated by Davies (266, 267) are listed in Table 3.

From analysis of the destruction rates for oil-in-water and water-in-oil emulsions, Davies was able to relate the group numbers with the ratio of coalescence rates for these two types of emulsion. Another correlation was shown to exist to this ratio and the two equilibrium concentrations of the surfactant in the aqueous and oil phases, (c^w/c^o—-distribution coefficient). Finally, the Davies' theory leads to the relation:

$$\mathrm{HLB} = 7 + 0.36 \ln(c^w/c^o) \qquad (120)$$

Comparing this expression with Eq. (10), which determines the difference between the standard chemical potentials of surfactants in the aqueous and oil phases (i.e., by the definition of the free energy of the surfactant transfer from the oil phase into the aqueous phase):

$$\mu_{0i}^w - \mu_{0i}^o = RT \ln K_i^0 \qquad (121)$$

where It can be easily seen that the HLB is related to the free energy (or the work of transfer) of the surfactant (w^{wo}) from one phase (water) to the other (oil). Therefore, $w^{wo}=RT\ln(c^w/c^o)$, and, consequently, the energetic interpretation of HLB numbers can be presented as

$$\mathrm{HLB} = 7 + 0.36 w^{wo}/\mathrm{RT} \qquad (122)$$

It is seen from the comparison of Eqs (119) and (122) that the additivity of HLB numbers follows from the additivity of the transfer work, because the group numbers in Eq. (118) are proportional to the partial values of transfer work w_i^{wo} characteristic to the individual groups which constitute the surfactant molecule:

$$g_i = 0.36 w_i^{wo}/RT \qquad (123)$$

The transfer work can be calculated from the coefficient K_i^o of the surfactant distribution coefficient between the two phases. The values of transfer work for a number of substances are tabulated, for example, in Ref. 262. For a ho-

Table 3 Group Numbers for Some Chemical Groups Calculated by Davies (266, 267)

$-SO_4Na$	38.7	−OH	1.9
−COOK	21.1	−O−	1.3
−COONa	19.1	$-(CH_2CH_2-O)-$	0.33
$-N^+$ (tert, amine)	9.4	CH_3-, $-CH_2-$, −CH=	−0.475
−COOH	2.1	Benzyl	−1.66

mologous series of a surfactant, the transfer work can be expressed as

$$w^{wo}/RT = a - bn_c \quad (124)$$

where a and b are constants which correspond to the transfer energy of one hydrophilic group and one methylene group, respectively, and n_c is the number of carbon atoms in the lipophilic part of the molecule. Similar relations are valid also for nonionic surfactants where the specific energy of transfer is calculated per oxyethylene group. If an energetic equilibrium exists between the hydrophilic and lipophilic parts of the surfactant molecule, i.e., $w^{wo}/RT = 0$, then it follows from Eq. (122) that the HLB = 7. For example, with respect to the series of aliphatic acids, according to the condition $a - bc_n = 0$, pentanoic acid is hydrophilic, while hexanoic acid, the next in the series, is lipophilic. Similarly, for the Tritons X homologous series, X-35 is hydrophilic, while X-15 is lipophilic.

While the HLB number concepts proposed by Griffin and Davies certainly facilitate the choice of surfactants and oils with regard to their practical applications, the theoretical deficiencies of these systems are also well known, and were discussed in a number of publications. For example, the additivity principle of the Griffin HLB with respect to mixtures of surfactants is held only within a rather narrow range of surfactants' HLB and necessary HLB numbers for oils (265, 268, 269). No account is taken for the concentration of surfactants, the temperature, or admixtures of electrolytes and other substances. When HLB numbers for nonionic surfactants are calculated from the Griffin equation [see (258)], the hydrophility is estimated only from the mass portion of oxyethylene groups, regardless of their location and the structure of the lyophilic chain. To take account of these effects and the influence of the medium, both for nonionic and ionic surfactants, the concept of effective HLB values was introduced (270, 271). It was shown that the addition of acetone, urea, dioxane, and other substances lead to the increase of the effective HLB numbers for nonionic surfactants, while the addition of glycerine, on the contrary, results in a decrease of the HLB value. The addition of alcohols and polyethylene glycols lead to more complicated changes in the HLB values (270, 271).

In the framework of Davies' concept, the relation [Eq. (119)] is empirical. This relation implies the additivity of group numbers. There is evidence for the fact that the hydrophilicity and lyophilicity of various groups depend on their position in the molecule; this is true, e.g., for isomers. The location of the benzene ring within the alkyl benzene sulfonates affects the distribution coefficient between water and oil, that is, the HLB value. Similar effects were observed with respect to the location of the polar group in the molecules of sodium alkyl sulfates (272). Principal relations of the Davies theory were derived from the analysis of the emulsion coalescence rates, where the Smoluchowsky theory was applied. In this analysis, no account was taken for the difference, which exists between emulsions of low stability, described by this theory, and stable emulsions where the coalescence stage is regulated by the properties of thin liquid films. The assumption of the Davies' model that the repulsive energetic barrier in oil-in-water emulsions does not depend on the lyophilic chain length, while for water-in-oil emulsions this barrier does not depend on the nature of polar groups, contradicts experimental data. Also, some arbitrariness exists in the relation between the behavior of emulsions and HLB numbers. According to Davies, values of HLB > 7 correspond to stable O/W emulsions, while stable W/O emulsions can be obtained for HLB < 7. It was shown experimentally, however, that the formation of stable O/W emulsions is possible for HLBs in the range 2-17, while the HLB interval corresponding to stable W/O emulsions is 2 to 10, see Ref. 262. Also the influence of the concentration of a surfactant on the type and stability of the emulsion remains unclear. For example, at low concentrations O/W emulsions are stable, while when the concentration exceeds 4-6%, a phase inversion takes place, which results in the formation of stable W/O emulsions (267, 273). A comparison between the HLB numbers of Griffin and Davies was made in a number of studies, for example, in Refs 262 and 274). For nonionic surfactants, these numbers are mutually inconsistent.

The HLB scale of Davies is based on the difference between the work of transfer of a surfactant molecule (or its constituents) from the vacuum into aqueous and oil phases. It can be expected that, similar to this difference, the ratio of these values can be used as a measure for the HLB (261). The work of surfactant transfer into a phase from the vacuum can be calculated as $w = w_h + w_l$, where the subscripts "h" and "l" refer to the hydrophilic and lipophilic parts of the surfactant molecule, respectively. This leads to the definition of the HLB indices (261):

$$\chi = w^w/w^o = (w_h^w + w_l^w)/(w_h^o + w_l^o) \quad (125)$$

$$\chi_l = w_h^{wo}/w_l^{ow} = (w_h^o - w_h^w)/(w_l^o - w_l^w), \quad (126)$$

where w_h^{wo} is the work required for the transfer of the hydrophilic group from the aqueous phase into the oil phase,

and w_1^{ow} is the work corresponding to the transfer of the lipophilic group from the oil phase into water. If a balance between the hydrophilic and lipophilic group exists, then $\chi = \chi_1 = 1$ The HLB index χ can be either positive or negative, with lipophilic substances corresponding to $-\infty < \chi < 1$, while for hydrophilic substances $1 < \chi < \infty$. The index x_1 being the ratio of two positive values, is positive. Using Eq. (117), one obtains from Eqs (125) and (126):

$$\chi = 1 - (RT/w^o)\ln(c^w/c^o) \quad (127)$$

$$\chi_1 = 1 - (RT/w_1^{ow})\ln(c^w/c^o) \quad (128)$$

It is seen that, unlike the scale by Davies, where the distribution coefficient of the surfactant is only necessary to calculate the HLB, to determine χ and χ_1 one requires some additional information regarding the work necessary for the transfer of the surfactant into the oil phase, or the difference between the works of transfer of lipophilic group from the oil phase into the aqueous one. Also, the ratio:

$$\chi_2 = w_h^w/w_l^o \quad (129)$$

is used as HLB index (275). This value is always possible, being the ratio of two negative values. The disadvantage of the indices x, x_1, and xx_2 compared with Griffin's and Davies' HLB numbers is that they are not additive.

A number of attempts have been made to estimate the HLB from the comparison of the work of surfactant-molecule transfer not between the adjacent bulk phases, but from bulk phases into the surface layer, that is, to use the adsorption work as basis for such estimates. The adsorption work from the aqueous phase is $w(z) - w^w$, while the adsorption work from the oil phase is given by the relation $w(z) - w$. Here, z is the coordinate of the hydrophilic-lipophilic center (HLC) of a surfactant molecule, which corresponds usually to the minimum of $w(z)$ (261). This minimum work of transfer of a surfactant molecule corresponds to the maximum at the plot of the concentration distribution in the surface layer. Usually the location of the minimum of $w(z)$ (i.e., HLC) is displaced from the geometric interface towards the aqueous phase. It is seen from the above relations that the adsorption work, unlike the work of transfer from bulk phases, is not a definite and unambiguous characteristic. Usually the local value of the work $w\{z\}$ is substituted by the mean (integral) work w^σ, related to the entire adsorption layer. Due to the inhomogeneity of the interface region, the adsorption work cannot be calculated additively from the work of adsorption for particular groups of the molecule, because these work values depend on the location of the group within the surface layer. Clearly, an interrelation should exist between the adsorption work and HLB characteristics. A trivial approach is based on the comparison of the adsorption work differences. In this case the difference between the adsorption works is just the work necessary for the transfer of the surfactant molecule from one phase into another; this work is the basic value in Davies' concept. The ratio of adsorption works, the so-called hydrophilic-oleophilic ratio (HOR) is often used (261, 262, 276-278):

$$HOR = w^{0\sigma}/w^{w\sigma} \quad (130)$$

Various expressions for HOR were proposed, expressed via the surfactant distribution coefficient between the phases, and the surfactant's adsorption activity (5). The advantage of HOR as compared to the HLB system is that, for a particular choice of the standard state, this index does not depend on the surfactant concentration, the type of the organic phase, or the presence of various additives soluble in water and oil. Methods were also proposed to determine the HOR for mixtures of surfactants (262). For these systems, however, this index is not additive anymore. The HOR values for mixtures are shifted towards that characteristic for the component which possesses the higher value of the distribution coefficient. Another deficiency of the HOR concept is its suggestiveness: it was mentioned above that this value depends on the coordinate of the HLC. However, for the HOR values other than unity, the HLC position-dependent work of the introduction of a surfactant molecule into the surface layer is uniquely determined by the HOR.

To summarize, among all the proposed characteristics of the HLB, Davies' HLB scale is the most substantiated and most widely used, in spite of the number of deficiencies noted above. Here, the recent publication (279), which relates the electroacoustophoretic behavior of emulsions with Davies' HLB numbers, can be referred to as an example.

X. CONCLUSIONS

The behavior of emulsions as a particular type of disperse system is controlled by many factors. There is a large number of properties of the corresponding liquid/ liquid interface which can be determined by well-established methods, such as dynamic surface tensions, adsorbed amount, exchange of matter across the interface, and dilational and shear rheology. Although first models exist, a general view

does not exist yet of how important the individual properties are in respect of emulsion stability or its destabilization. In practice, personal experience and trial and error procedures are most frequently used so far. The access to quantitative methods and extensive studies of model systems will for sure improve the possibilities of designing emulsions with a predefined behavior. This contribution only summarizes the experimental possibilities at extended liquid interfaces rather than providing a link to particular emulsion properties. An overall understanding of real emulsions will certainly require the study of the entire present encyclopedia, and then still questions remain open to be answered in future work.

ACKNOWLEDGMENTS

The work was financially supported by projects of the European Community (INCO ERB-IC15-CT96-0809), the DFG (Mi418/9-1 and Mi418/7-1), the Fonds der Chemischen Industrie (RM 400429), the German Canadian Agreement on Co-operation in Scientific Research and Technological Development (KAN MPT 22), and the ESA (Topical Team and Fast project).

NOMENCLATURE

A surface area
A_0 surface area at equilibrium
c concentration
c^w, c^0 concentration in the aqueous and oil phases
D diffusion coefficient
dA change in interfacial area
dW^A mechanical work due to interfacial tension
f frequency
g gravitational acceleration
HLB hydrophilic/lipophilic balance
k rate constant of transition from state 1 into state 2
K distribution coefficient
MW molecular weight
N^A total interfacial mole number
P pressure
r bubble radius
R gas constant
r_{cap} capillary radius
S^A interfacial entropy
t time
T absolute temperature
U^A interfacial internal energy
V volume
W_0 integral work
x direction normal to the interface
z coordinate normal to the surface

Greek symbols

α a constant
$\beta = (\omega)1/\omega_2)^{\alpha}$
γ surface tension
γ_0 surface tension of the pure solvent
$\Gamma = \Gamma_1\Gamma_2$ total adsorption
δ relative oscillation amplitude
$\triangle H_i$ molar standard enthalpy of transfer
$\triangle\pi\rho$ density difference
ε_d dilational elasticity
η_d dilational viscosity
η_s shear viscosity
Θ relative area change
$\lambda = k/\varpi$ dimensionless rate constant
μ^A interfacial chemical potential
$\Pi = \gamma_0 - \gamma$ surface tension
ω_1, ω_2 partial molar areas
$\varpi - 2\pi f$ circular frequency

REFERENCES

1. O Reynolds. Phil Trans Roy Soc London A177: 1577—165, 1886.
2. VG Levich. Physico-chemical Hydrodynamics. Englewood Cliffs, NJ: Prentice Hall, 1962.
3. AD Scheludko. Adv Colloid Interface Sci 1: 391—130, 1967.
4. IB Ivanov. Pure Appl Chem 52: 1241—1262, 1980.
5. A Sonin, A Bonfillon, D Langevin. J. Colloid Interface Sci 162: 323—330, 1994.
6. HA Barnes. Colloids Surfaces A 91: 89—95, 1994
7. TF Tadros, B Vincent. In: P Becher, ed. Encyclopedia of Emulsion Technology. Vol 1. New York: Marcel Dekker, 1983, p 130.
8. GV Jeffreys, JL Hawksley. AIChE J 11: 413—421, 1965.
9. DR Woods, KA Burrill. J Electroanal Chem 37: 191—203, 1972.
10. AJS Liem, DR Woods. AIChE Symp Ser 70: 8—15, 1974.
11. PG Murdoch, and DE Leng, Chem Eng Sci 26: 1881—1896, 1971.
12. IB Ivanov, TT Traykov. Int J Multiphase Flow 2: 397—410, 1976.
13 AD Barber, S Hartland. Can J Chem Eng 54: 279—288, 1976.

14. Z Zapryanov, AK Malhotra, N Aderangi, DT Wasan. Int J Multiphase Flow 92: 105—129, 1983.
15. DT Wasan, K Sampath, N Aderangi. AIChE Symp Ser 192: 93—97, 1980.
16. RRRP Borwankar, LA Lobo, DT Wasan. Colloids Surfaces A 69: 135—146, 1992.
17. V Bergeron. Langmuir 13: 3474—3482, 1997.
18. A Espert, R von Klitzing, P Poulin, A Collin, R Zana, D Langevin. Langmuir 14: 4251—4260, 1998.
19. E Dickinson. Curr Opinion Colloid Interface Sci 3: 633—638, 1998
20. A Williams, JJM Janssen, A Prins. Colloids Surfaces A 125: 189—200, 1997.
21. E Manev, RJ Pugh. J Colloid Interface Sci 186: 493—497, 1997.
22. JK Angarska, KD Tachev, PA Kralchevsky, A Mehreteab, G Broze. J Colloid Interface Sci 200: 31—45, 1998.
23. D Sentenac, SD Dean. J Colloid Interface Sci 196: 35—47, 1997.
24. IB Ivanov, PA Kralchevsky. Colloids Surfaces A 128: 155—175, 1997.
25. IB Ivanov, DS Dimitrov. In: IB Ivanov, ed. Thin Liquid Films. New York: Marcel Dekker, 1988, p 379.
26. D Langevin. Curr Opinion Colloid Interface Sci 3: 600—607, 1998.
27. R Miller, R Wiistneck, J Krágel, G Kretzschmar. Colloids Surfaces A 111: 75—118, 1996.
28. H Fruhner, KD Wantke. Colloids Surfaces A, 114: 53—60, 1996
29. J Kragel, AV Makievski, VI Kovalchuk, VB Fainerman, R Miller. Colloids Surfaces A (submitted).
30. J Krágel, DO Grigoriev, AV Makievski, R Miller, VB Fainerman, PJ Wilde, R Wüstneck. Colloids Surfaces B 12: 391—397, 1999.
31. VB Fainerman, EH Lucassen-Reynders, R Miller. Colloids Surfaces A 143: 141—165, 1998.
32. JA Butler. Proc Roy Soc Ser A, 138: 348—375, 1932.
33. P Joos. Bull Soc Chim Belg 76: 591—600, 1967.
34. B von Szyszkowski. Z Phys Chem (Leipzig) 64: 385—398, 1908.
35. I Langmuir. J Am Chem Soc 39: 1848—1907, 1917.
36. EH Lucassen-Reynders. J Colloid Sci 19: 584—585, 1964.
37. EH Lucassen-Reynders. J Phys Chem 70: 1777—1785, 1966.
38. EH Lucassen-Reynders. J Colloid Interface Sci 41: 156—167, 1972.
39. EH Lucassen-Reynders. J Colloid Interface Sci 85: 178—185, 1982.
40. EH Lucassen-Reynders. Progr Surface Membrane Sci 10: 253—320, 1976.
41. R Van den Bogaert, P Joos. J Phys Chem 84: 190—194, 1980.
42. VB Fainerman, R Miller, R WuUstneck, AV Makievski. J Phys Chem 100: 7669—7675, 1996
43. VB Fainerman, R. Miller, R. Wiistneck, J Phys Chem 101: 6479—6483, 1997
44. VB Fainerman, R Miller, R Wüstneck. J Colloid Interface Sci 183: 26—34, 1996.
45. EH Lucassen-Reynders. Colloids Surfaces A 91: 79—88, 1994.
46. JT Davies. Proc Roy Soc Ser A 208: 224—231, 1951.
47. JT Davies. Proc Roy Soc Ser A 245: 417—132, 1958.
48. RP Borwankar, DT Wasan. Chem Eng Sci 43: 1323—1337, 1988.
49. I Prigogine. The Molecular Theory of Solutions. Amsterdam: North-Holland, 1968.
50. EA Guggenheim. Mixtures. Oxford: Clarendon Press, 1952.
51. RC Read, JM Prausnitz, TK Sherwood. The Properties of Gases and Liquids. 3rd ed. New York, London, Paris, Tokyo: McGraw-Hill, 1977.
52. AN Frumkin. Z Phys Chem (Leipzig) 116: 466—484, 1925.
53. BB Damaskin, AN Frumkin, SL Djatkina. Izv AN SSSR Ser Chim 2171—2175, 1967.
54. BB Damaskin. Izv AN SSSR Ser Chim 346—351, 1969.
55. EH Lucassen-Reynders. In: EH Lucassen-Reynders, ed. Anionic Surfactants, Physical Chemistry of Surfactant Action. New York—Basel: Marcel Dekker, 1981, p 1.
56. JA Tedoradze, RA Arakeljan, ED Belokolos. Elektrokhimija 2: 563—569, 1966.
57. BB Damaskin. Elektrokhimija 5: 249—255, 1969.
58. BB Damaskin, AN Frumkin, NA Borovaja. Elektrokhimija 8: 807—815, 1972.
59. MJ Rosen, XY Hua. J Colloid Interface Sci 86: 164—172, 1982.
60. XY Hua, MJ Rosen. J Colloid Interface Sci 87: 469—477, 1982.
61. VB Fainerman, SV Lylyk Kolloidn Zh 45: 500—508, 1983.
62. VV Krotov. Kolloidn Zh 47: 1075—1082, 1985.
63. VB Fainerman. Zh Fiz Khim 62: 1003—1010, 1988.
64. VB Fainerman. Zh Fiz Khim 60: 681—685, 1986.
65. VB Fainerman. Kolloidn Zh 48: 512—519, 1986.
66. J Rodakiewicz-Nowak. J Colloid Interface Sci 85: 586—597, 1982.
67. M Karolczak, DM Mohilner. J Phys Chem 86: 2840—2848, 1982.
68. DM Mohilner, H Nakadomari, PR Mohilner. J Phys Chem 81: 244—252, 1977.
69. E Helfand, HL Frisch, JL Lebowitz. J Chem Phys 34: 1037—1044, 1961.
70. R Parsons. J Electroanal Chem 7: 136—144, 1964.
71. E Tronel-Peyroz. J Phys Chem 88: 1491—1496, 1984.
72. H Diamant, D Andelman. J Phys Chem 100: 13732—13742, 1996.
73. R Miller, EV Aksenenko, L Liggieri, F Ravera, VB Fainerman. Langmuir 15: 1328—1336, 1999.

74. EH Lucassen-Reynders, J Lucassen, D Giles. J Colloid Interface Sci 81: 150—162, 1981.
75. VV Kalinin, CJ Radke. Colloids Surfaces A 114: 337—350, 1996.
76. CA MacLeod, CJ Radke. Langmuir 10:3555—3566, 1994.
77. VYa Poberezhnyi, LA Kul'skiy. Kolloidn Zh 46: 735—742, 1984.
78. VYa Poberezhnyi, TZ Sotskova, LA Kul'skiy. Khim i Tekhnol Vody 18: 570—582, 1996.
79. PM Vlahovska, KD Danov, A Mehreteab, G Broze. J Colloid Interface Sci 192: 194—206, 1997.
80. PA Kralchevsky, KD Danov, G Broze, A Mehreteab. Langmuir 15:2351—2365, 1999.
81. VM Muller, BV Derjaguin. J Colloid Interface Sci 61:361—369, 1977.
82. AV Makievski, VB Fainerman, M Bree, R Wüstneck, J Krägel, R Miller. J Phys Chem 102: 417—425, 1998.
83. VB Fainerman, R Miller. In: D Möbius, R Miller, eds. Proteins at Liquid Interfaces. Vol. 7. Amsterdam: Elsevier, 1998, pp 51—102.
84. P Joos, G Serrien. J Colloid Interface Sci, 145: 291—294, 1991.
85. VB Fainerman, R Miller. Langmuir 15: 1812—1816, 1999.
86. R Miller, VB Fainerman, AV Makievski, J Krägel, R Wüstneck. Colloids Surfaces A, 161:151—157, 2000.
87. JF Padday. In: E Matijevic, ed. Surface and Colloid Science. Vol 1. New York: Wiley, 1968, p 101.
88. DS Ambwani, T Fort Jr. In: RJ Good, RR Stromberg, eds. Surface and Colloid Science. Vol 11. New York: Plenum Press.
89. AW Adamson. Physical Chemistry of Surfaces. 5th ed, New York: Wiley, 1990.
90. AI Rusanov, VA Prokhorov. In: D Möbius, R Miller, eds. Studies of Interface Science. Amsterdam: Elsevier, 1996.
91. P Chen, DY Kwok, RM Prokop, OI del Rio, SS Susnar, AW Neumann. In: D Möbius, R Miller, eds. Studies of Interface Science. Vol 6. Amsterdam: Elsevier, 1998, pp 61—138.
92. R Miller, VB Fainerman. In: D Möbius, R Miller, eds. Studies of Interface Science. Vol 6. Elsevier, Amsterdam, 1998, pp 139—186.
93. AM Seifert. In: D Möbius, R Miller, eds. Studies of Interface Science. Vol 6. Amsterdam: Elsevier, 1998, pp 187—238.
94. L Liggier, F Ravera. In: D Möbius, R Miller, eds. Studies of Interface Science. Vol 6. Amsterdam: Elsevier, 1998, pp 239—278.
95. F MacRitchie. Chemistry at Interfaces. San Diego, New York: Academic Press, 1990.
96. JD Andrade. Surface and Interfacial Aspects of Biomaterial Polymers. Vol 2. New York: Plenum, 1985.
97. A Passerone, R Ricci. Bubbles in Interfacial Research. In: D Möbius, R Miller, eds. Studies of Interface Science. Vol 6. Amsterdam: Elsevier, 1998, pp 475—524.
98. DY Kwok, P Chiefalo, B Khorshiddoust, S Lahooti, MA Cabrerizo-Vilchez, OI del Rio, AW Neumann. In: R Sharma, ed. Surfactant Adsorption and Surface Solubilization. ACS Symposium Series 615. Washington, DC: American Chemical Society. 1995, ch. 24.
99. JF Padday. In: E Matijevic, ed. Surface and Colloid Science. Vol 1. New York, London, Sydney, Toronto: Wiley-Interscience, 1969, p 39.
100. FC Goodrich. In: E Matijevic, ed. Surface and Colloid Science. Vol 1. New York, London, Sydney, Toronto: Wiley-Interscience, 1969, p 1.
101. AFH Ward, L Tordai. J Phys Chem 14: 453—164, 1946.
102. FW Pierson, S Whittaker. J Colloid Interface Sci 52: 203—213, 1976.
103. R Miller. Colloid Polymer Sci 258: 179—185, 1980.
104. JT Davies, JAC Smith, DG Humphreys. Proc Int Conf Surf Act Subst 2: 281—287, 1957. 105. J Kloubek. J Colloid Interface Sci 41: 1—6, 1972.
106. VB Fainerman. Kolloidn Zh 41: 111—115, 1979.
107. D Ilkovic, J Chim Phys Physicochem Biol 35: 129—135, 1938.
108. P Delahay, I Trachtenberg. J Am Chem Soc 79: 2355—2362, 1957.
109. P Delahay, CT Fike. J Am Chem Soc 80: 2628—2630, 1958.
110. P Joos, M Van Uffelen. J Colloid Interface Sci 171: 297—305, 1995.
111. A Passerone, L Liggier, N Rando, F Ravera, E. Ricci. J Colloid Interface Sci 146: 152—162, 1991.
112. RS Hansen. J Phys Chem 64: 637—641, 1960.
113. VB Fainerman, SA Zholob, R Miller. Langmuir 13: 283—289, 1997.
114. M Ferrari, L Liggieri, F Ravera, C Amodio, R Miller. J Colloid Interface Sci 186: 40—45, 1997.
115. L Liggier, F Ravera, M Ferrari, A Passerone, R Miller. J Colloid Interface Sci 186:46—52, 1997.
116. JL Cayias, RS Schechter, WH Wade. In: KL Mittal, ed. Adsorption at Interface. ACS Symposium Series 8. Washington, DC: American Chemical Society, 1975, pp 234—247.
117. VK Bansal and DO Shah. In: KL Mittal, ed. Micellization, Solubilization, and Microemulsions. Vol 1. New York: Plenum Press, 1977, pp 87—114.
118. JL Cayias, RS Schechter, WH Wade. J Colloid Interface Sci 59: 31—44, 1977.
119. L Cash, JL Cayias, G Fournier, D Macallister, T Schares, RS Schechter, WH Wade. J Colloid Interface Sci 59: 39—44, 1977.
120. El Franses, JE Puig, Y Talmon, WG Miller, LE Scriven, HT Davis. J Phys Chem 84: 1547—1556, 1980.
121. R Aveyard, BP Binks, TA Lawless, J Mead. J Chem Soc Faraday Trans 1 81: 2155—2168, 1985.

122. R Aveyard, BP Sinks, J Mead. J Chem Soc Faraday Trans 1 81:2169—2177, 1985.

123. R Aveyard, BP Binks, J Mead. J Chem Soc Faraday Trans 1 82: 1755—1770, 1986.

124. R Aveyard, BP Binks, S Clark, J Mead. J Chem Soc Faraday Trans 1 82: 125—142, 1986.

125. D Guest, D Langevin. J Colloid Interface Sci 112: 208—220, 1986.

126. R Aveyard, BP Binks, J Mead. J Chem Soc Faraday Trans 1 83: 2347—2357, 1987.

127. R Aveyard, BP Binks, TA Lawless, J Mead. Can J Chem 66: 3031—3037, 1988.

128. R Aveyard, BP Binks, PDI Fletcher, JR Lu. J Colloid Interface Sci 139: 128—138, 1990. 129. WD Harkins, H Zollman. Am Chem Soc 48: 69—81 1926.

130. AM Cazabat, D Langevin, J Meuntier, A Pouchelon. Adv Colloid Interface Sci 16: 175—199, 1982.

131. JW Gibbs. The Scientific Papers of J Willard Gibbs. New York: Dover, 1960.

132. HB Callen. Thermodynamics and an Introduction to Thermostatics. 2nd ed. New York: John Wiley, 1985.

133. Y Rotenberg, L Boruvka, AW Neumann. J Colloid Interface Sci 93: 169—183, 1983. 134. P Cheng, D Li, L Boruvka, Y Rotenberg, AW Neumann. Colloids Surfaces, 43: 151—167, 1990.

135. S Lahooti, OI del Rio, P Cheng, AW Neumann. In: JK Spelt, AW Neumann, eds. Applied Surface Thermodynamics. New York: Marcel Dekker, 1996, pp 441—507.

136. B Vonnegut. Rev Sci Instrum 13: 6—9, 1942.

137. HM Princen, IYZ Zia, SG Mason. J Colloid Interface Sci 23: 99—107, 1967.

138. JC Slattery, JD Chen. J Colloid Interface Sci 64: 371—373, 1978.

139. PK Currie, JV Nieuwkoop. J Colloid Interface Sci 87: 301—316, 1982.

140. A Voigt, O Thiel, D William, Z Policova, W Zingg, AW Neumann. Colloids Surfaces 58: 315—326, 1991.

141. R Miller, R Sedev, K-H Schano, C Ng, AW Neumann. Colloids Surfaces 69:209—216, 1993.

142. DY Kwok, MA Cabrerizo-Vilchez, Y Gomez, SS Susnar, IO del Rio, D Vollhardt, R Miller, AW Neumann. In: V Pillai, DO Shah, eds. Dynamic Properties of Interfaces and Association Structures. Champaign, IL: American Oil Chemists Society Press, 1996, pp 278—296.

143. DY Kwok, D Vollhardt, R Miller, D Li, AW Neumann. Colloids Surfaces A: Physicochem Eng Aspects 88: 51—58, 1994.

144. DY Kwok, S Tadros, H Deol, D Vollhardt, R Miller, MA Cabrerizo-Vilchez, AW Neumann. Langmuir 12: 1851—1859, 1996.

145. R Wüstneck, P Enders, TH Ebisch, R Miller. Thin Solid Films 298: 39—46, 1997.

146. J Li, R Miller, R Wüstneck, H Möhwald, AW Neumann. Colloids Surfaces A: Physicochem Eng Aspects 96: 295—299, 1995.

147. J Li, R Miller, H Mohwald. Colloids Surfaces A: Physicochem Eng Aspects 114: 113—121, 1996.

148. DY Kwok, LK Leung, CB Park, AW Neumann. Polym Eng Sci, 38: 757—764, 1998. 149. M Wulf, S Michel, K Grundke, OI del Rio, DY Kwok, AW Neumann. J Colloid Interface Sci 210:172—181, 1998.

150. SS Susnar, HA Hamza, AW Neumann. Colloids Surfaces A: Physicochem Eng Aspects 89:169—180, 1994.

151. MA Cabrerizo-Vilchez, Z Policova, DY Kwok, P Chen, AW Neumann. Colloids Surfaces B: Biointerfaces 5: 1—9, 1995.

152. D Duncan, D Li, J Gaydos, AW Neumann. J Colloid Interface Sci 169: 256—261, 1995. 153. A Amirfazli, DY Kwok, J Gaydos, AW Neumann. J Colloid Interface Sci 205: 1—11, 1998.

154. D Li, AW Neumann. J Colloid Interface Sci 148: 190—200, 1992.

155. DY Kwok, CNC Lam, A Li, AW Neumann. J Adhesion, 68: 229—255, 1998.

156. DY Kwok, CNC Lam, A Li, A Leung, R Wu, E Mok, A W Neumann. Colloids Surfaces A: Physicochem Eng Aspects 142: 219—235, 1998.

157. HT Patterson, KH Hu, TH Grindstaff. J Polym Sci C: Polym Symposia 34: 31—43, 1971. 158. J Ryden, PÅ Albertsson. J Colloid Interface Sci 37: 219—222, 1971.

159. JJ Elmendorp, G de Vos. Polym Eng Sci 26: 415—417, 1986.

160. M Heinrich, BA Wolf. Polymer, 33: 1926—1931, 1992.

161. AM Seifert, JH Wendorff. Colloid Polym Sci 270: 962—971, 1992.

162. DD Joseph, MS Arney, G Gillberg, H Hu, D Hultman, C Verdier, TM Vinagre. J Rheol 36:621—662, 1992.

163. J Lyklema. Fundamentals of Interface and Colloid Science. Vol I. London: Academic Press, 1993.

164. R Miller, G Loglio, U Tesei. Colloid Polymer Sci 270: 598—601, 1992.

165. F Ravera, L Liggier, A Passerone, A Steinchen. J Colloid Interface Sci 163: 309—314, 1994.

166. CA MacLeod, CJ Radke. J Colloid Interface Sci 166: 73—88, 1997.

167. VB Fainerman. SA Zholob, R Miller. Langmuir 13: 283—289, 1997.

168. DC England, JC Berg. AIChE J 17: 313—322, 1971.

169. E Rubin, CJ Radke. Chem Eng Sci 35: 1129—1138, 1980.

170. TS Sørensen, M Hennenberg. In: TS Sørensen, ed. Dynamics and Instabilities in Fluid Interfaces, Lecture Notes in Physics 105. Berlin: Springer-Verlag, 1979.

171. M Hennenberg, A Sanfeld, PM Bish. AIChe J 27: 1002—1008, 1981.
172. F Ravera, M Ferrari, L Liggieri, R Miller, A Passerone. Langmuir 13: 4817—4820, 1997. 173. M Ferrari, L Liggieri, F Ravera. J Phys Chem B 102: 10521—10527, 1998.
174. AFH Ward, L Tordai. J Chem Phys 14:453—461, 1946.
175. RS Hansen. J Phys Chem 64: 637—641, 1960.
176. F Ravera, M Ferrari, L Liggieri, R Miller. Progr Colloid Polymer Sci 105: 346—350, 1997.
177. R Miller. Colloid Polymer Sci 259: 375—381, 1981.
178. G Loglio, U Tesei, R Miller, R Cini. Colloids Surfaces A 61: 219—226, 1991.
179. EH Lucassen-Reynders, J Lucassen. Colloids Surfaces A 85: 211—219, 1994.
180. SS Dukhin, G Kretzschmar, R Miller In: D Mobius, R Miller, eds. Studies in Interface Science. Vol 1. Amsterdam: Elsevier, 1995.
181. R Miller, VB Fainerman, J Krägel, G Loglio. Curr Opinion Colloid Interface Sci 2: 578—583, 1997.
182. R Miller, R Wüstneck, J Krägel, G Kretzschmar. Colloids Surface A 111: 75—118, 1996. 183. J Lucassen, M van den Tempel. Chem Eng Sci 27: 1283—1291, 1972.
184. J Lucassen, M van den Tempel. J Colloid Interface Sci 41: 491—498, 1972.
185. SM Sun, MC Shen. J Math Anal Appl 172: 533—566, 1993.
186. BA Noskov, DO Grigoriev, R Miller. J Colloid Interface Sci 188: 9—15, 1997.
187. BA Noskov, DO Grigoriev, R Miller. Langmuir 13: 295—298, 1997.
188. DO Johnson, KJ Stebe. J Colloid Interface Sci 168: 21—35, 1994.
189. KD Wantke, H Fruhner. In: Studies in D Mobius, R Miller, eds. Studies in Interface Science. Vol 6. Amsterdam: Elsevier, 1998, pp 327—365.
190. P Joos, M van Uffelen. Colloids Surfaces A 100: 245—253, 1995.
191. M van Uffelen, P Joos. J Colloid Interface Sci 158: 452—159, 1995.
192. T Horozov, P Joos. J Colloid Interface Sci 173: 334—342, 1995.
193. LT Lee, D Langevin, B Farnoux. Physical Review Letters 67: 2678—2681, 1991.
194. A Bonfillon, D Langevin. Langmuir 9: 2172—2177, 1993.
195. A Prins, MA Bos, FJG Boerboom, HKAI van Karlsbeek. In: D Möbius, R Miller, eds. Studies in Interface Science. Vol 7. Amsterdam: Elsevier, 1998, pp 221—265.
196. R Miller, Z Policova, R Sedev, AW Neumann. Colloids Surfaces A 76:179—185, 1993.
197. P Chen, Z Polikova, SS Susnar, CR Pace-Asciak, PM Demin, AW Neumann. Colloids Surfaces A 114: 99—112, 1996.
198. JB Li, R Miller, H Möhwald. Colloids Surfaces A 114: 123—130, 1996.
199. J Benjamins, A Cagna, EH Lucassen-Reynders. Colloids Surfaces A 114: 245—254, 1996.
200. R Miller, J Krägel, AV Makievski, R Wüstneck, JB Li, VB Fainerman, AW Neumann. Proceedings of the Second World Emulsion Congress, Bordeaux, 1997, Vol 4, pp 153—163. 201. R Wüstneck, B Moser, G Muschiolik. Colloids Surfaces A, Colloids Surfaces B 15: 263—273, 1999.
202. AV Makievski, R Miller, VB Fainerman, J Krägel, R Wüstneck. In: E Dickinson, JM Rodiguez Patino, eds. Food Emulsions and Foams: Interfaces, Interfaces, Interactions and Stability, Special Publication No. 227. Cambridge, England: Royal Society of Chemistry, 1999, pp 269—284.
203. R Nagarajan, DT Wasan. J Colloid Interface Sci 159: 164—173, 1993.
204. L Liggieri, F Ravera, A Passerone J Colloid Interface Sci 169: 226—237, 1995.
205. L Liggieri, F Ravera, A Passerone. J Colloid Interface Sci 140: 436—443, 1990.
206. YT Tian, RG Holt, RE Apfel. Theory Phys Fluids 7: 2938—2949, 1995.
207. YT Tian, RG Holt, RE Apfel. J Colloid Interface Sci 187: 1—10, 1997.
208. YH Kim, K Koczo, DT Wasan. J Colloid Interface Sci 187: 29—44, 1997.
209. R Miller, AV Makievski, VB Fainerman, J Krägel, F Ravera, L Liggieri, G Loglio. In: J Banhart, ed., Proceedings of the Workshop "Foams", Leuven, Belgium, 1999.
210. HA Wege, JA Holgado-Terriza, AW Neumann, MA Cabrerizo-Vilchez. Colloids and Surfaces A 156: 509—517, 1999.
211. R Miller, G Loglio, U Tesei, KH Schano. Adv Colloid Interface Sci 37: 73—96, 1991.
212. EK Zholkovskij, VI Kovalchuk, VB Fainerman, G Loglio, J Krägel, R Miller, SA Zholob, SS Dukhin. J Colloid Interface Sci 224: 47—55, 2000.
213. VI Kovalchuk, EK Zholkovskij, J Krägel, R Miller, VB Fainerman, R Wüstneck, G Loglio, SS Dukhin. J Colloid Interface Sci 224: 245—254, 2000.
214. M Joly. In: E Matijevic, ed. Surface and Colloid Science. Vol 5. New York: Wiley-Interscience, 1972, pp 1—93.
215. FC Goodrich. In: KL Mittal, ed. Solution Chemistry of Surfactants. Vol 2. New York: Plenum Press, 1979, pp 733—748.
216. J Lucassen. In: EH Lucassen-Reynders, ed. Anionic Surfactants: Physical Chemistry of Surfactant Action. New York: Marcel Dekker, 1981, pp 217—265.
217. DA Edwards, H Brenner, DT Wasan. Interfacial Transport Processes and Rheology. Boston, MA: Butterworth-Heinemann, 1991

218. B Noskov, G Loglio. Colloids Surf A 143: 167—183, 1998.

219. B Warburton. Curr Opinion Colloid Interface Sci 1:481—486, 1996.

220. R Miller, VB Fainerman, J Krägel, G Loglio. Curr Opinion Colloid Interface Sci 2: 578—583, 1997.

221. AK Malhotra, DT Wasan. In: IB Ivanov, ed. Thin Liquid Films, Surfactant Science Series, Vol 29. New York: Marcel Dekker, 1988, pp 829—890.

222. EH Lucassen-Reynders. Food Struct 12:1—12, 1993.

223. B Murray, E Dickinson. Food Sci Technol Int 2: 131—145, 1996.

224. B Murray. In: D Möbius, R Miller, eds. Proteins at Liquid Interfaces. Amsterdam: Elsevier, 1998, pp 179—220.

225. B Warburton. In: AA Collyer, ed. Techniques in Rheological Measurements. London: Chapman & Hall, 1993, pp 55—95.

226. J Benjamins, F van Voorst Vader. Colloids Surfaces A 65: 161—174, 1992.

227. R Nagarajan, DT Wasan. Rev Sci Instrum 65: 2675—2679, 1994.

228. HO Lee, TS Jiang, KS Avramidis. J Colloid Interface Sci 146: 90—122, 1991.

229. SS Feng, RC MacDonald, BM Abraham. Langmuir 7: 572—576, 1991.

230. R Nagarajan, SI Chung, DT Wasan. J Colloid Interface Sci 204: 53—60, 1998.

231. R Miller, J Krägel, AV Makievski, R Wüstneck, JB Li, VB Fainerman, AW Neumann. Proteins at liquid/liquid interfaces—-adsorption and rheological properties. Proceedings of the Second World Emulsion Congress, Bordeaux, 1997, Vol 4, pp 153—163.

232. J Krägel, S Siegel, R Miller, M Born, KH Schano. Colloids Surfaces A 91: 169—180, 1994.

233. I Lakatos, J Lakatos-Szabo. Colloid Polymer Sci 275: 493—501, 1997.

234. FO Opawale, DJ Burgess. J Colloid Interface Sci 197: 142—150, 1998.

235. RA Mohammed, AI Bailey, PF Luckham, SE Taylor. Colloids Surfaces A 91: 129—139, 1994.

236. AE Cardenas-Valera, AI Bailey. Colloids Surfaces A 79: 115—127, 1993.

237. JY Zhang, LP Zhang, JA Tang, L Jiang. Colloids Surfaces A 88: 33—39, 1994.

238. JY Zhang, XP Wang, HY Liu, JA Tang, L Jiang. Colloids Surfaces A 132: 9—16, 1998. 239. M Faergemand, BS Murray, E Dickinson. J Agric Food Chem 45: 2514—2519, 1997. 240. LG Ogden, AJ Rosenthal. J Colloid Interface Sci 191: 38—47, 1997.

241. LG Ogden, AJ Rosenthal. J Am Oil Chem Soc 75: 1841—1847, 1998.

242. R Wustneck, J Krägel, R Miller, PJ Wilde, DK Sarker, DC Clark. Food Hydrocoll 10: 395—405, 1996.

243. RMA Azzam, NM Bashara. Ellipsmetry and Polarized Light. Amsterdam: North Holland, 1979.

244. R Reiter, H Motschmann, H Orendi, A Nemetz, W. Knoll. Langmuir 8: 1784—1788, 1992.

245. R Teppner, S Bae, K Haage, H Motschmann. Langmuir 15: 7002—7007, 1999.

246. D Ducharme, A Tessier, RM Leblanc. Rev Sci Instrum 58: 571--578, 1987.

247. M Paudler, J Ruths, H Riegler. Langmuir 8: 184—189, 1992.

248. D Ducharme, J-J Max, C Salesse, RM Leblanc. J Phys Chem 94: 1925—1932, 1990.

249. J Lekner. Theory of Reflection of Electromagnetic and Particle Waves, Boston, MA: Martinus Nijhoff 1987.

250. SWH Eijt, MM Wittebrood, MAC Devillers, T Rasing. Langmuir 10: 4498—4502, 1994. 251. JA De Feijter, J Benjamins, FA Veer. Biopolymers 17: 1759—1772, 1978.

252. RW Collins, DE Aspnes, EA Irene, eds. Spectroscopic ellipsometry. Proceedings of the Second International Conference, Charleston, SC, 1997.

253. M Harke, R Teppner, O Schulz, H Orendi, H Motschmann. Rev Sci Instrum 68: 3130—3134, 1997.

254. AI Rusanov, VI Pshenitsyn. Dokl Akad Nauk SSSR 187: 619—629, 1969.

255. A Hirtz, W Lawnik, GH Findenegg. Colloids Surfaces 51: 405—418, 1990.

256. BB Sauer, H Yu, M Yazdanian, G Zografi. Macromolecules 22: 2332—2337, 1989.

257. DG Goodall, ML Gee, G Stevens, J Perera, D Beaglehole. Colloids Surfaces A 143: 41—52, 1998.

258. WC Griffin. J Soc Cosmetic Chem 1: 311—326, 1949; 5: 249—262, 1954.

259. P Beecher. Emulsions, New York: Reinhold, 1965.

260. LA Morris. Manuf Chem Aerosol News 36: 66—69, 1965.

261. AI Rusanov. Chem Rev 27: 1—326, 1997.

262. PM Kruglyakov. Studies in Interface Science. Vol 9. Amsterdam: Elsevier, 2000.

263. WB Borman, GD Hall. J Pharm Soc 52: 442—455, 1964.

264. T Legras. Ann Pharm France 30: 211—232, 1972.

265. N Ohba. Bull Chem Soc Japan 35: 1016—1020, 1962; 35: 1021—1032, 1962.

266. JT Davies. Proceedings of the Second International Congress on Surface Activity. Vol 1. London: Butterworths, 1957, pp 440.

267. JT Davies, EK Rideal. Interfacial Phenomena. New York: Academic Press, 1963.

268. K Shinoda, T Yoneyama, H Tsutsumi. J Disp Sci Technol 1: 1—9, 1980.

269. L Marszall. J Disp Sci Technol 2: 443-454, 1981.

270. L Marszal. J Colloid Interface Sci 60: 570--579, 1977; 65: 589—596, 1978.

271. L Marszal. Tenside Surfactants Detergents 16: 303—311, 1979.

272. IJ Lin, JP Friend, Y Zimmels. J Colloid Interface Sci 45: 378—392, 1973.
273. S Rigelman, G Pichon, Am Perfumer 77: 31—50, 1962.
274. N Schott. J Pharm Soc 60: 648—662, 1971.
275. P Winsor. Solvent Properties of Amphiphilic Compounds. London: Butterworths, 1954.
276. PM Kruglyakov, AF Koretskij. Dokl AN SSSR 197: 1106—1109, 1971.
277. GMM Cook, WR Rodwood, AR Taylor, DA Haydon. Kolloid ZZ Polym 227: 28—37, 1968.
278. SH Ikeda. Adv Colloid Interface Sci 18: 93—125, 1982.
279. OB Ho. J Colloid Interface Sci 198: 249—260, 1998.